NASA CR-66045

A DIGITAL COMPUTER SIMULATION OF HIGH-ALTITUDE PARACHUTE RESPONSE TO WIND GRADIENTS

By

Robert L. Ammons

June 23, 1965

Prepared for

National Aeronautics & Space Administration

Langley Research Center

Langley Station

Hampton, Virginia

In Fulfillment of

Contract No. NAS 1-4537

Prepared by

Thiokol Chemical Corporation

Astro-Met Division

P.O. Box 1497 Ogden, Utah

A DIGITAL COMPUTER SIMULATION OF HIGH-ALTITUDE PARACHUTE RESPONSE TO WIND GRADIENTS

By

Robert L. Ammons

June 23, 1965

Prepared for
National Aeronautics & Space Administration
Langley Research Center
Langley Station
Hampton, Virginia

In Fulfillment of
Contract No. NAS 1-4537

Prepared by
Thiokol Chemical Corporation
Astro-Met Division
P.O. Box 1497 Ogden, Utah

ABSTRACT

The response of two parachute systems---impervious hemisphere and disc-gap-band---was studied as a function of wind shear and altitude. Both systems were simulated on a digital computer as rigid bodies. The computer program included the effects of Magnus forces and viscous damping. Equations for a parachute falling in a wind field at 0° angle of attack are presented, as is a technique for determining error as a function of altitude on either parachute. The computer program dynamic model and equations of motion are summarized, and all computer data outputs are supplied.

TABLE OF CONTENTS

LIST OF FIGURES

LIST OF FIGURES (Cont.)

LIST OF FIGURES (Cont.)

NOTATION

1.	α	=	angle of attack (degrees)
2.	b	=	numerical factor (dimensionless)
3.	$C_{D\ eff.}$	=	$\dfrac{W}{1/2\rho\ V_z^2 S_{ref}}$
4.	$C_{D\ act.}$	=	$\dfrac{F_D}{1/2\rho \lvert V_R \rvert^2 S_{ref}}$
5.	D	=	diameter (feet)
6.	E	=	error = $V_w - V_p$ (feet per second)
7.	e	=	Napierian base
8.	F_D	=	drag force (pounds)
9.	g	=	gravitational acceleration (feet per second^2)
10.	h	=	altitude (feet)
11.	ℓ	=	line length (feet)
12.	m	=	mass (slugs)
13.	n	=	number of lines
14.	ω	=	spin rate (radians per second)
15.	ρ	=	density (pound-second^2 per feet^4)
16.	S_{ref}	=	$\dfrac{\pi D^2}{4}$ (feet^2)
17.	t	=	time (seconds)
18.	τ	=	period of oscillation (seconds)
19.	V_p	=	parachute velocity - $\vec{V}_x + \vec{V}_y$ (feet per second)
20.	V_R	=	resultant velocity (feet per second)

21.	V_w	=	wind velocity (feet per second)
22.	V_z	=	fall rate (feet per second)
23.	W_s	=	store weight (pounds)
24.	W_t	=	total weight (pounds)
25.	x,y,z	=	space coordinates

SECTION I

PROBLEM STATEMENT AND CONCLUSIONS

The response of two parachute systems (impervious hemisphere and disc-gap-band) was studied as a function of wind shear (dV_w/dh) and altitude. A brief comparison of the two systems follows:

	Impervious Hemisphere	Disc-Gap-Band
Flying (Reference) Diameter (ft.)	15.0	12.5
Line Length (ft.)	28.0	18.75
Number of Lines	24	18
Total Weight (lb.)	8.3	8.0
Store Weight (lb.)	6.5	5.0
Nominal C_D (dimensionless)	1.40	1.34
Stable Angle of Attack (deg.)	45	0

The two parachute systems, with principal dimensions, are illustrated in Figures 1a and 1b; aerodynamic coefficients are summarized in Figures 2a and 2b. Figure 3 shows the form of the wind field through which each parachute descent was simulated. Figure 4 is a comparison of descent rates vs. altitude for the two parachute systems.

When the five values of V_w are combined with the five values of $2\Delta h$ (as listed below), 25 separate wind fields result:

V_w (ft./sec.)	$2\Delta h$ (ft.)
30	5,000
40	10,000
60	20,000
100	30,000
200	40,000

Thus, each parachute was subjected to simulated wind shears ranging from 0.0015 sec.$^{-1}$ to 0.08 sec.$^{-1}$. The results of these computer runs are appended in the form of direct computer output listings. Analysis of these listings has resulted in a number of conclusions;

1. For a given parachute configuration, measurement error associated with a wind shear is inversely proportional to air density and directly proportional to the velocity-altitude gradient; that is,

$$E = (2m/C_D S) \quad (1/\rho) \quad (dV_w/dh)$$

$$= (V_z^2/g) \quad (dV_w/dh).$$

2. The altitude increment through which the parachute falls while its horizontal velocity approaches to within E of the actual wind velocity is a function of fall rate alone. It can be found by the equation $\Delta h = b(V_z^2/g)$, which gives the altitude interval Δh, in which the parachute attains a horizontal velocity of $V_w \pm E(1 \pm 1/e^b)$. These two relationships were first suspected when plots of the wind-measurement error as a function of altitude were examined. These plots showed the product $E\rho$ to be nearly constant for either parachute. Subsequent dimensional analysis showed the error equation to be of the form given above, and finally a solution to the differential equation of motion of the parachute in a wind gradient (Appendix A) confirmed the "steady-state" error function.

3. Perturbing moments (such as a Magnus effect) are required in order to cause the unstable hemispherical parachute to cone, rather than oscillate in a plane.

4. The wind-following error for the coning hemispherical parachute is of the same form as that for the disc-gap-band, with a

sinusoidal error component superimposed as a consequence of parachute oscillation. This error function is of the form

$$E = (V_z^2/g)\ (dV_w/dh) + K \sin\ (\omega t + \vartheta),$$

where ω is the precession rate of the system in radians per second. The effect of this precession component on wind-following error may be seen clearly in Figure 10. Figure 16 is a comparison of the function (V_z^2/g) for the two parachutes studied and allows the specific combinations of weight and drag area studied to be compared. The difference in wind-following error implied by Figure 16 is, in fact, due to a difference in drag-to-weight ratio, or descent rate, between the two systems.

5. Finally, it was found that the coning parachute exhibited a variable effective drag coefficient and did not fall with a constant dynamic pressure over the altitude range studied. The drag coefficient was found to vary from approximately 0.8 at 230,000 feet to 1.5 at 150,000 feet. This effect, shown in Figures 5, 6, and 7, is apparently brought about by the combination of lift, drag, and Magnus forces on the parachute, coupled with the three-dimensional phugoid motion of the system.

SECTION II

SUMMARY OF COMPUTER RUNS

Early computer runs showed that the hemispherical parachute, when released at altitude, oscillated in a plane with a total excursion of approximately $\pm 45^{\circ}$. The system, as described by early versions of the six-degree-of-freedom computer program, did not have sufficient cross-wind perturbing force to cause the parachute to oscillate in a conical mode.

The computer program was modified to include the effects of a Magnus force brought about by the action of the cross velocity combined with the parachute spin about the longitudinal axis of the system. The addition of this Magnus force causes the hemispherical parachute to fall with a coning motion such that the path described by the system center of gravity is a helix, with radius and wavelength both functions of spin rate. This oscillation is a type of three-dimensional phugoid, with the parachute longitudinal axis maintaining a constant angle of attack.

Further refinements to the program included modification of the viscous damping term before actual data runs were commenced. The final program is described in Appendix C.

A total of 63 computer runs was conducted on the hemispherical parachute in order to establish aerodynamic coefficients which would simulate the actual in-flight observed behavior of this parachute at high altitudes.[1,2] As a result of these studies the coning period of the hemispherical parachute was maintained at an average of 7 seconds over the altitude interval of interest.

---

[1] Whitock, Charles H. and Murrow, Harold N., "Performance Characteristics of a Preformed Elliptical Parachute at Altitudes Between 200,000 and 100,000 Feet, Obtained by In-Flight Photography," NASA TND-2183, Feb. 1964.

[2] Murrow, Harold N., "Observations of Parachute Characteristics at Altitudes Above 100,000 Feet by Means of In-Flight Photography," presented at Symposium on Parachute Technology and Evaluation, El Centro, Calif. April 7-19, 1964.

Preliminary runs on the stable disc-gap-band configuration showed that parachute to be relatively unaffected by Magnus forces, and it was concluded that data runs need not include the effect of spin. A total of 33 computer runs verified this fact, and supplied preliminary data on parachute behavior.

Ten more computer runs were used to determine initial velocities for the two parachutes so that none of the data running time would be invalid while the parachutes were attaining their respective terminal velocities. The technique proved successful for the disc-gap-band parachute, but it was finally decided to release the hemispherical parachute from an altitude of 300,000 feet, with a constant density atmosphere from 300,000 to 240,000 feet, so that the system would be at terminal velocity when entering the first wind layer at 240,000 feet.

At the conclusion of these computer runs, 50 data runs were performed in which each of the two parachutes was subjected to a total of 25 sawtooth wind fields from altitudes of 240,000 feet to 150,000 feet. The wind fields were selected so they would be identical with those used in a previous analog study of the hemispherical parachute.[3]

---

[3] Murrow, Harold N. and Barker, Lawrence E., Jr. "An Analytical Study of the Wind-Following Characteristics of a Parachute at High Altitudes," presented at Instrument Society of America Fall Conference, Sept. 11-15, 1961.

SECTION III
RESULTS

Figures 8 and 9 contain typical plots of the two components of parachute horizontal velocity vs. altitude and time, and of the wind-sensing error vs. altitude and time. In addition, wind and parachute descent velocity are included as functions of altitude, and, for the hemispherical parachute, spin rate is shown as a function of altitude and time. These two figures show, typically, what is contained within the data runs. Figure 10 is a summary of wind-sensing error vs. altitude for the two parachute systems in the wind field noted on the figure; the periodic nature of the hemispherical parachute behavior can be clearly seen from the figure.

Of particular interest is the response of the two parachute systems to wind shears and to changes in the wind-velocity/altitude gradient. Since each parachute is falling through a sawtooth wind field, the parachute velocity is at times less than, and at times greater than, the actual wind velocity. This effect can be seen clearly in Figure 11.

As the parachute falls through the altitude interval Δh, its horizontal velocity increases, with the ratio of parachute velocity to wind velocity also increasing. As long as the wind velocity is greater than that of the parachute, the parachute velocity will continue to increase. However, when the wind velocity has decreased to the point that it is equal to the parachute velocity, the parachute velocity also begins to decrease. At the lower altitudes it can be seen that the parachute velocity inflection points occur closer and closer to the wind velocity inflections, and that the parachute velocity appears to lag the wind velocity by some "steady-state" error.

This "steady-state" error is of interest, as it is a measure of the difference between parachute and wind velocities in a changing wind field. Also of interest is the altitude through which the parachute falls while attaining this "steady-state" condition.

Figure 12 is a plot of error vs. altitude for the disc-gap-band parachute in various wind fields.* The error can be seen to fall within an envelope boundary, and at the lower altitudes to define this boundary curve. If this error boundary is plotted vs. altitude as in Figure 13, a definite exponential character is at once noted.

Analysis of the response of a rigid, six-degree-of-freedom parachute model (Appendix A) has shown that the exponential nature of the error boundary observed during the computer studies is, in fact, due to the exponential character of the atmosphere. Appendix A shows that the error function E is of the form $E = (V_z^2/g)\ (dV_w/dh)$. This equation allows the response characteristics of parachutes to be compared. When the equation is rearranged in the form

$$\frac{E}{dV_w/dh} = \frac{V_z^2}{g} ,$$

it can be seen that, for the same wind field, any parachute will exhibit an error proportional to the square of its descent rate.

For the two systems studied, Figure 16 shows the function (V_z^2/g) taken from computer listings. The difference between the two parachutes is simply due to their different drag-to-weight ratios.

The theoretical "steady-state" error $(V_z^2/g)\ (dV_w/dh)$ may be compared to the computer-determined error E by plotting the function (V_z^2/g) against $\frac{E}{dV_w/dh}$.

If the correlation between theoretical error and computer-determined error were perfect, all points would fall on the straight line

$$\frac{E}{dV_w/dh} = \frac{V_z^2}{g} .$$

Two measures of the degree of correlation are (1) to determine the slope of the least-squares straight line giving the best fit to the data being compared; and (2) to determine the standard error of the correlation, defined by

*All of the early conclusions were drawn from the disc-gap-band data since they did not contain the periodicity associated with the oscillating hemispherical parachute.

$$S = \left\{ \frac{1}{n} \left[\frac{E}{dV_w/dh} - \frac{V_z^2}{g} \right]^2 \right\}^{\frac{1}{2}} ,$$

where S is the standard error of correlation and n is the number of points being compared.

Figures 14 and 15 are plots of $\frac{E}{dV_w/dh}$ versus $\frac{V_z^2}{g}$ for the two parachutes, and show how the computed points compare with the theoretically perfect straight-line correlation.

The calculated least-squares slope and standard errors are as follows:

	Fig. 14 Disc-Gap-Band	Fig. 15 Hemispherical
Least-Squares Slope	1.00777	0.94938
Standard Error	47 ft.	161 ft.

The comparatively poorer correlation for the hemispherical parachute is apparently due to point scatter from the data reduction technique described in Appendix B.

Appendix A also shows the altitude interval, from a wind-velocity inflection point, through which the parachute falls in attaining a velocity $V_x = V_w \pm (V_z^2/g)(dV_w/dh)$, or in reaching the "steady-state" error condition, which is approximately equal to $\Delta h = 3V_z^2/g$. A plot of this function is shown in Figure 16 for the two parachutes.

The excellent results achieved on the disc-gap-band parachute prompted an effort to reduce equivalent data from the oscillating hemispherical parachute listings. Determination of the "mean steady-state" error for this parachute was hampered by the fact that the parachute velocity was oscillating about some mean value. Plots of position and velocity similar to Figure 8 showed that the parachute motion consisted of

a helix superimposed upon a velocity-altitude characteristic similar in nature to that for the disc-gap-band. Arithmetic averaging of parachute position vs. time, and attendant mean velocity and error determinations, proved of little value.

The technique described in Appendix B was arrived at as a method of determining "mean steady-state" error over altitude increments small enough that the data proved valid.

While developing this technique, it was discovered that plots of the hemispherical parachute's fall rate vs. altitude did not exhibit the characteristic of constant dynamic pressure usually associated with subsonic descent at terminal velocity. This effect can be seen clearly in Figure 5, which compares parachute fall rate from the computer listings to a constant dynamic pressure curve corresponding to the same fall rate at 150,000 feet. When this effect was discovered, computer runs on a nonspinning (and therefore nonoscillating) parachute were performed to see if the apparent variation in parachute effective drag coefficient was caused by the oscillation. Figure 6 shows the results of this comparison. The nonspinning parachute does indeed fall with a constant dynamic pressure!

Some mechanism, as yet unexplained, associated with the coning parachute brings about an increase in effective drag coefficient as the parachute descends.

Figure 7 shows the ratio of effective drag coefficient at any altitude to that at 150,000 feet. Also included on this figure is a similar curve used in previous analog studies of parachute behavior.[4]

---

[4] Murrow and Barker, loc. cit.

SECTION IV

RECOMMENDATIONS

1. Since wind-sensing error is proportional to wind gradient (dV_w/dz) and to the square of parachute descent velocity (V_z^2), the most fruitful area for accuracy improvement would seem to be a reduction of parachute descent rate.

2. As a consequence of instability, parachutes which exhibit an oscillating motion are contributing an additional error component to measured winds because of the motion of their centers of gravity. This error component should be eliminated by making all future wind measurements with a stable parachute system such as the disc-gap-band. Such a parachute would exhibit a much more favorable"signal-to-noise" ratio than the unstable impervious hemisphere.

3. Further, improvements in data reduction should take into account both wind gradient and altitude increment through which the parachute falls in attaining the "steady-state" error.

4. Finally, further research is needed on both the immediate practical problem of reducing the effects of parachute motions on fine-scale wind data, and in understanding the physical mechanisms producing both coning and change in effective drag coefficient.

NOTE

For definitions of notation used in Figures 8 and 9, pp. 20-103, see Appendix C, paragraphs 3, 4, and 5.

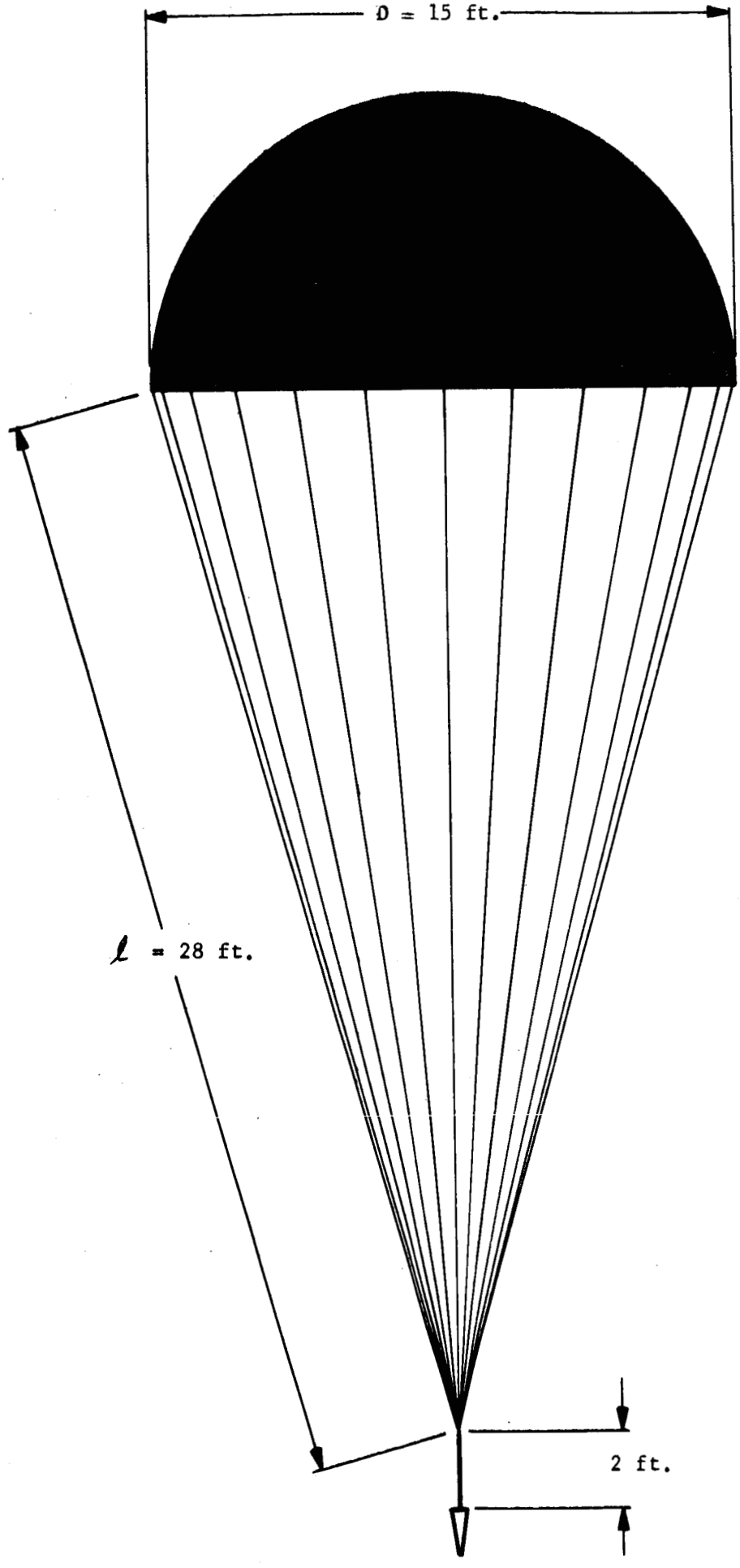

Figure 1a. Hemispherical Parachute

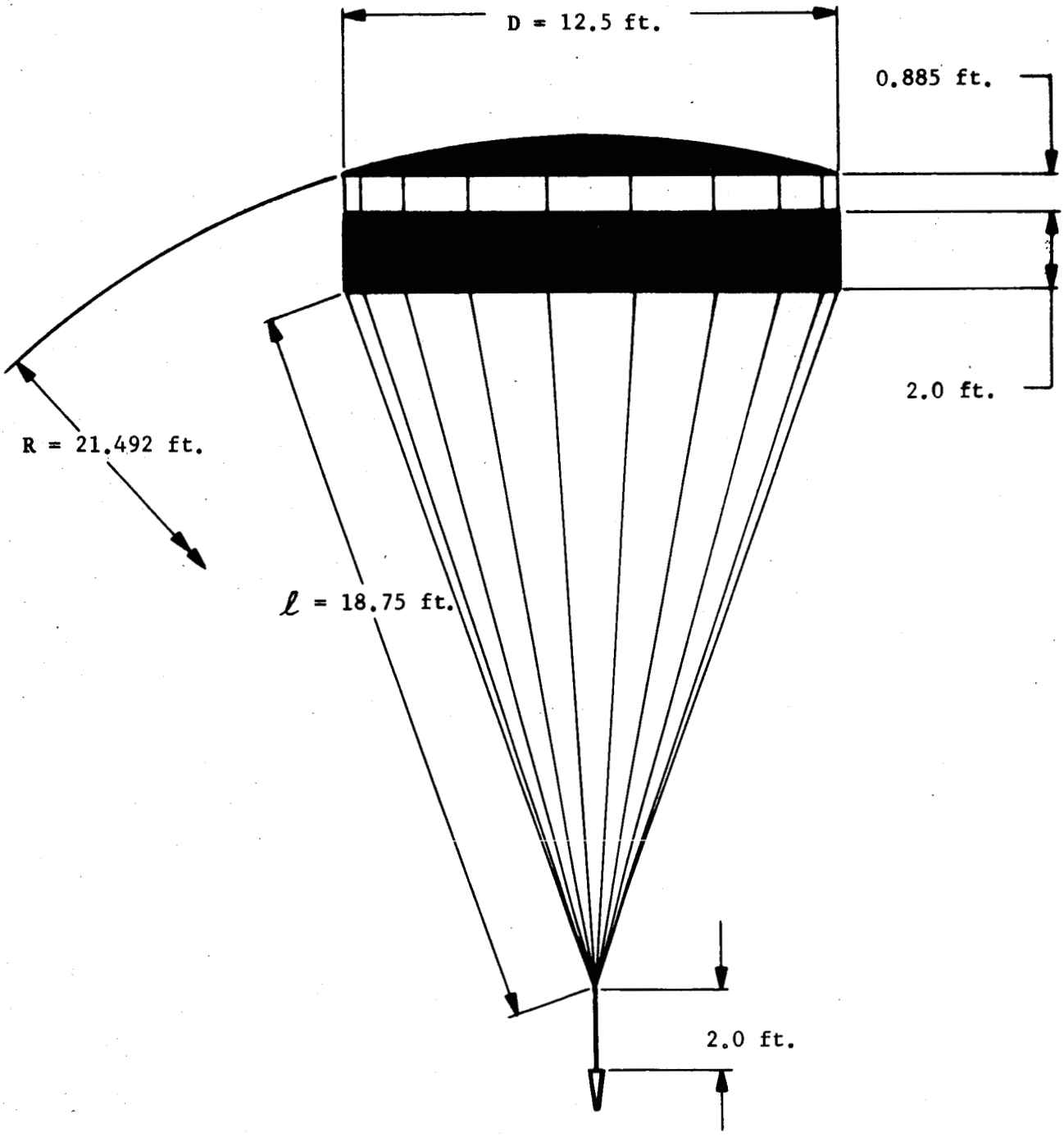

Figure 1b. Disc-Gap-Band Parachute

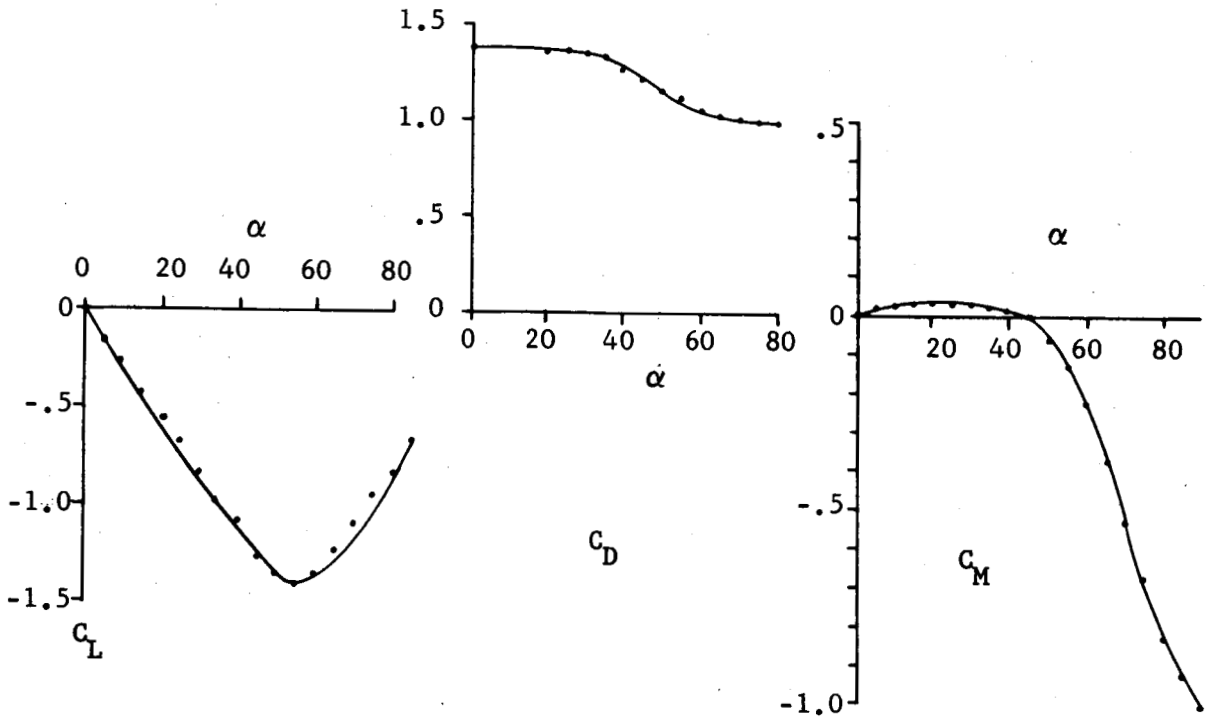

Procedure for converting C_N and C_T to C_L and C_D:

$$C_N = C_D \sin \alpha + C_L \cos \alpha$$

$$C_T = C_D \cos \alpha - C_L \sin \alpha$$

Figure 2a. Aerodynamic Coefficients for Hemispherical Parachute*

* Sources: (a) Hoerner, S.F., Fluid Dynamic Drag, published by author, 1958, pp 13-24. (b) Heinrich, H.G., "Drag and Stability of Parachutes," Aeronautical Engineering Review, June 1956.

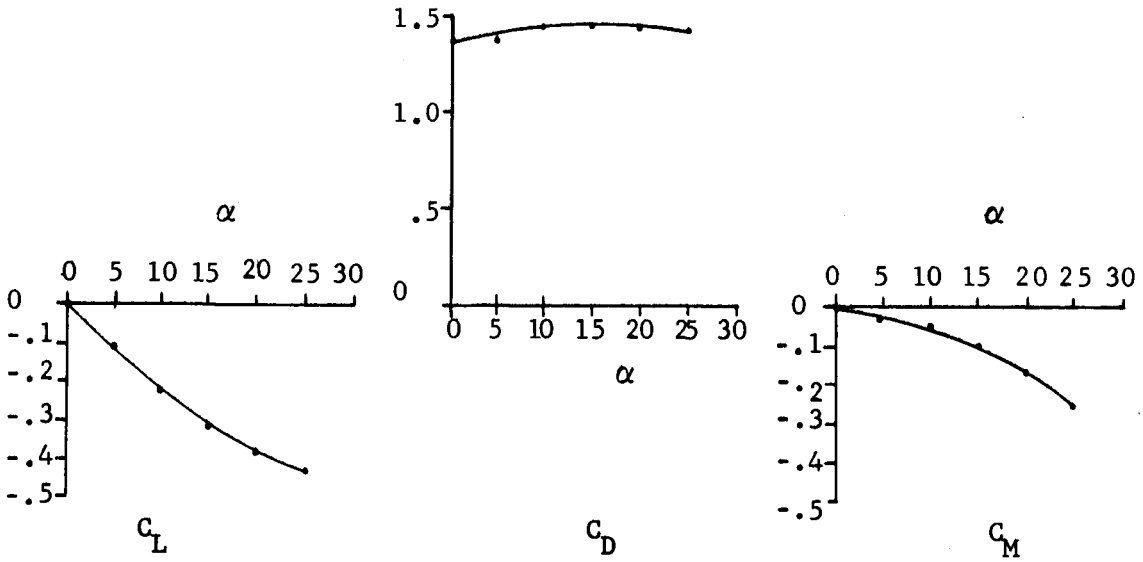

Procedure for converting C_N and C_T to C_L and C_D:

$$C_N = C_D \sin \alpha + C_L \cos \alpha$$

$$C_T = C_D \cos \alpha - C_L \sin \alpha$$

Figure 2b. Aerodynamic Coefficients for Disc-Gap-Band Parachute*

* Source: Heinrich, H.G., Haak, E.L., and Niccum, R.J., "High Altitude Disc-Gap-Band Parachute," report published by Department of Aeronautics and Engineering Mechanics, University of Minnesota, under sponsorship of G.T. Schjeldahl Co.

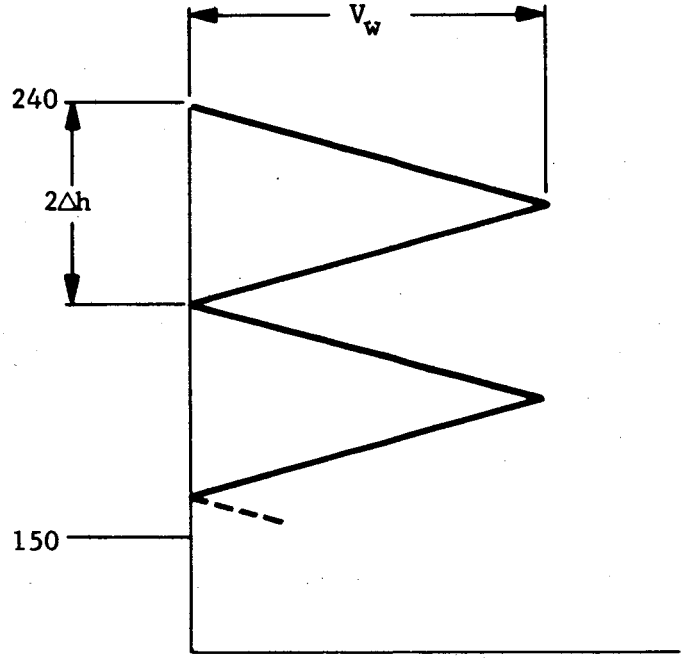

Figure 3. Typical Wind Profile as a Function of Altitude

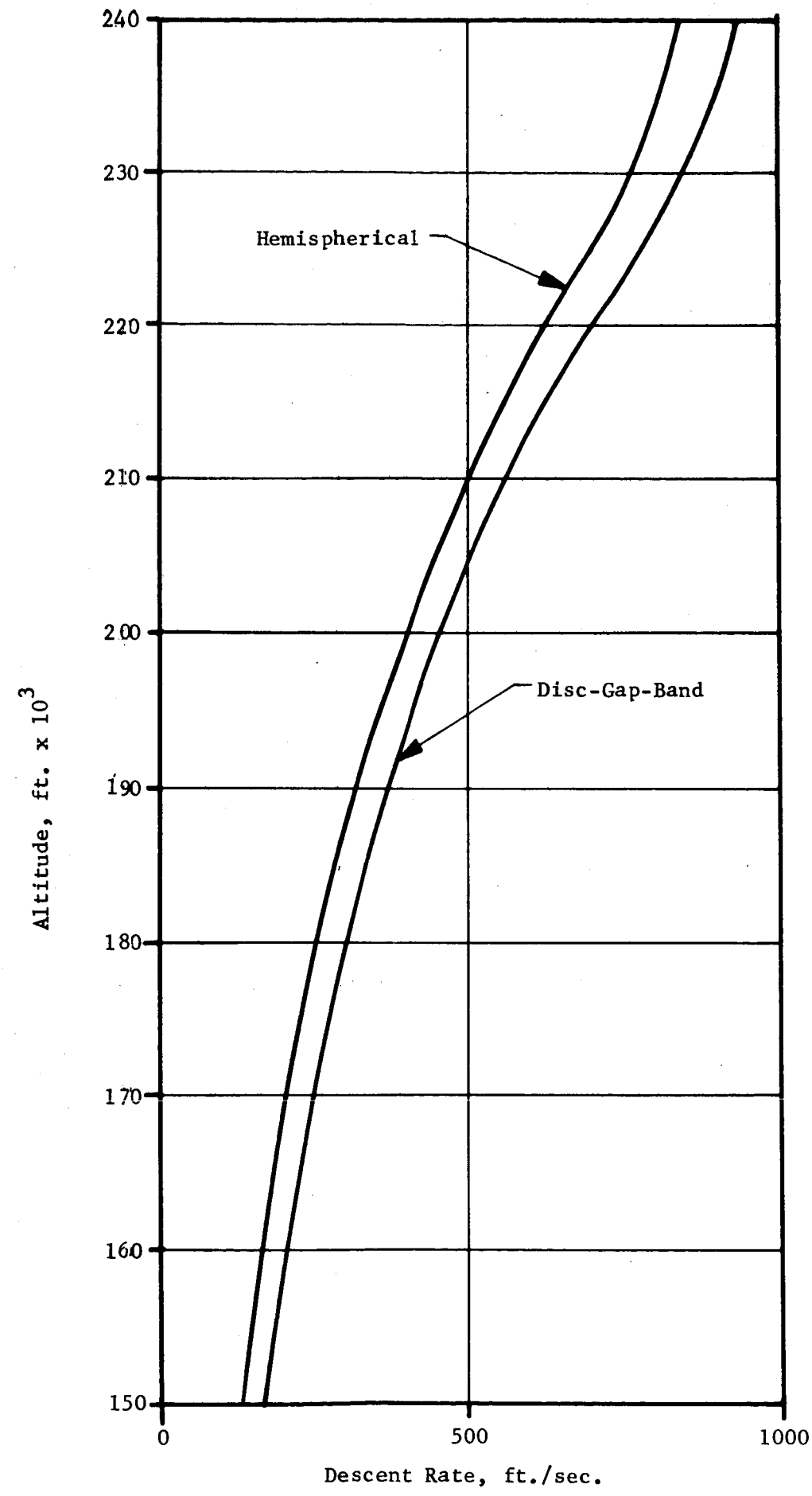

Figure 4. Comparison of Parachute Descent Rates vs. Altitude

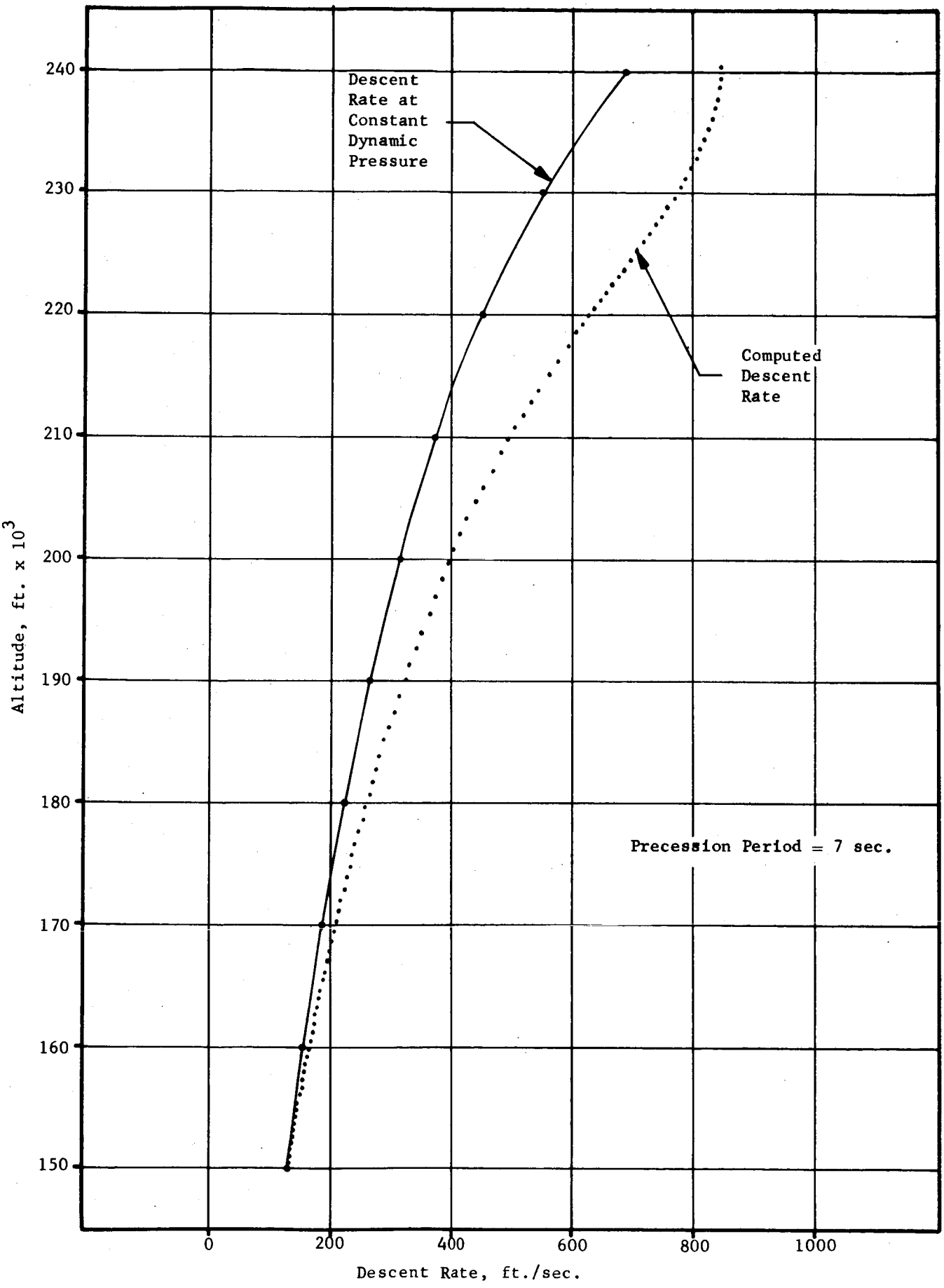

Figure 5. Descent Rate vs. Altitude for Hemispherical Parachute

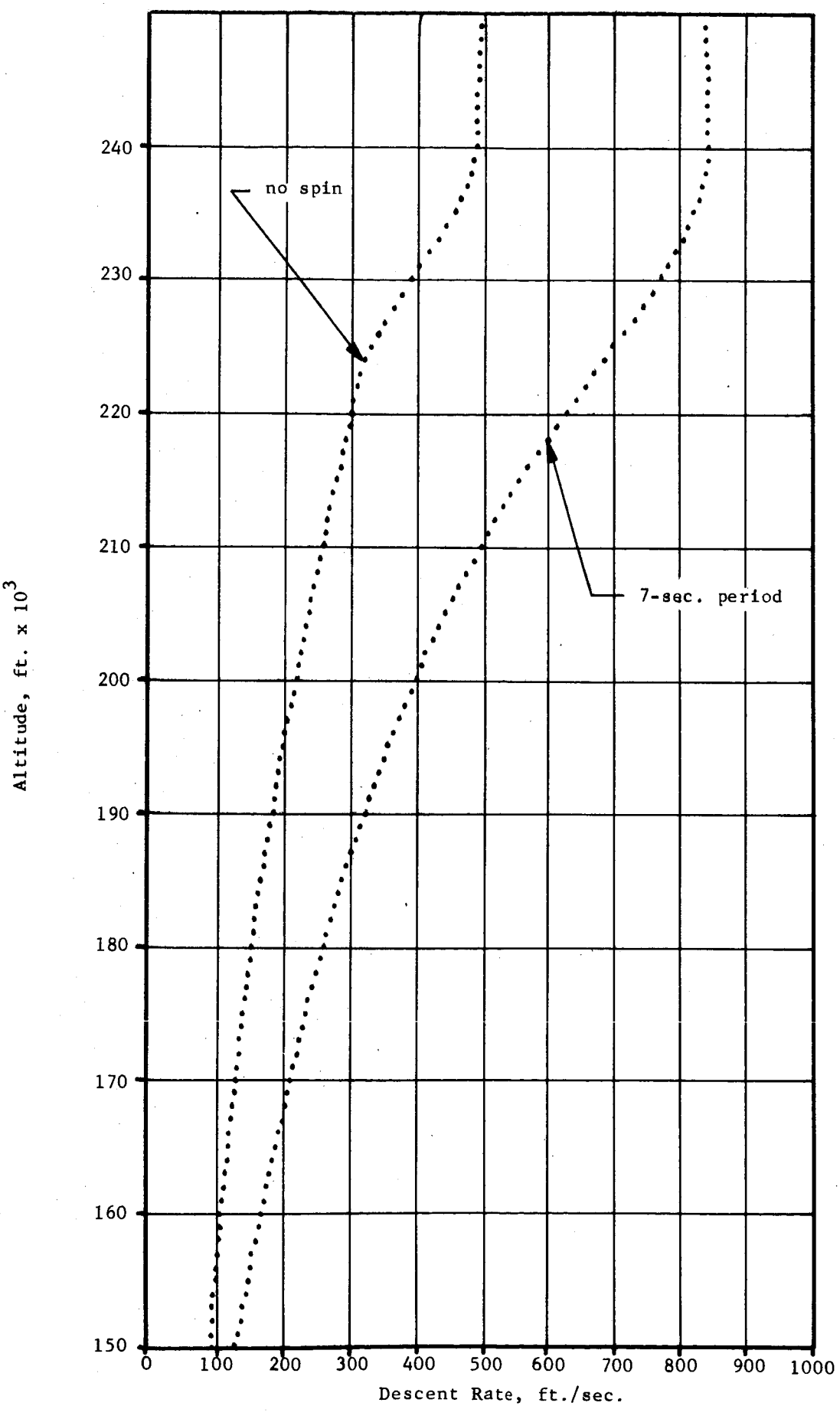

Figure 6. Descent Rate vs. Altitude for Coning and Nonconing Hemispherical Parachute

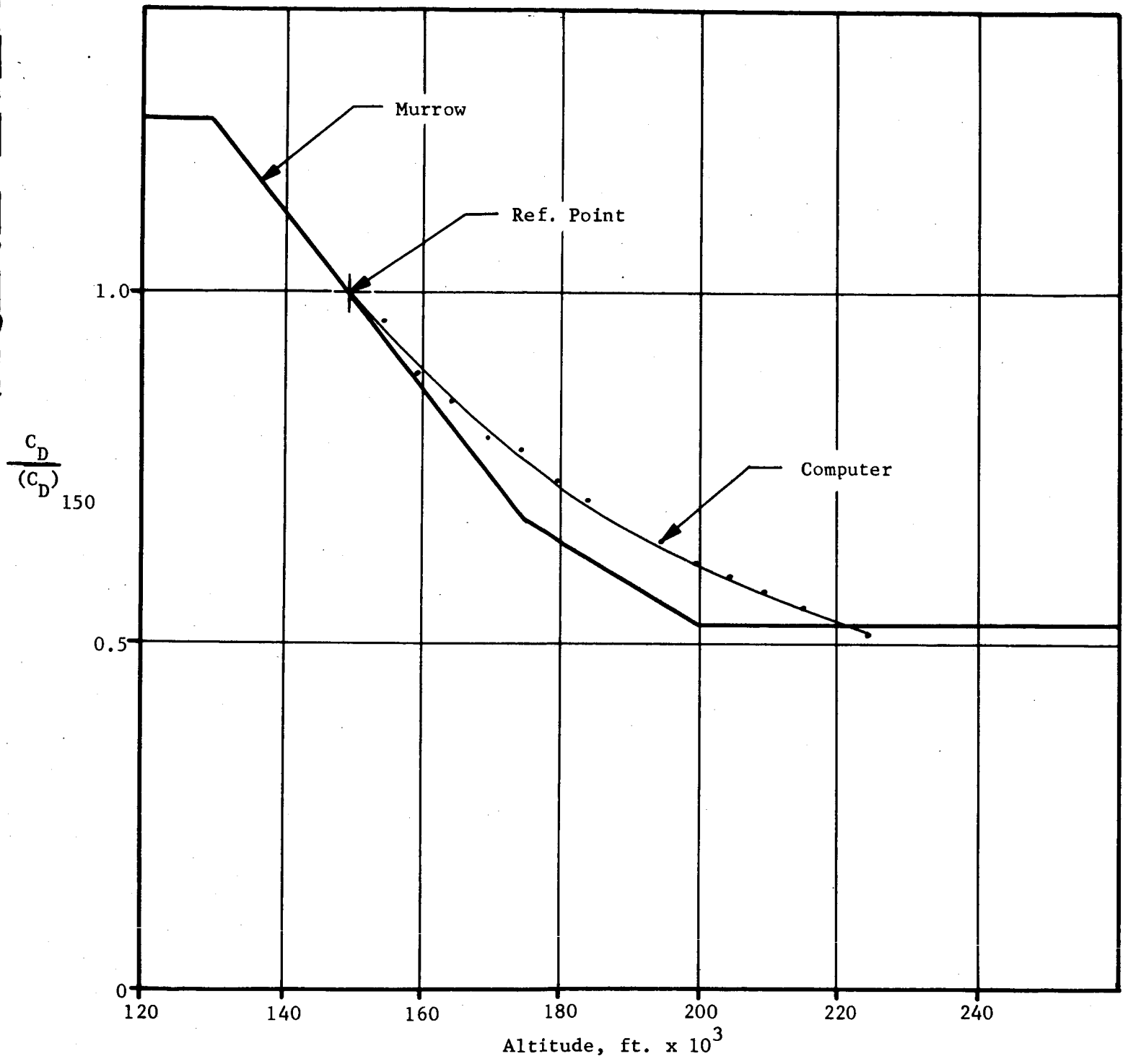

Figure 7. Oscillating Hemispherical Parachute Drag Coefficient vs. Altitude

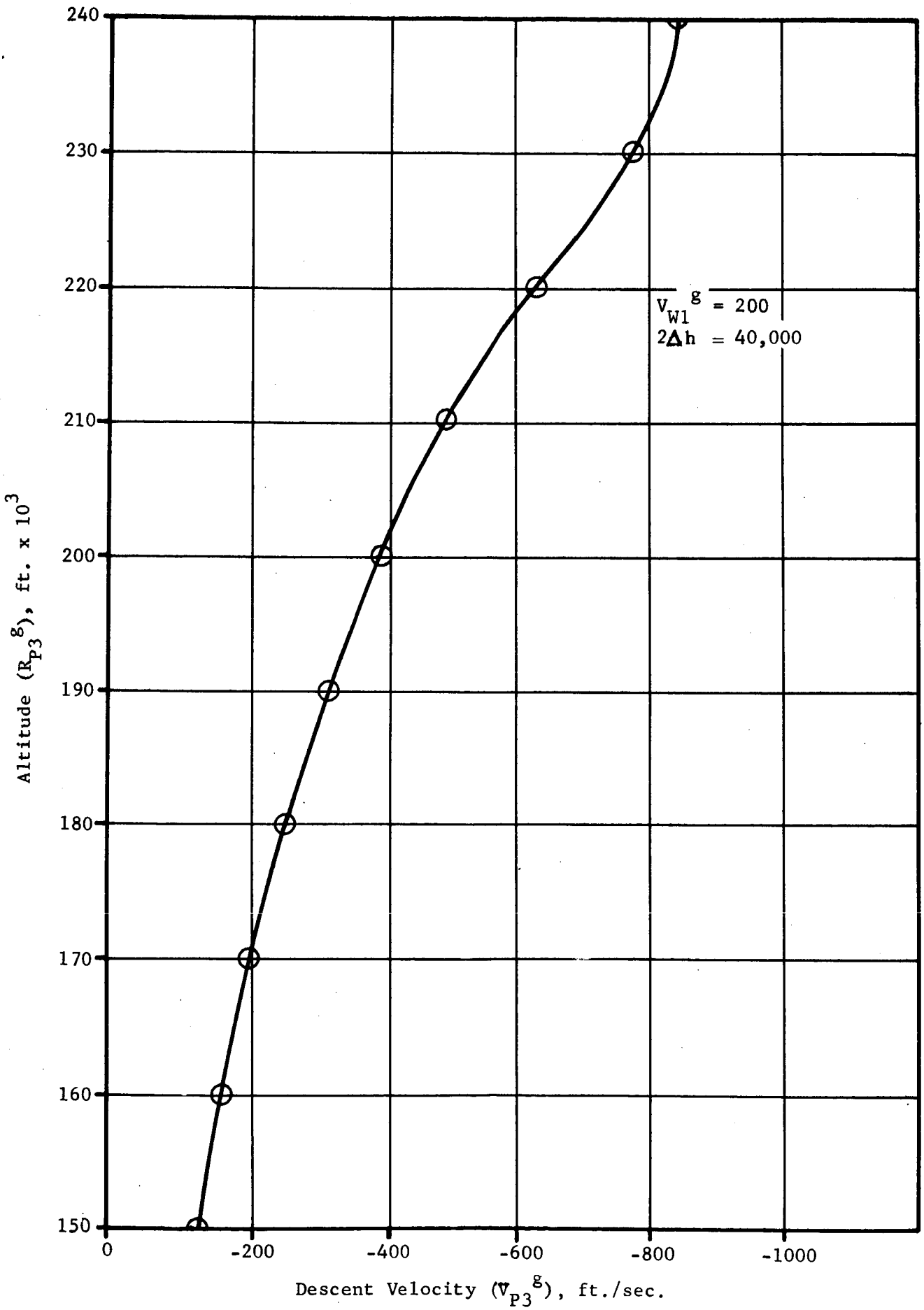

Figure 8a. Descent Velocity vs. Altitude for Hemispherical Parachute

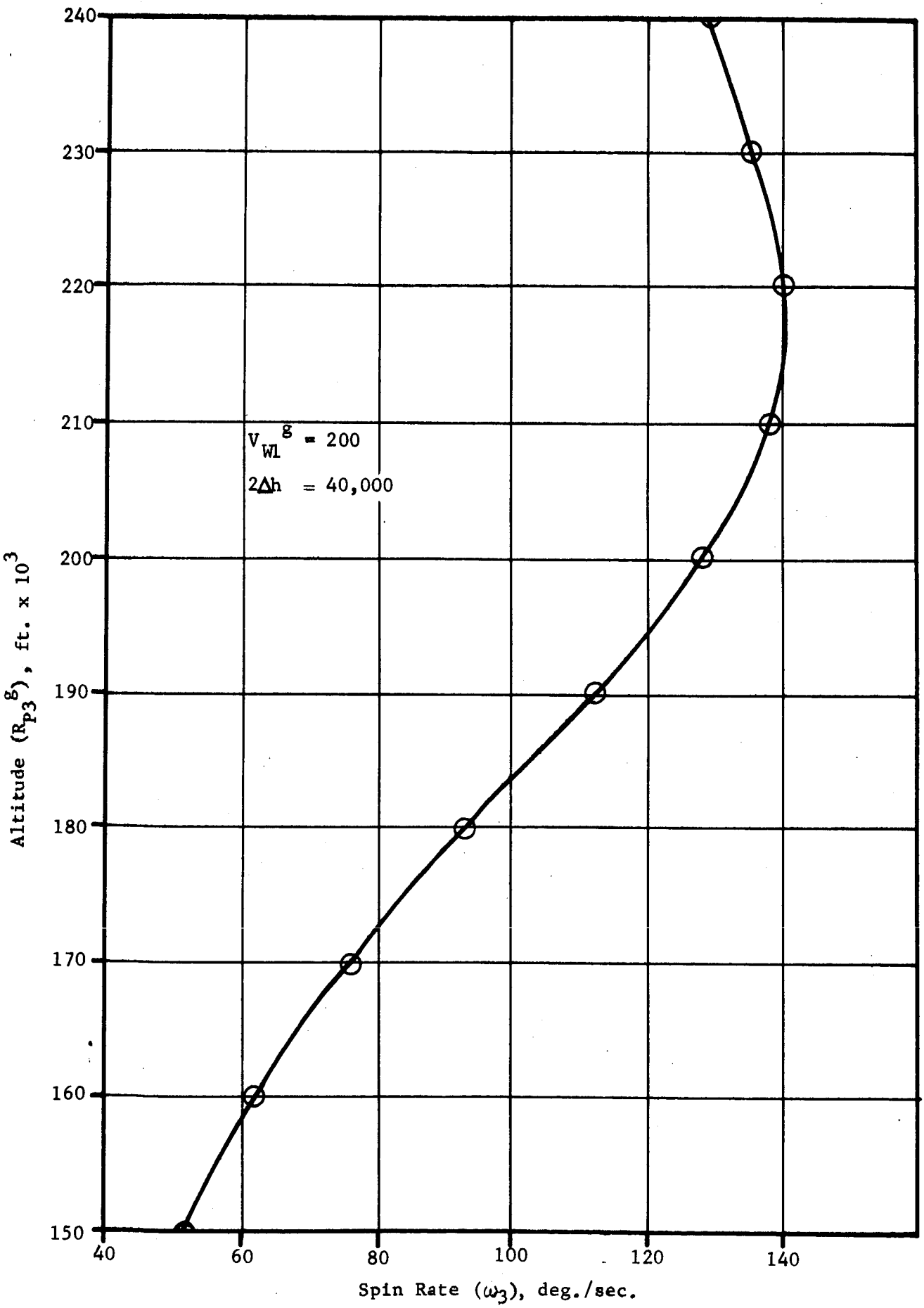

Figure 8b. Spin Rate vs. Altitude for Hemispherical Parachute

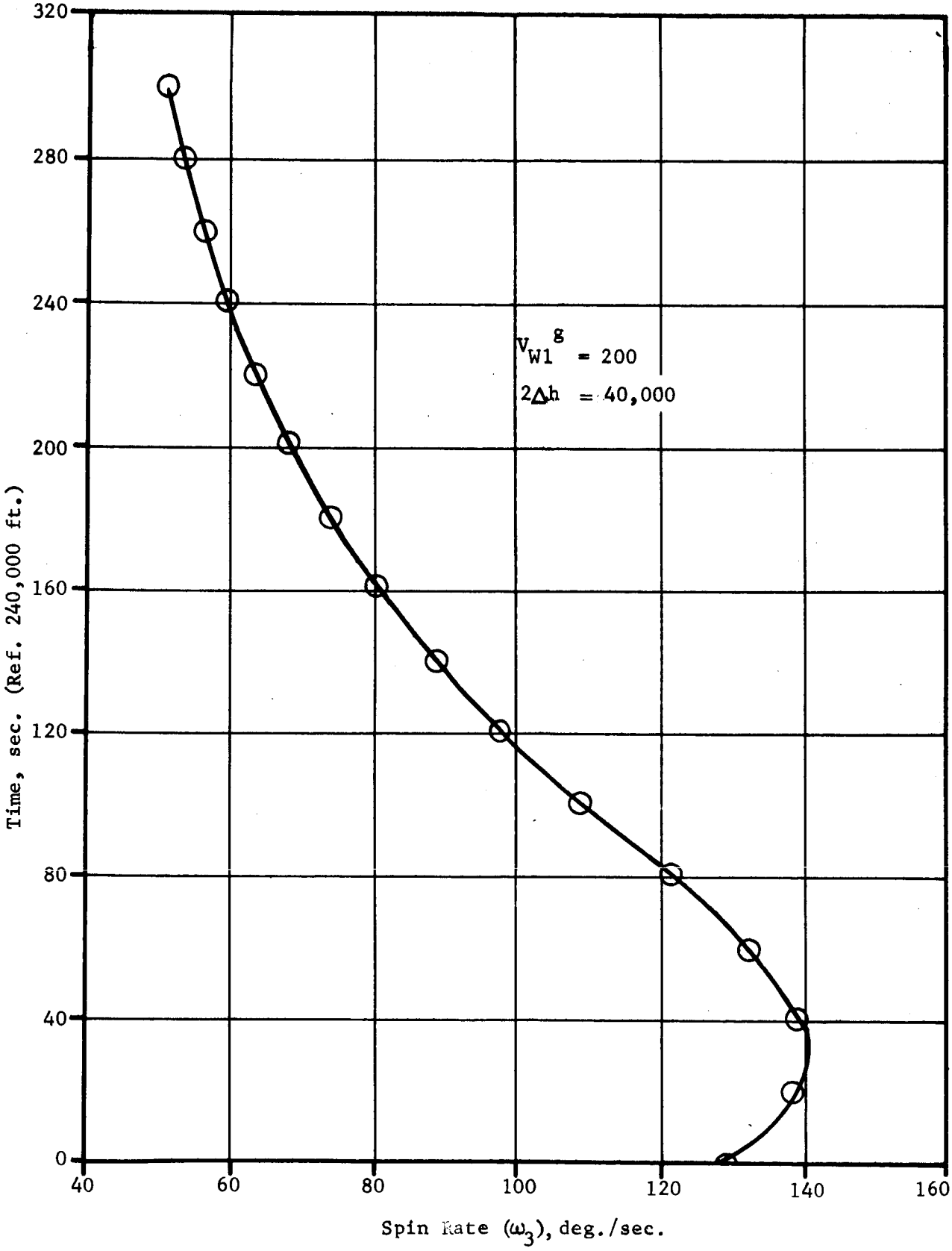

Figure 8c. Spin Rate vs. Time for Hemispherical Parachute

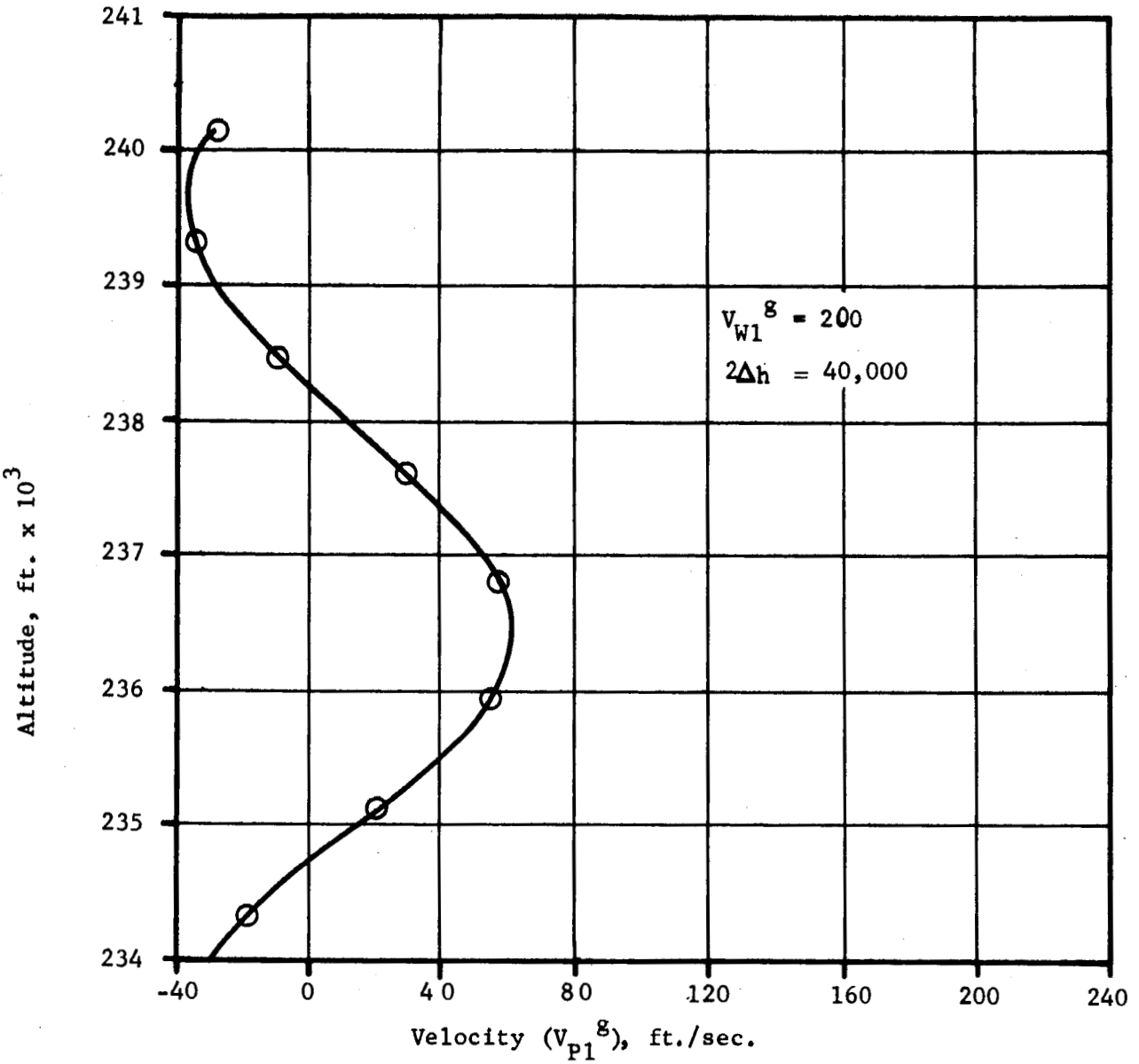

Figure 8d. Velocity vs. Altitude for Hemispherical Parachute

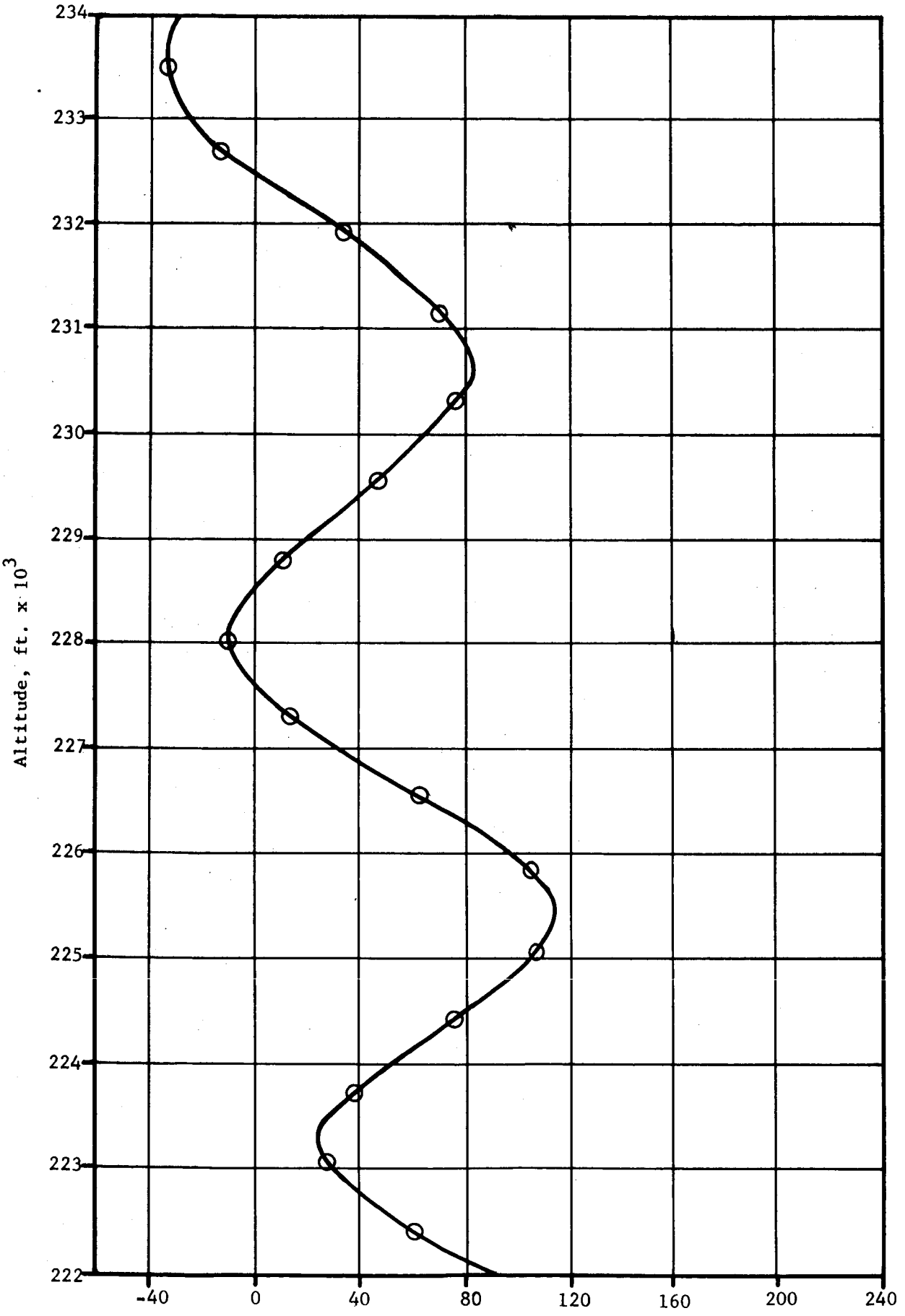

Figure 8d. (Page 2 of 8)

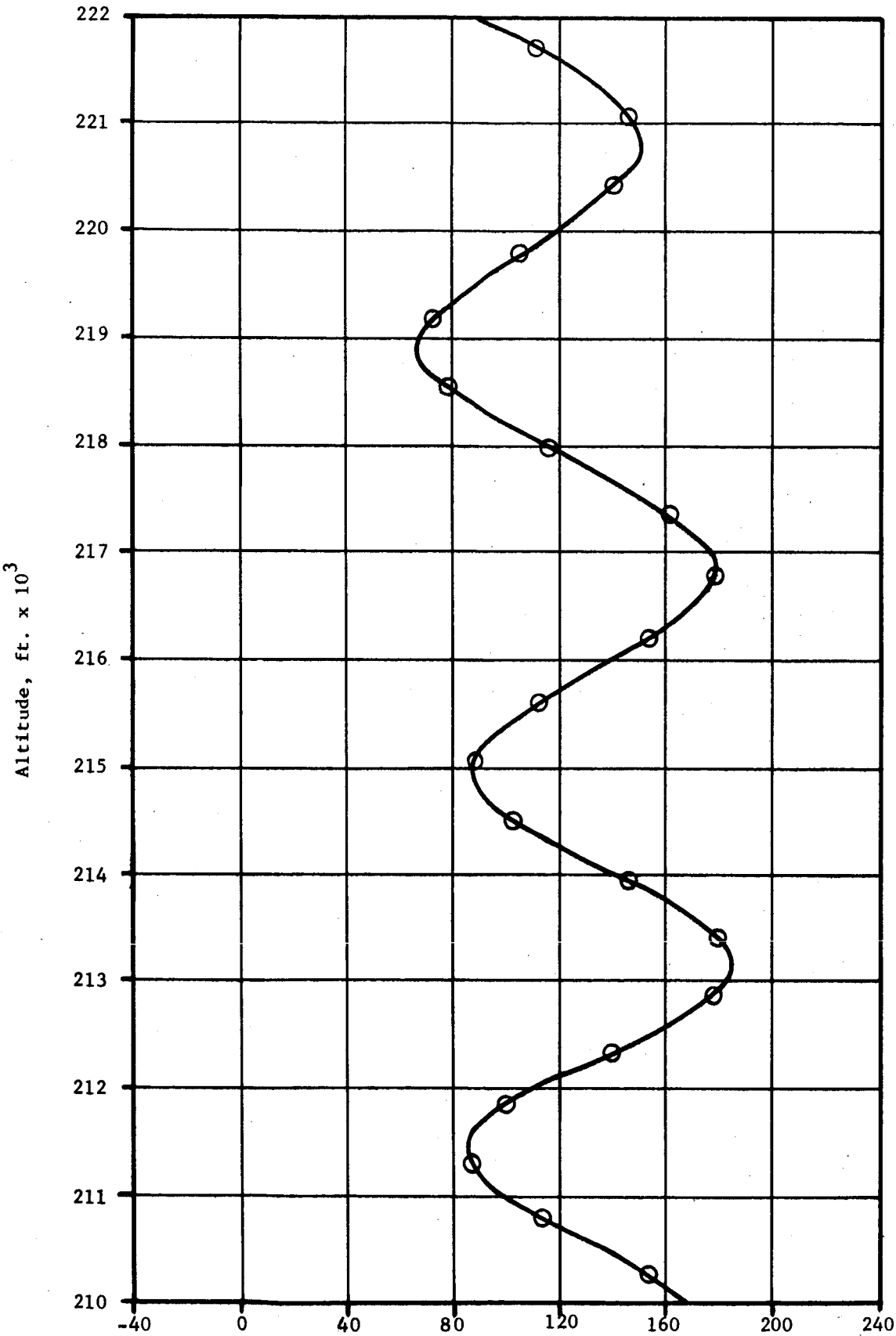

Figure 8d. (Page 3 of 8)

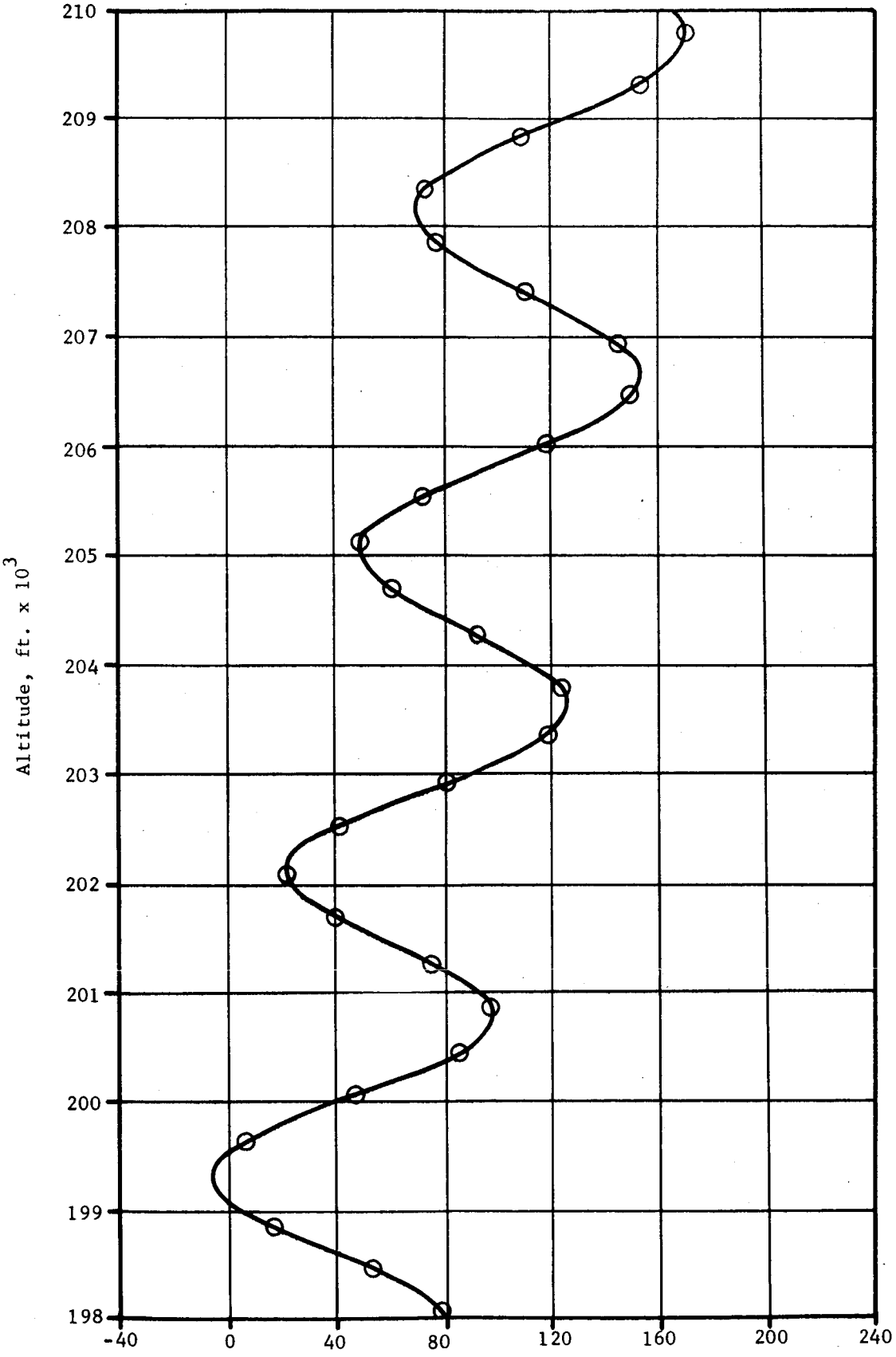

Figure 8d. (Page 4 of 8)

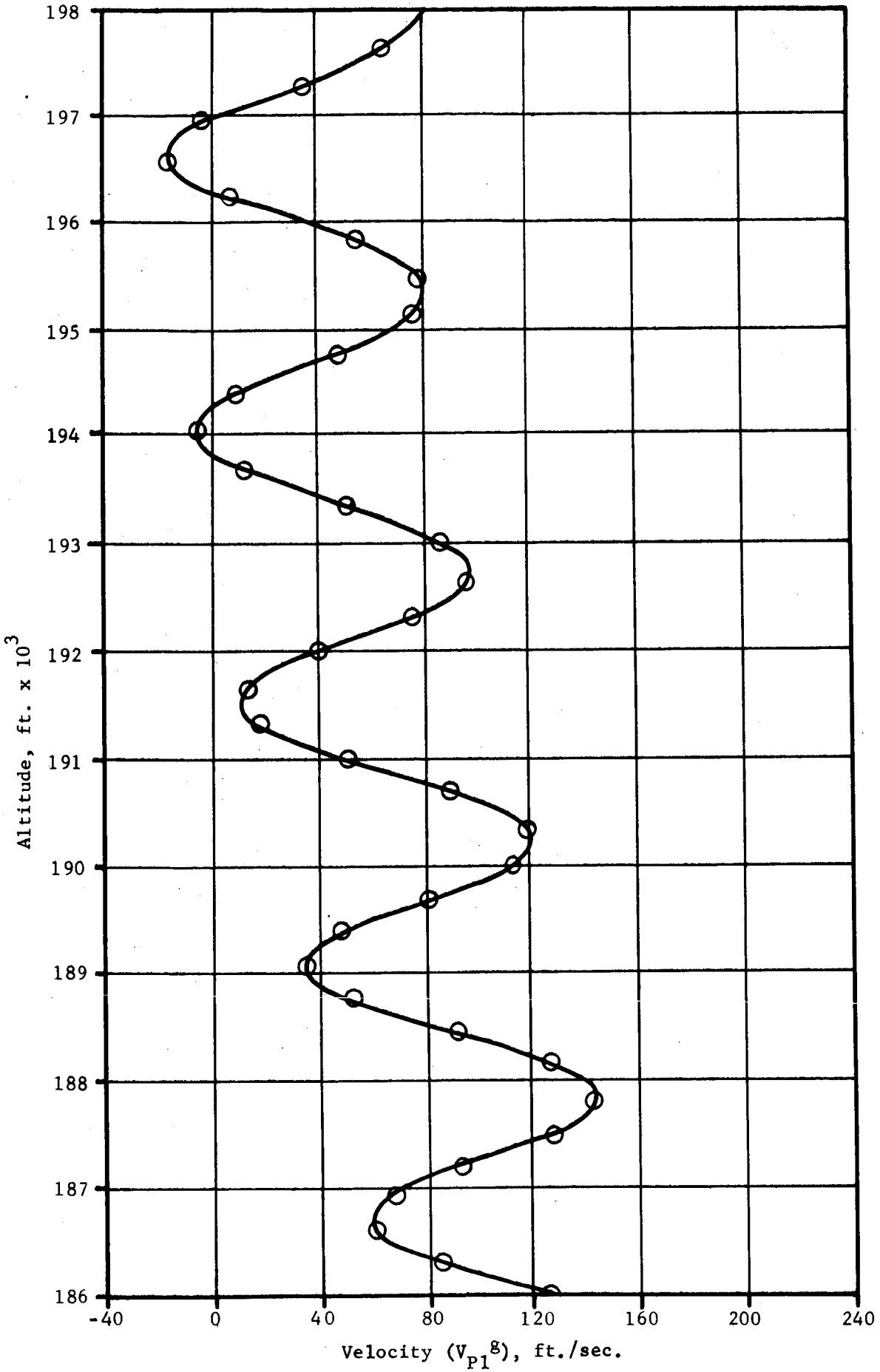

Figure 8d. (Page 5 of 8)

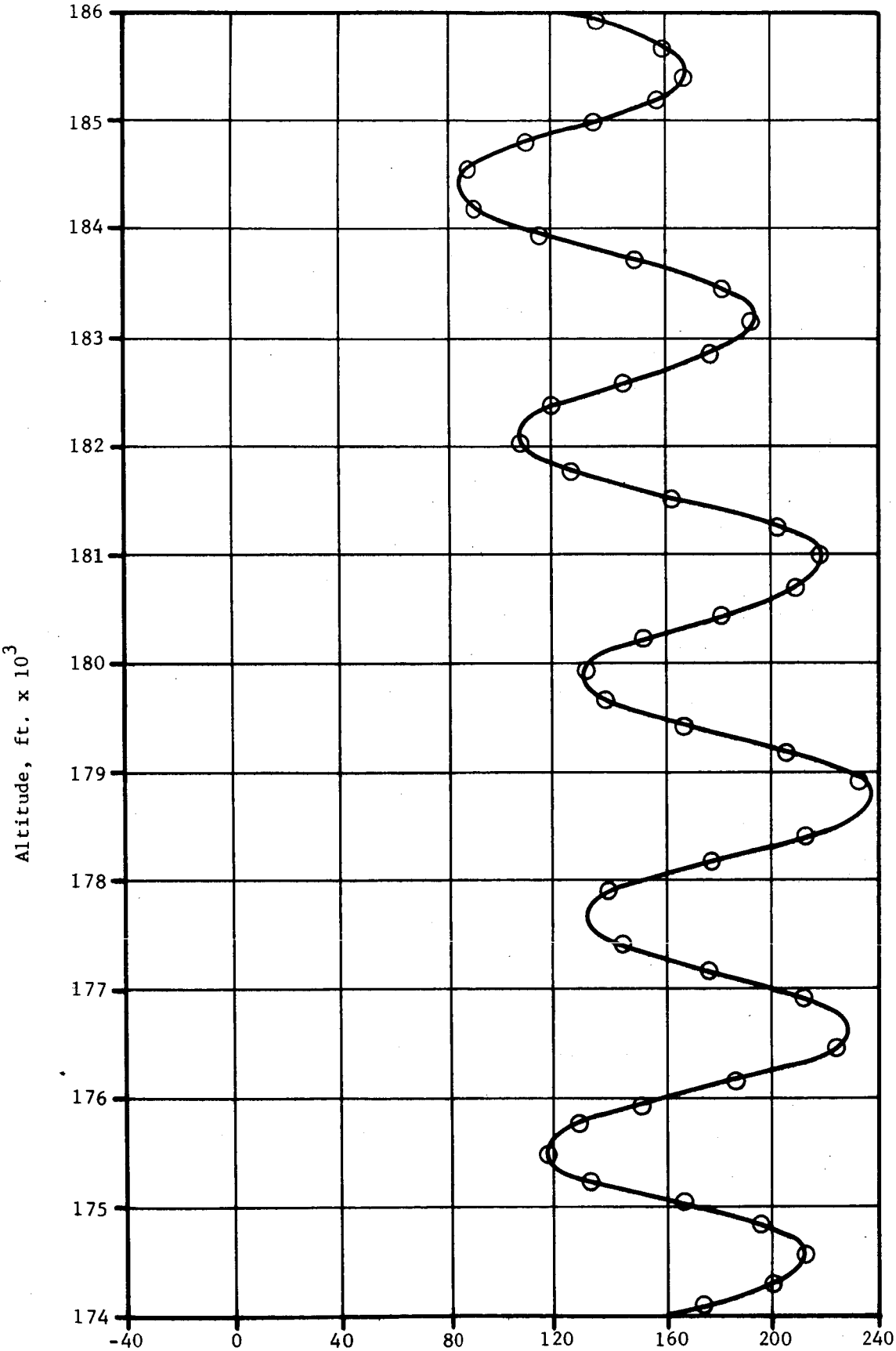

Figure 8d. (Page 6 of 8)

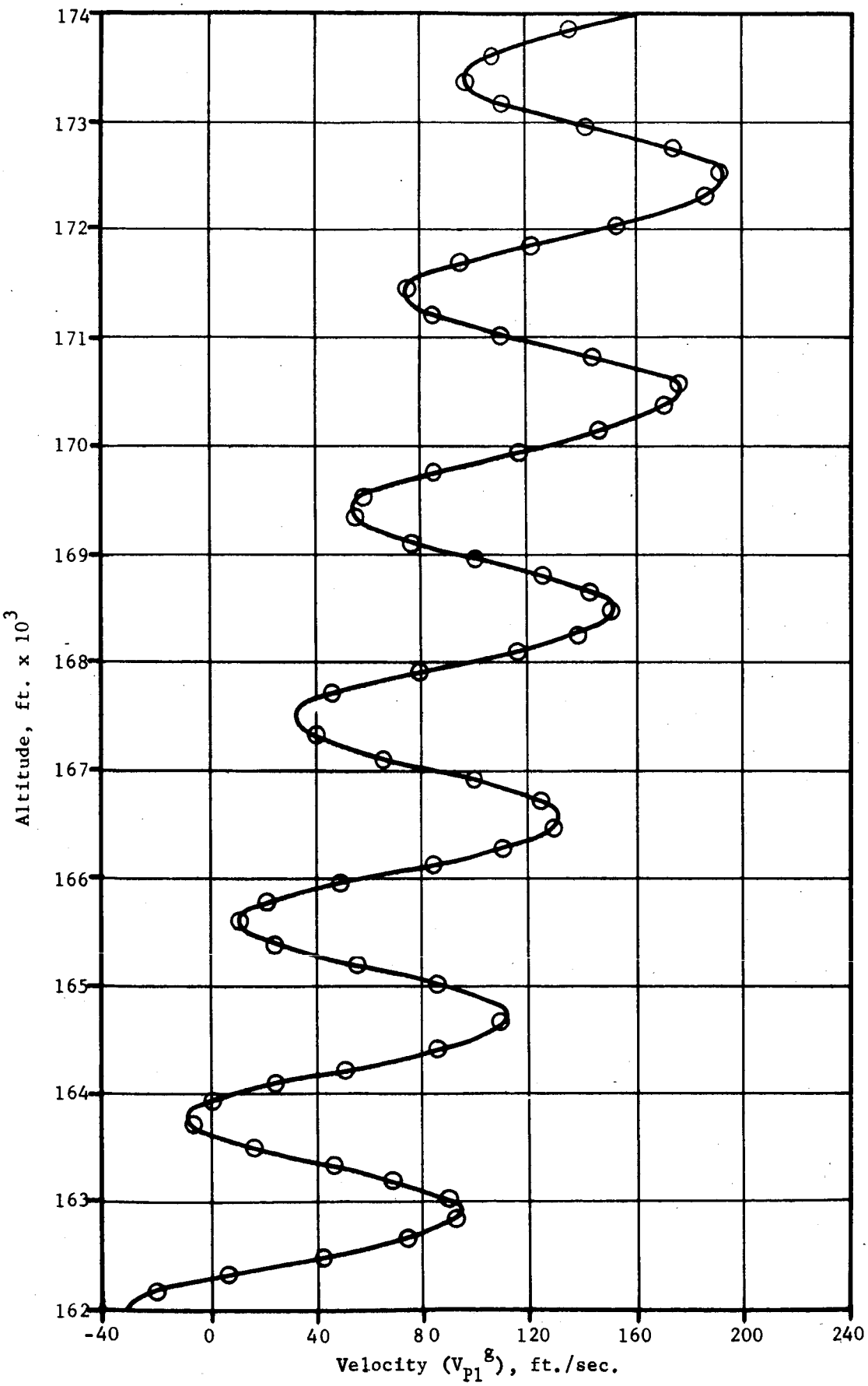

Figure 8d. (Page 7 of 8)

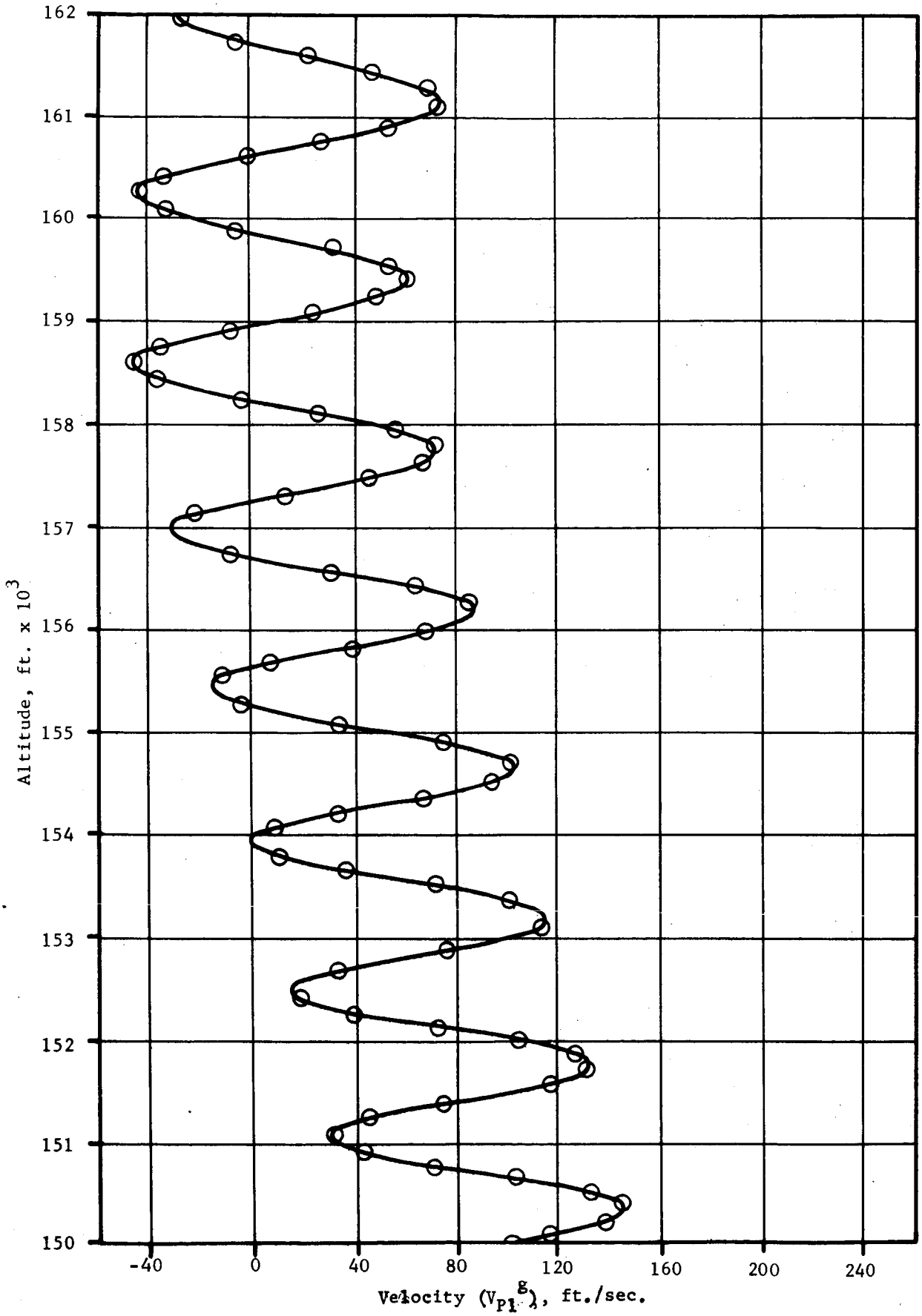

Figure 8d. (Page 8 of 8)

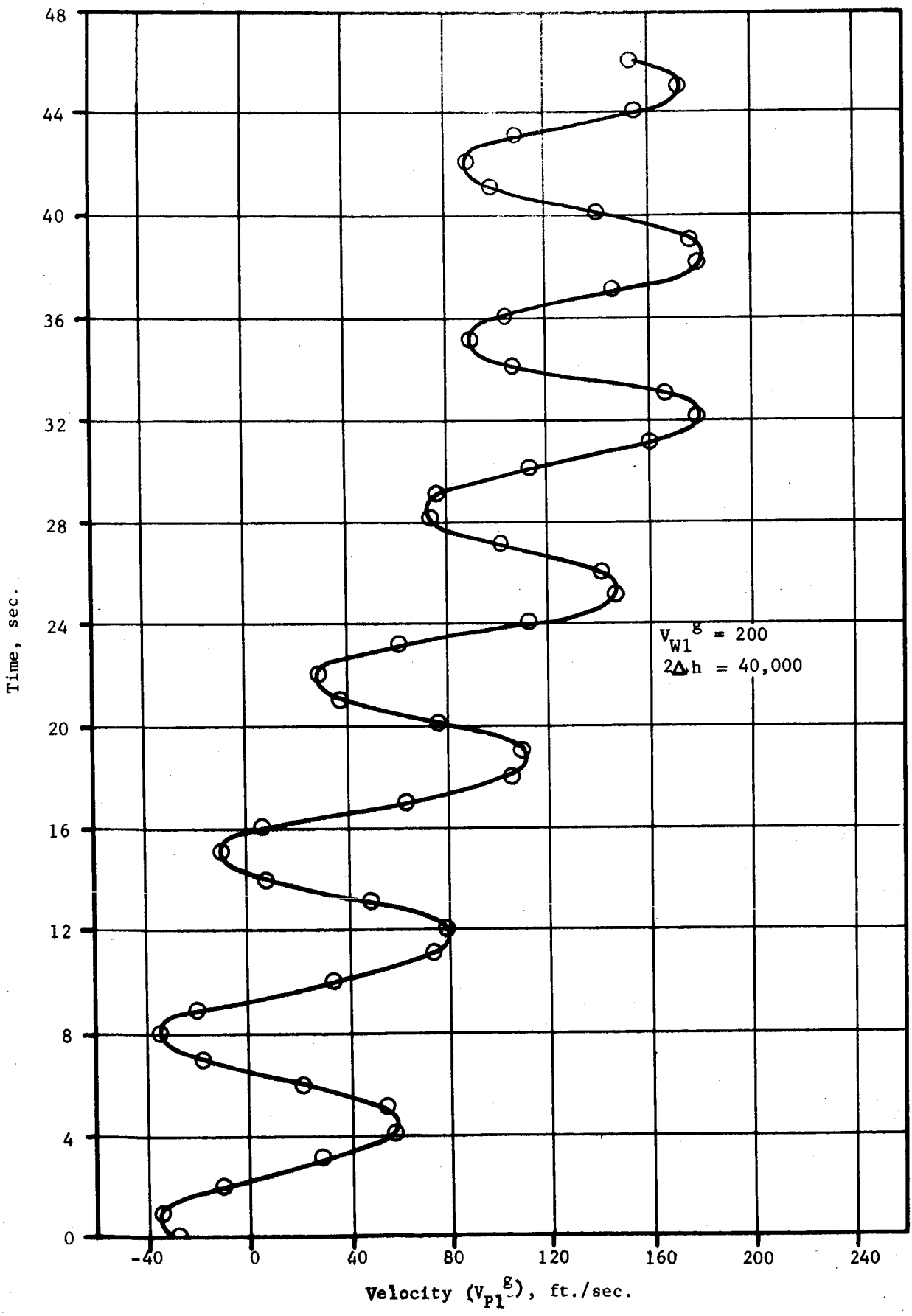

Figure 8e. Velocity vs. Time for Hemispherical Parachute

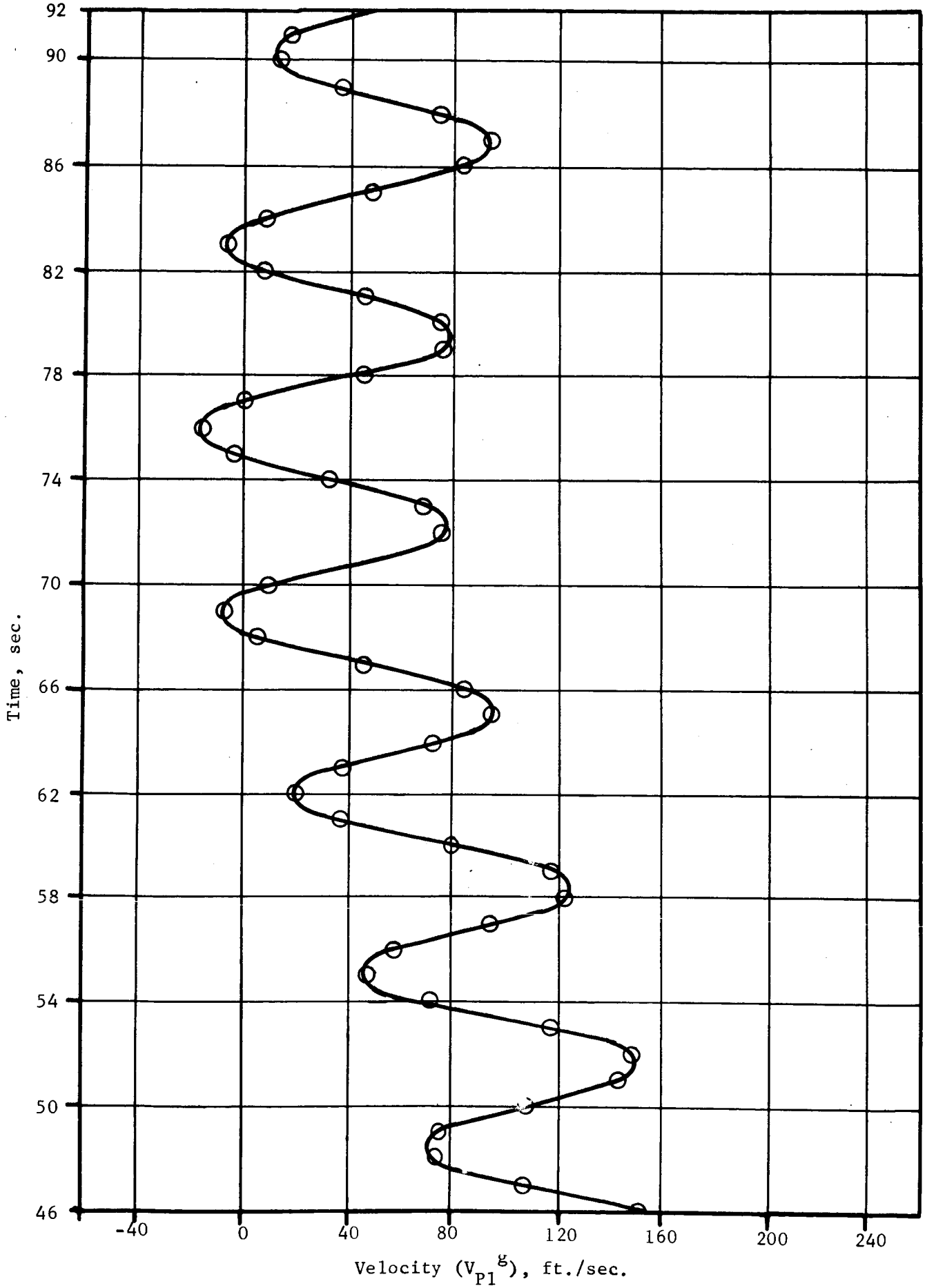

Figure 8e. (Page 2 of 7)

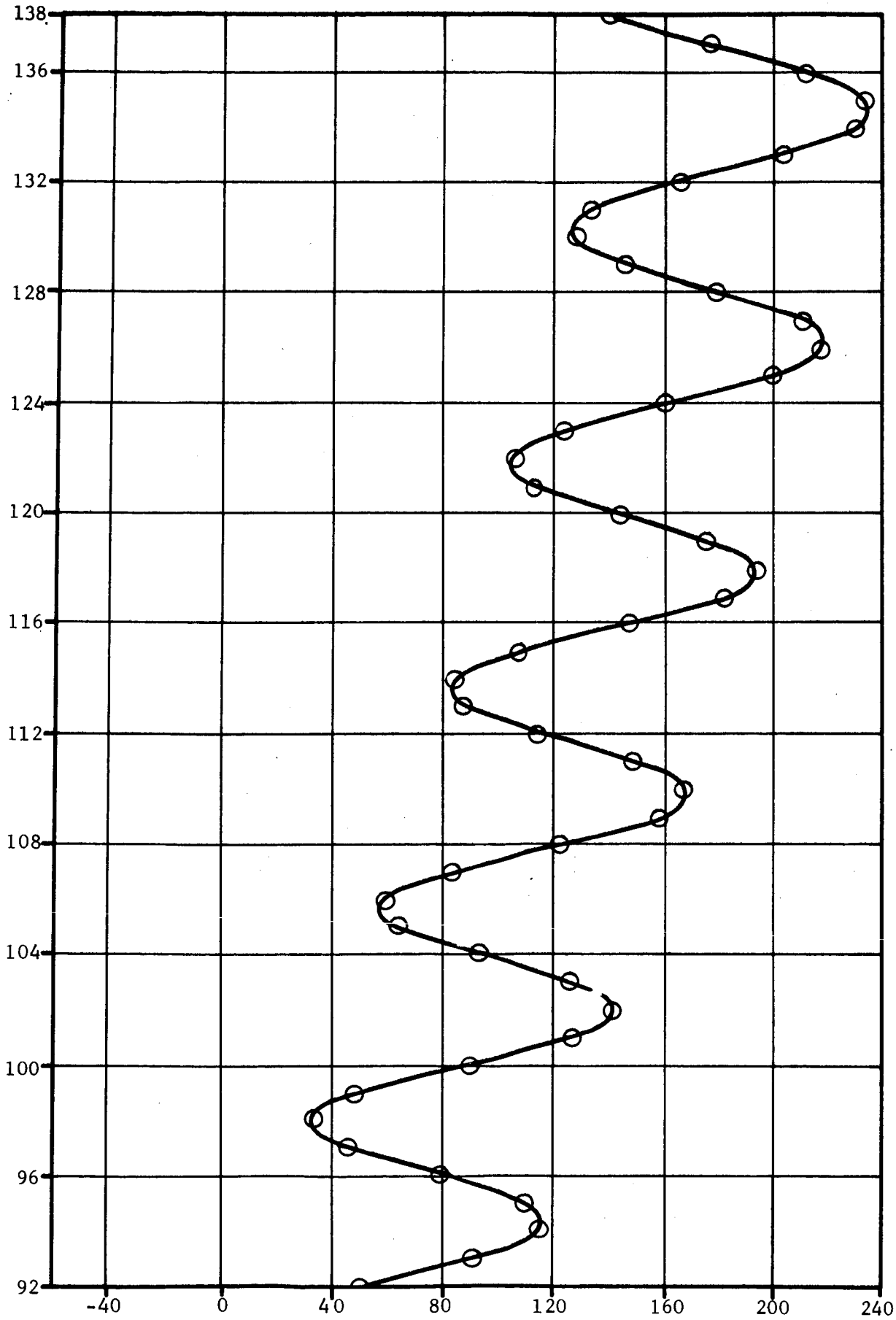

Figure 8e. (Page 3 of 7)

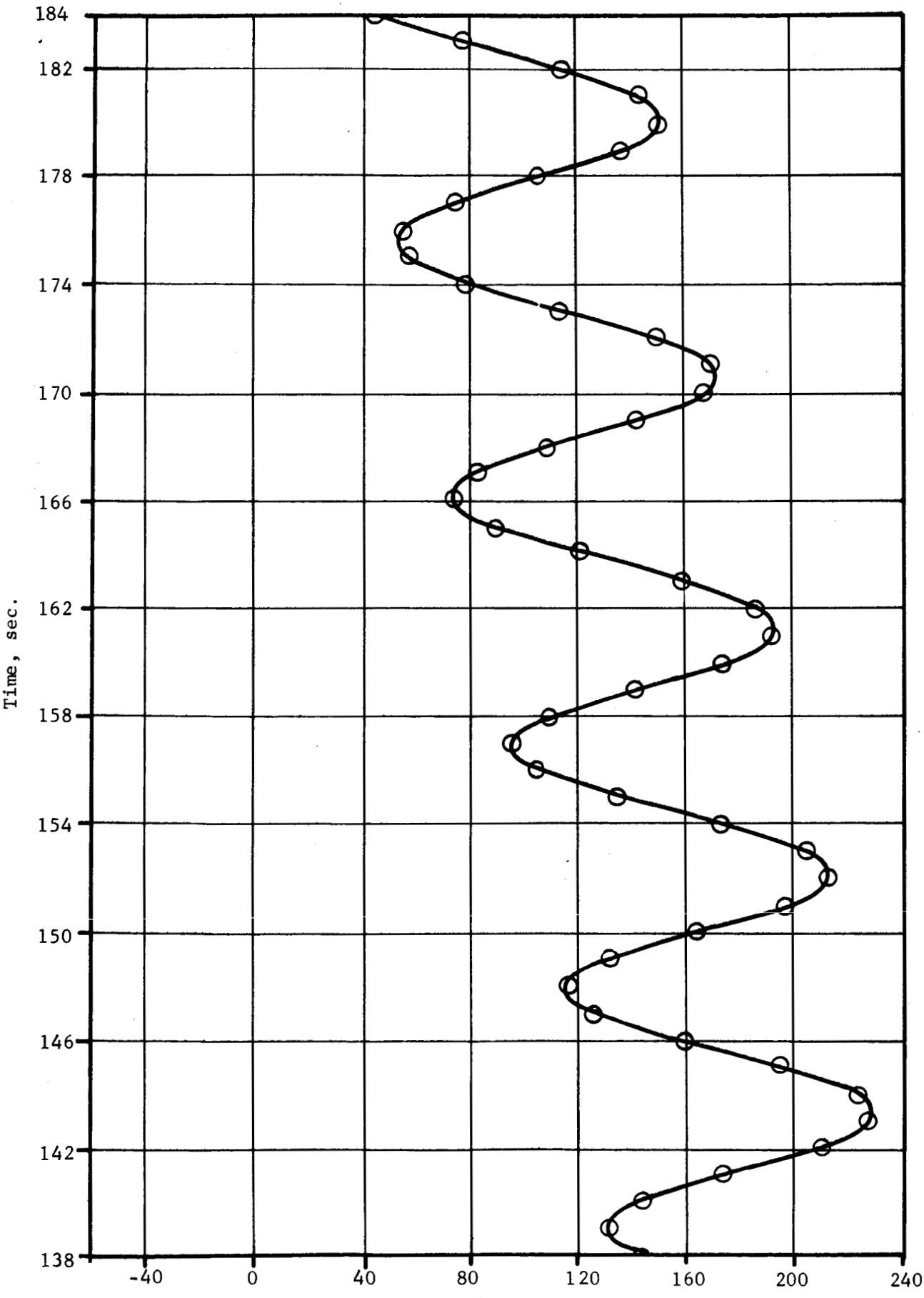

Figure 8e. (Page 4 of 7)

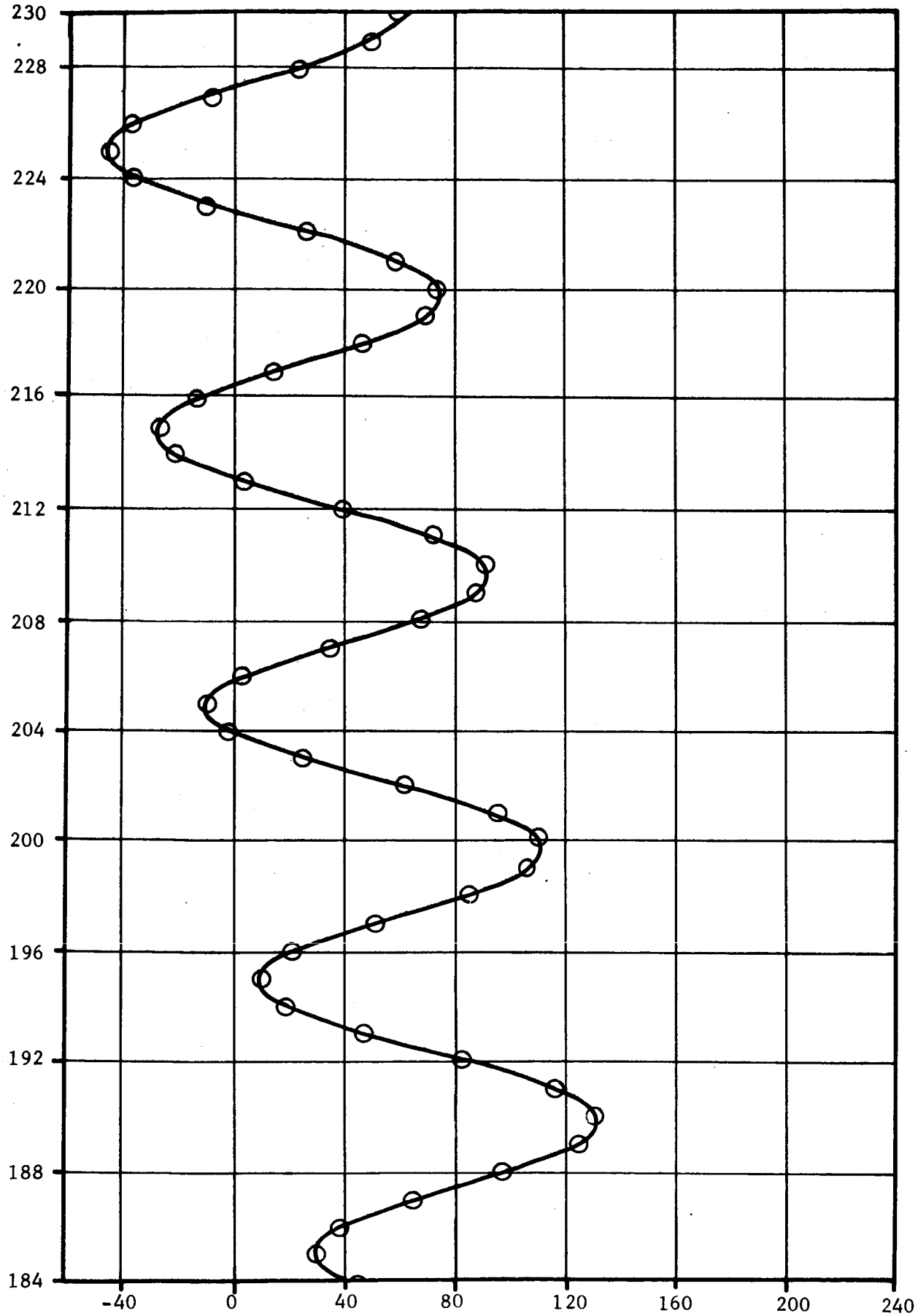

Figure 8e. (Page 5 of 7)

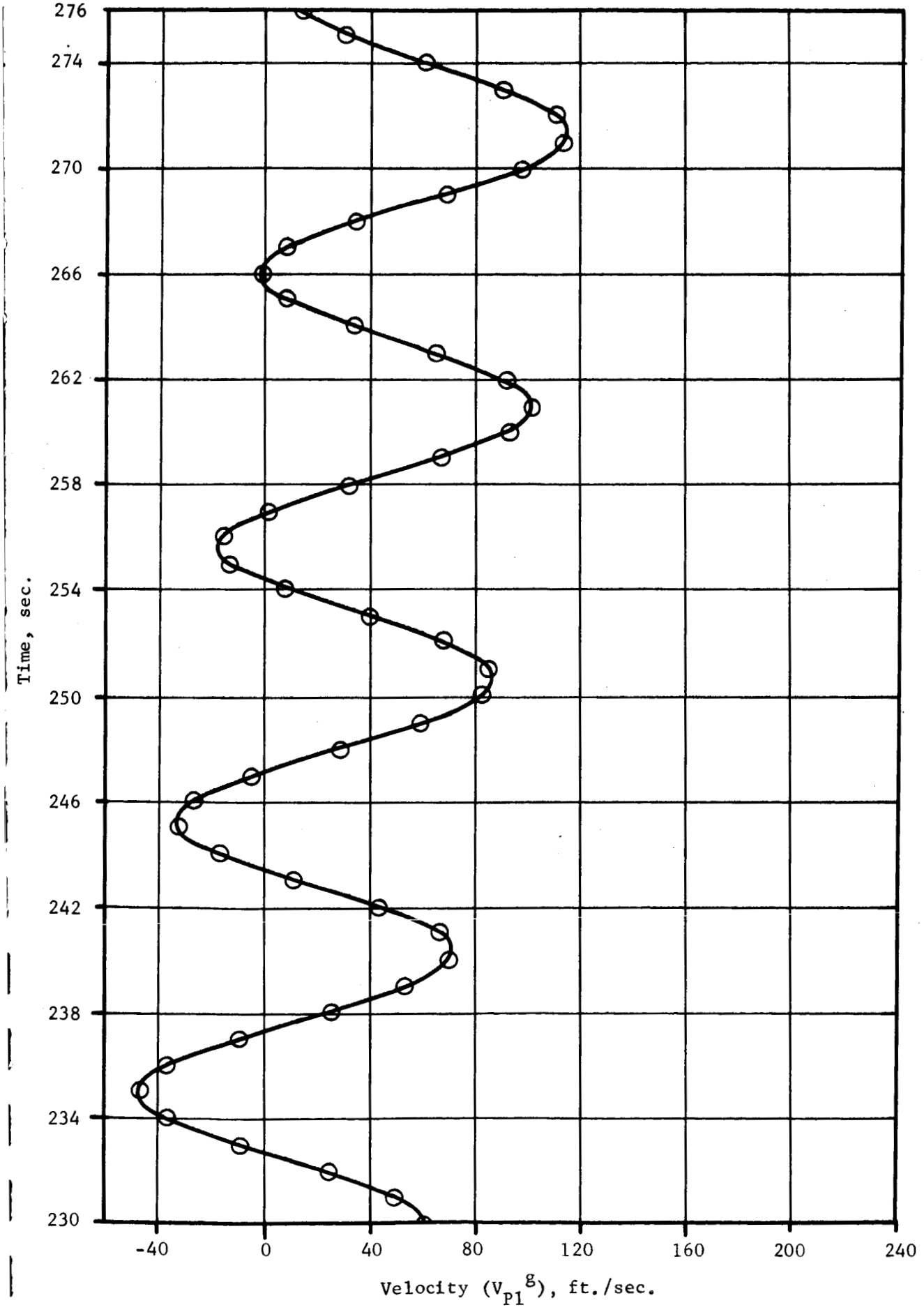

Figure 8e. (Page 6 of 7)

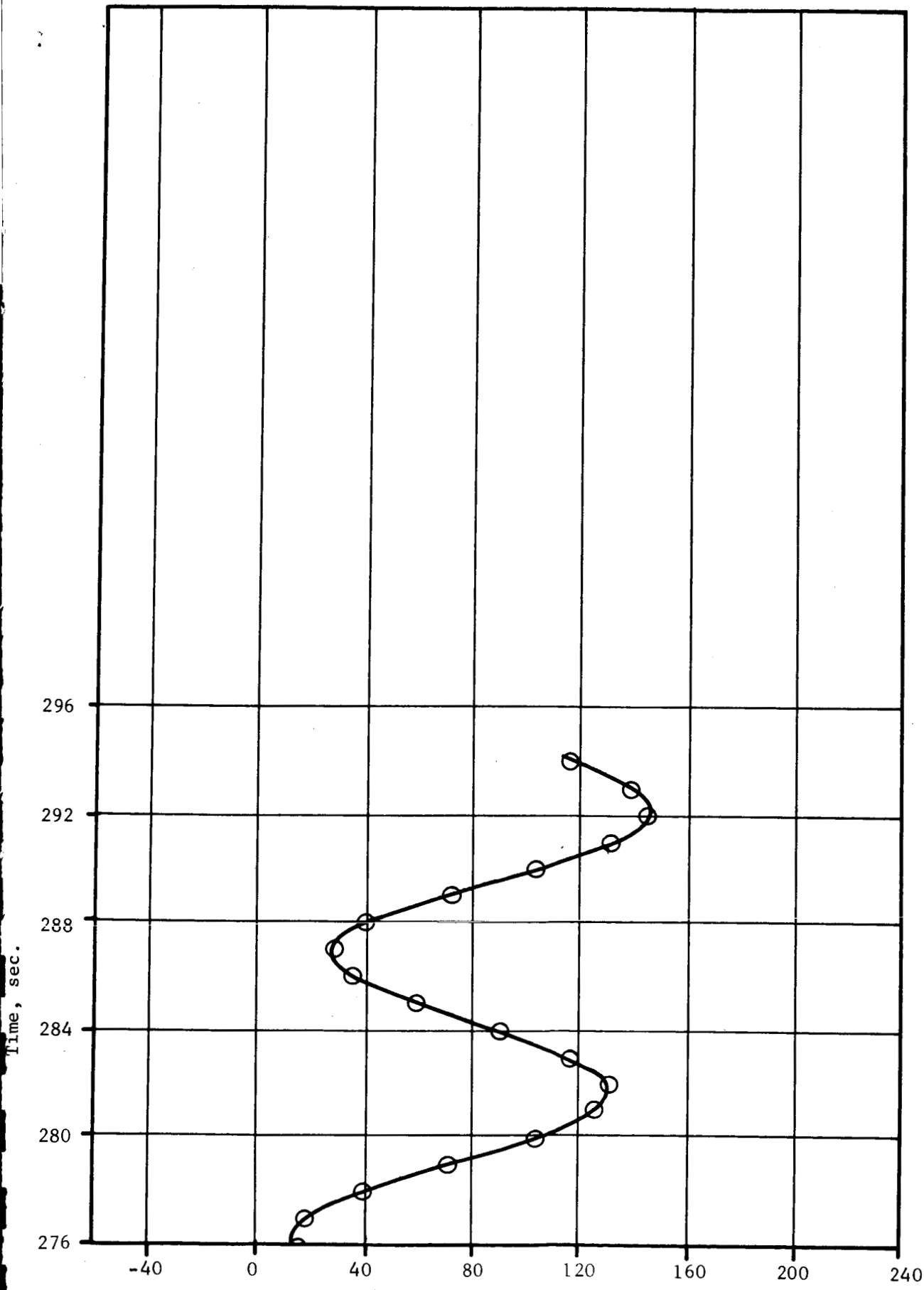

Figure 8e. (Page 7 of 7)

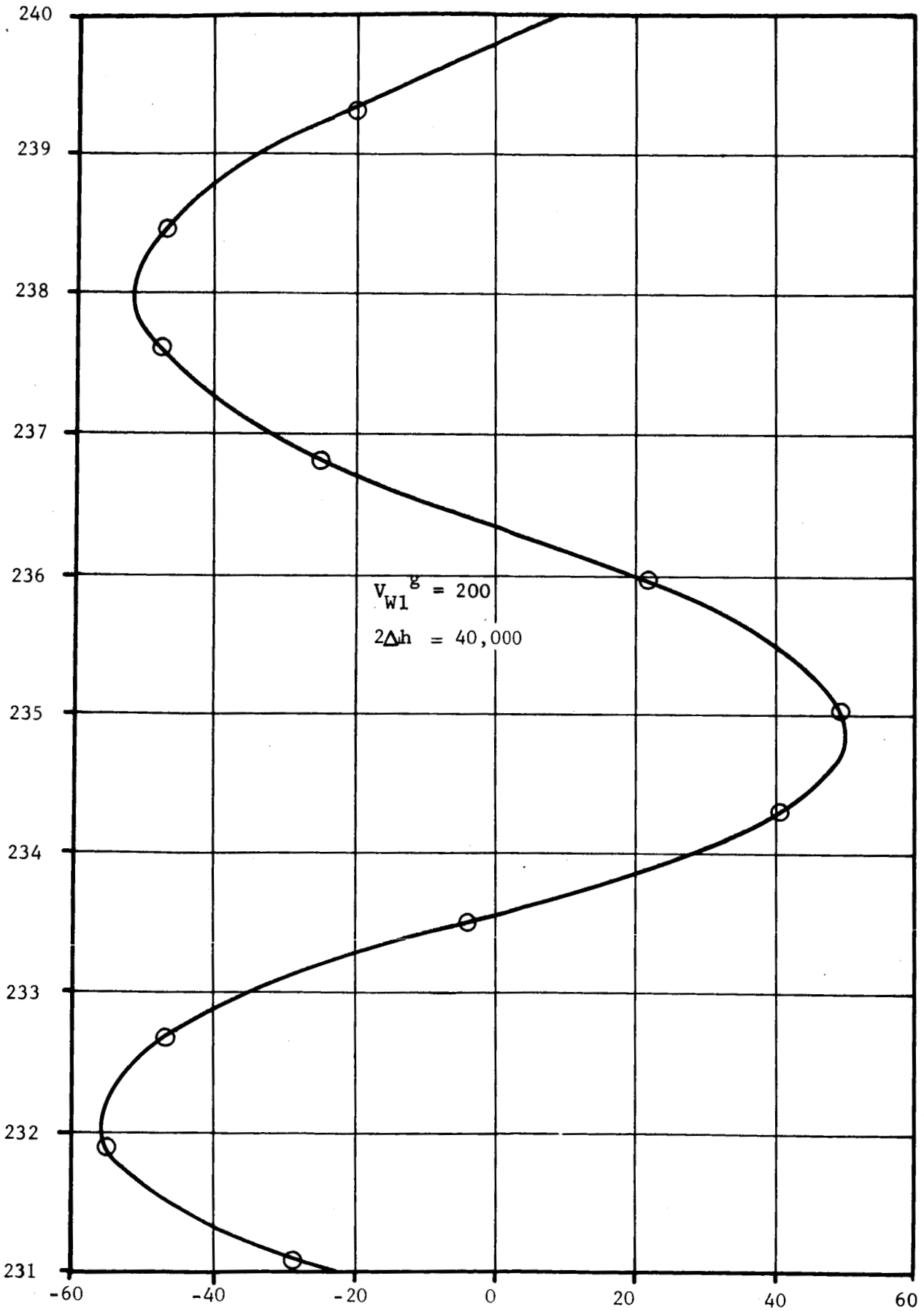

Figure 8f. Velocity vs. Altitude for Hemispherical Parachute

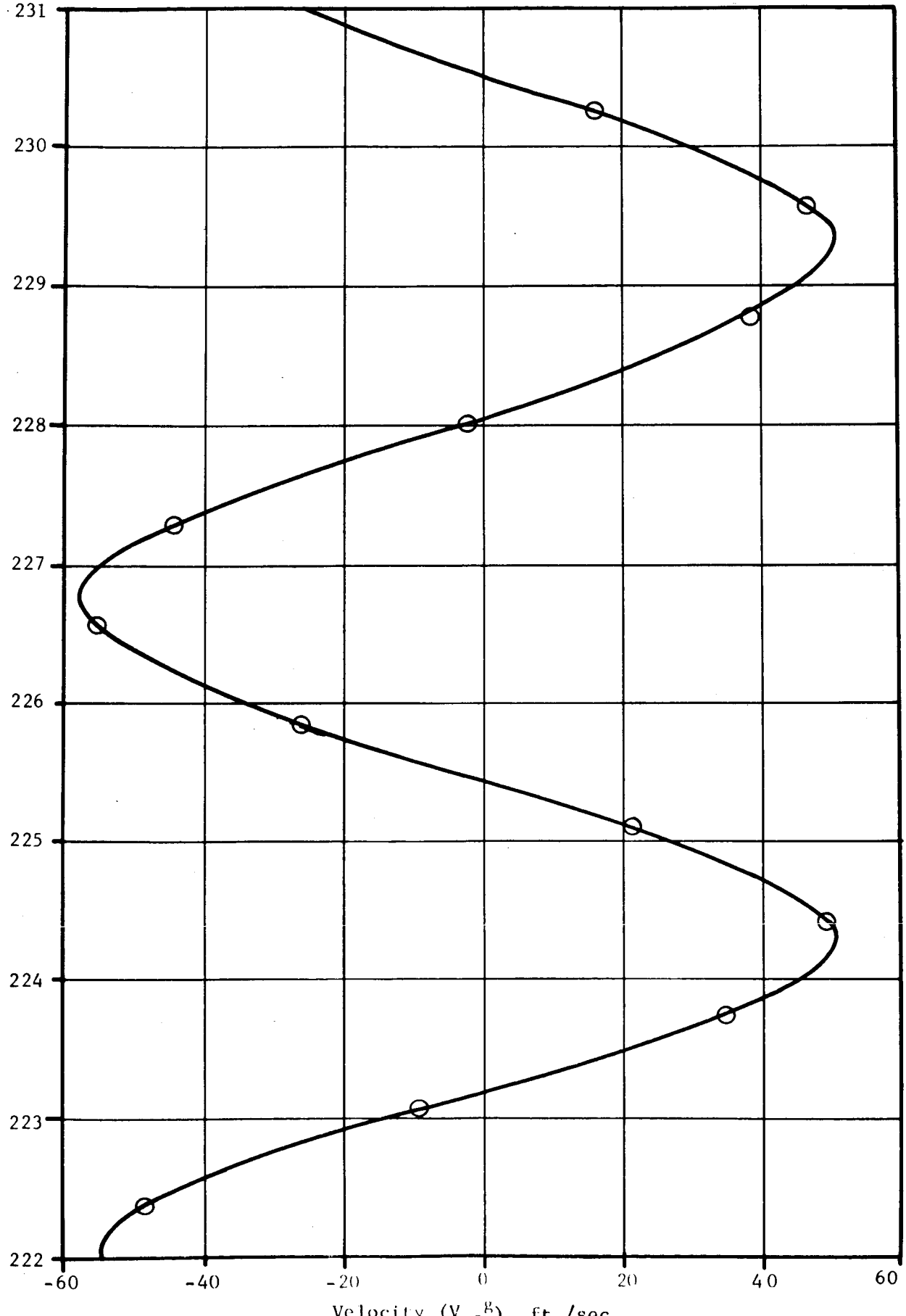

Figure 81. (Page 2 of 10)

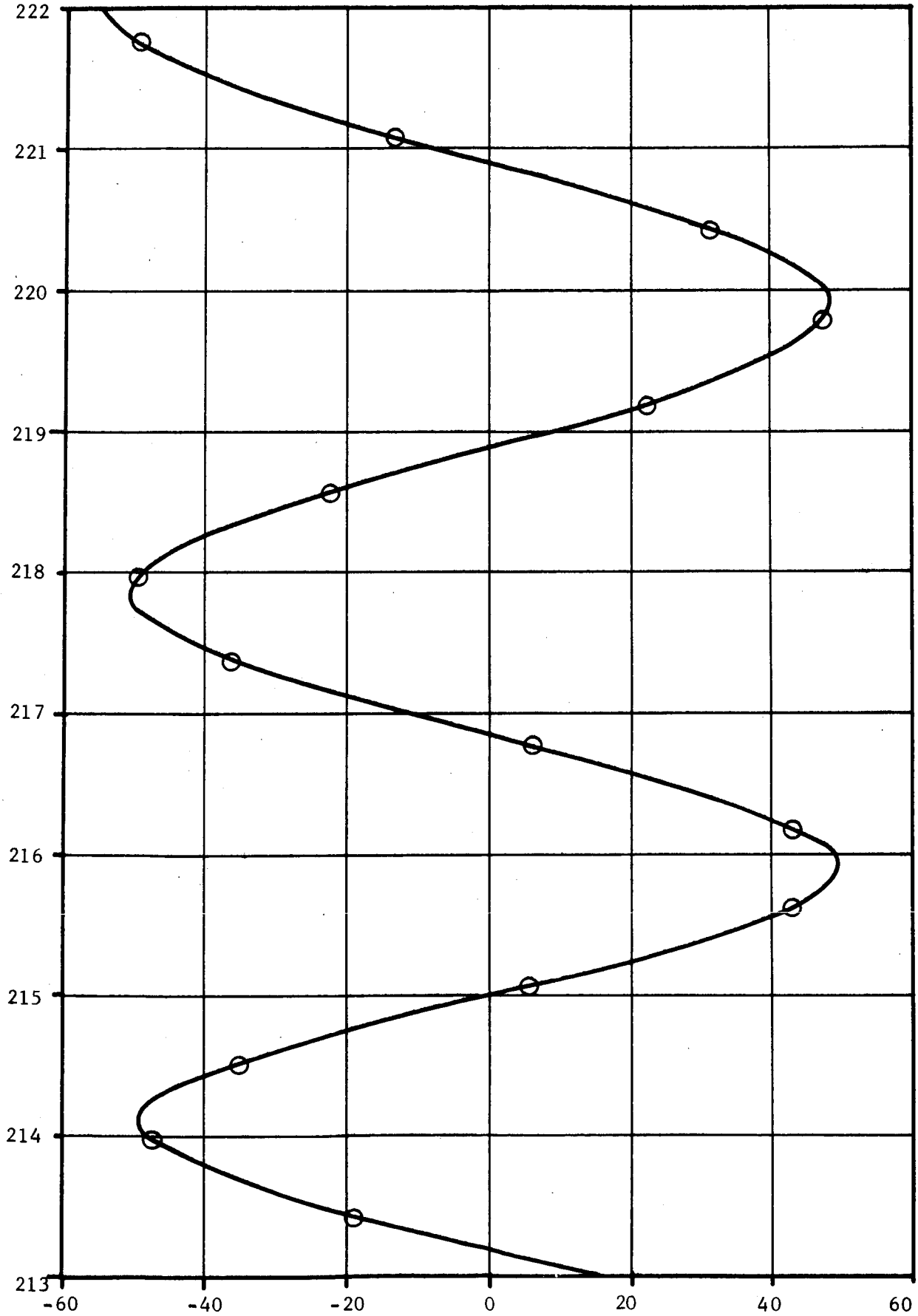

Figure 8f. (Page 3 of 10)

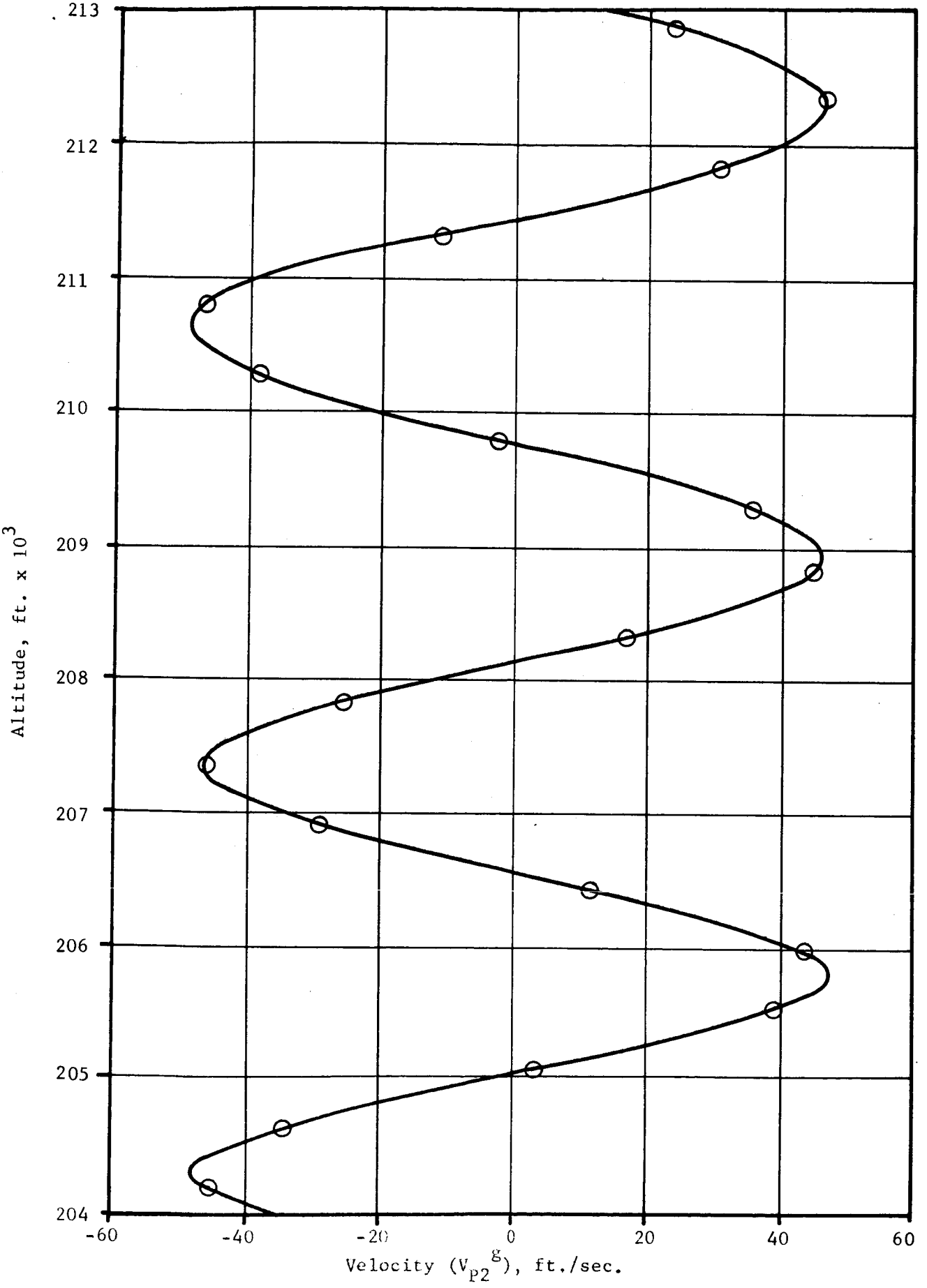

Figure 8f. (Page 4 of 10)

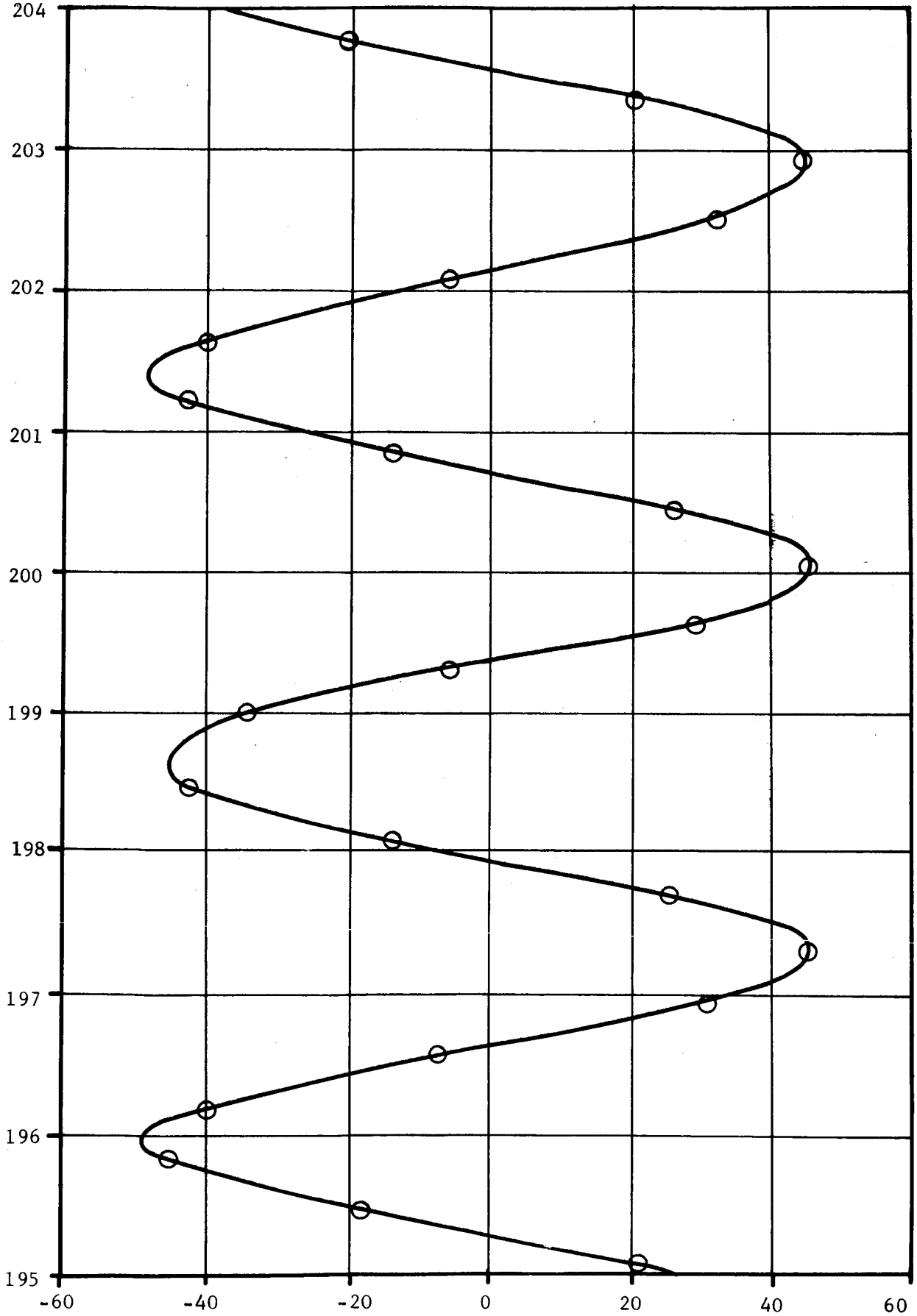

Figure 8f. (Page 5 of 10)

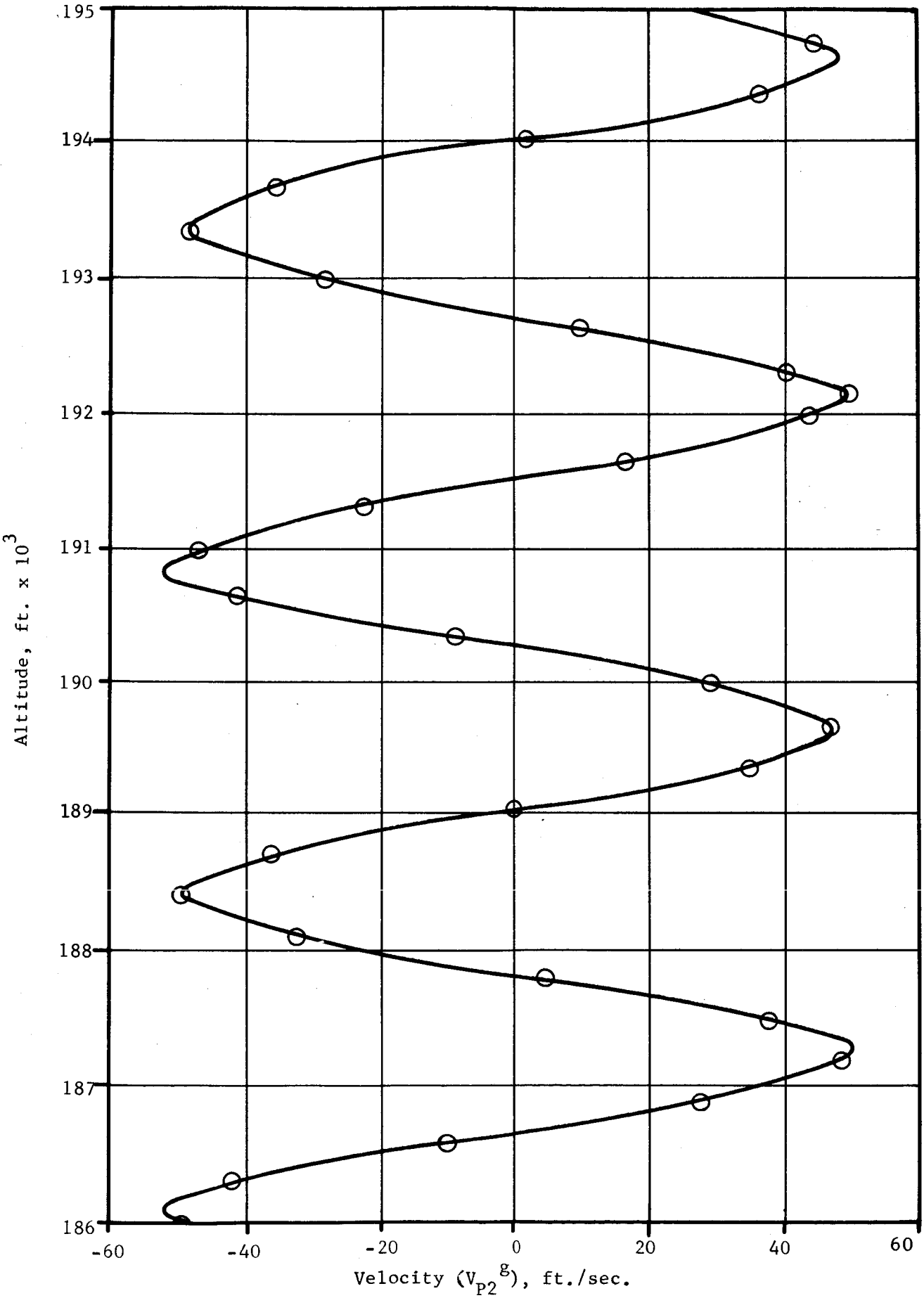

Figure 8f. (Page 6 of 10)

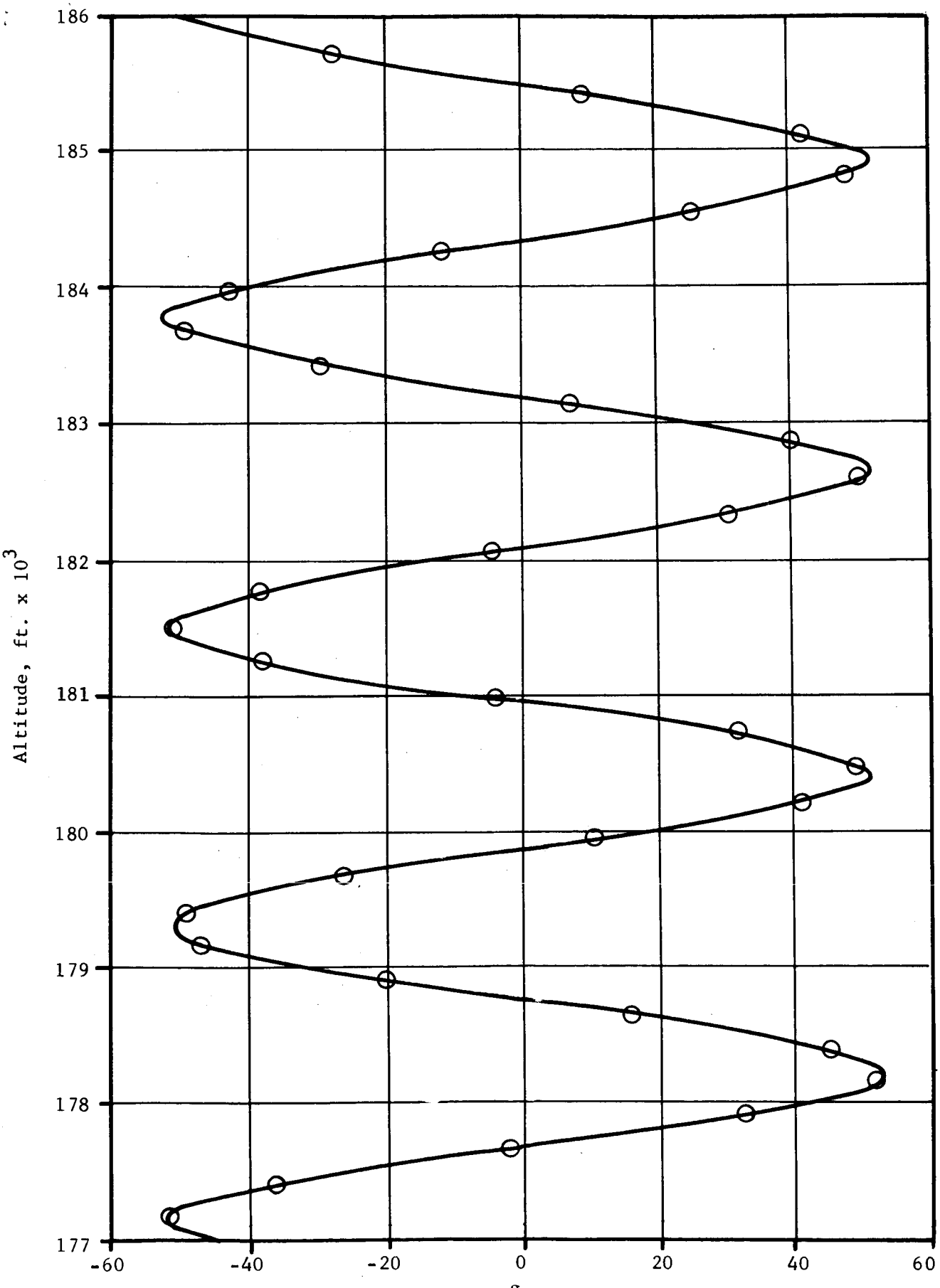

Figure 8f. (Page 7 of 10)

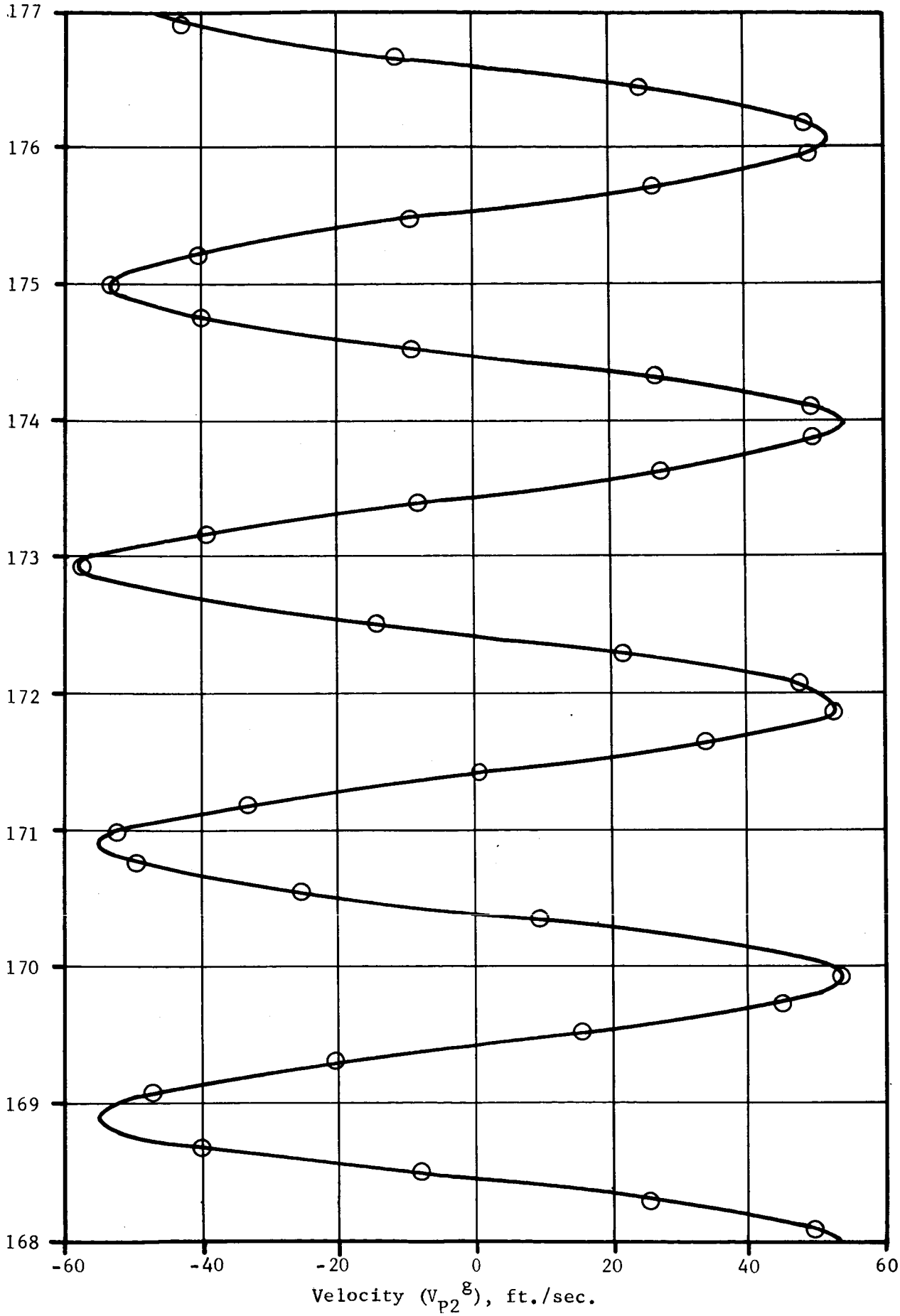

Figure 8f. (Page 8 of 10)

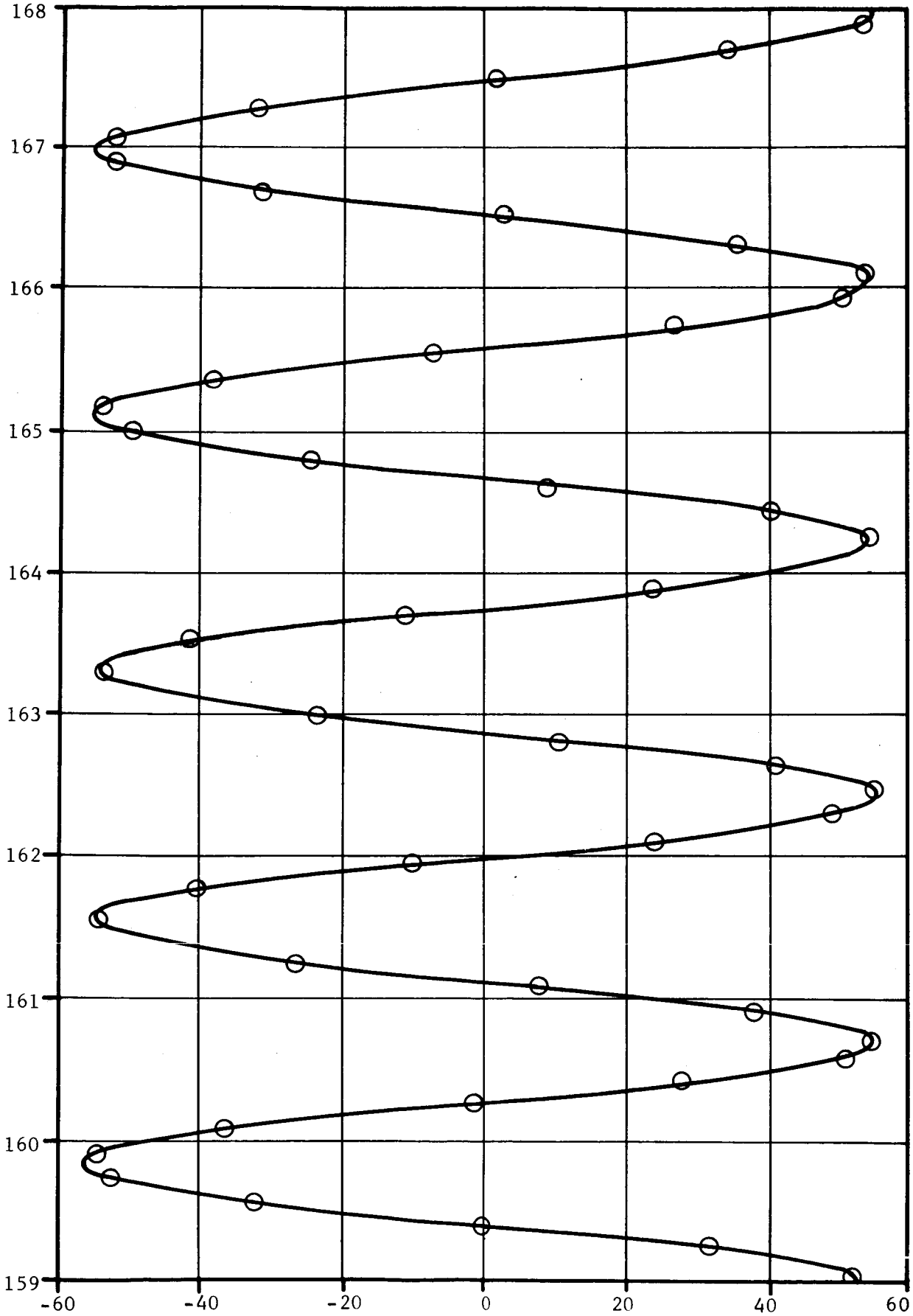

Figure 8f. (Page 9 of 10)

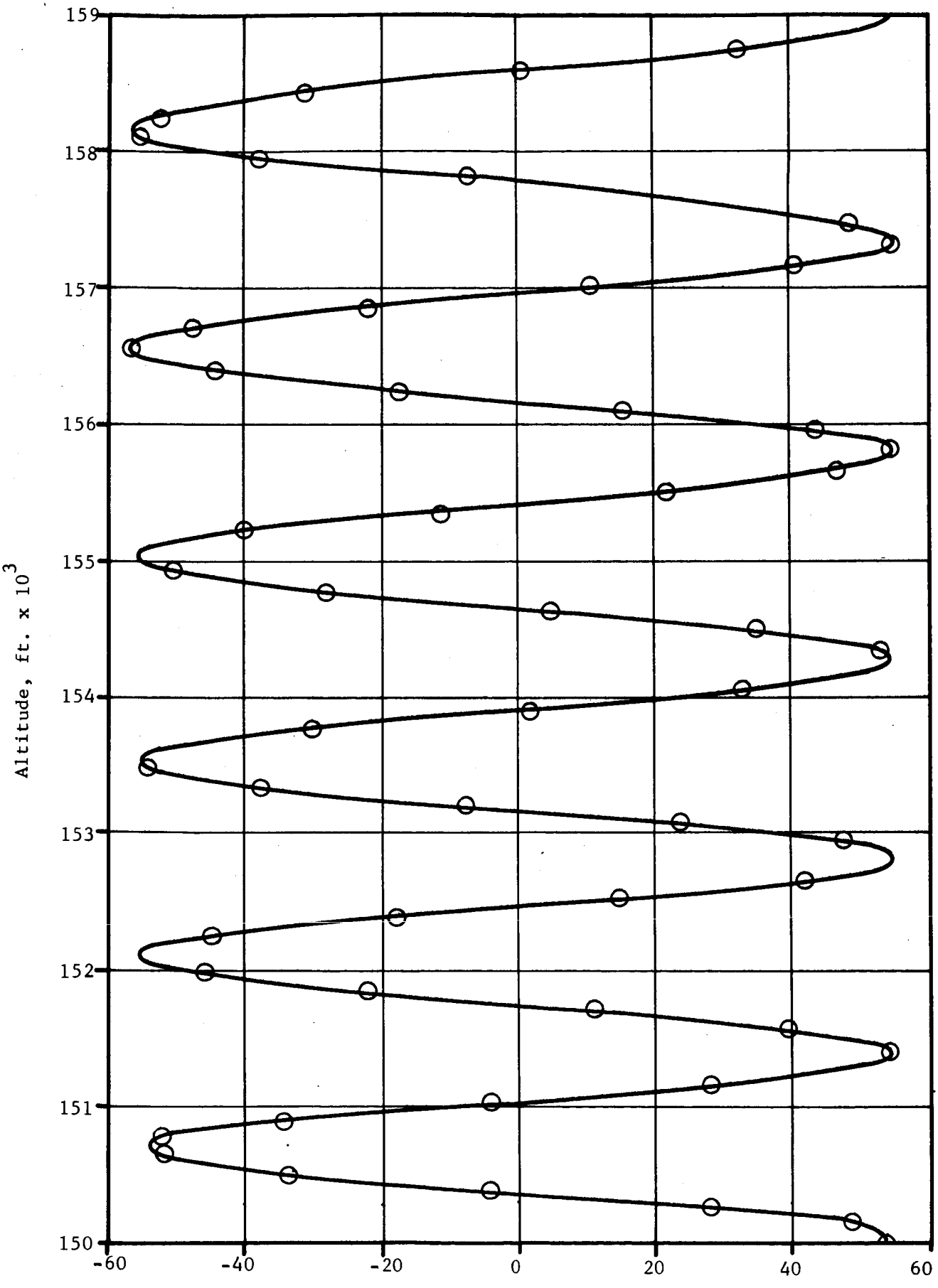

Figure 8f. (Page 10 of 10)

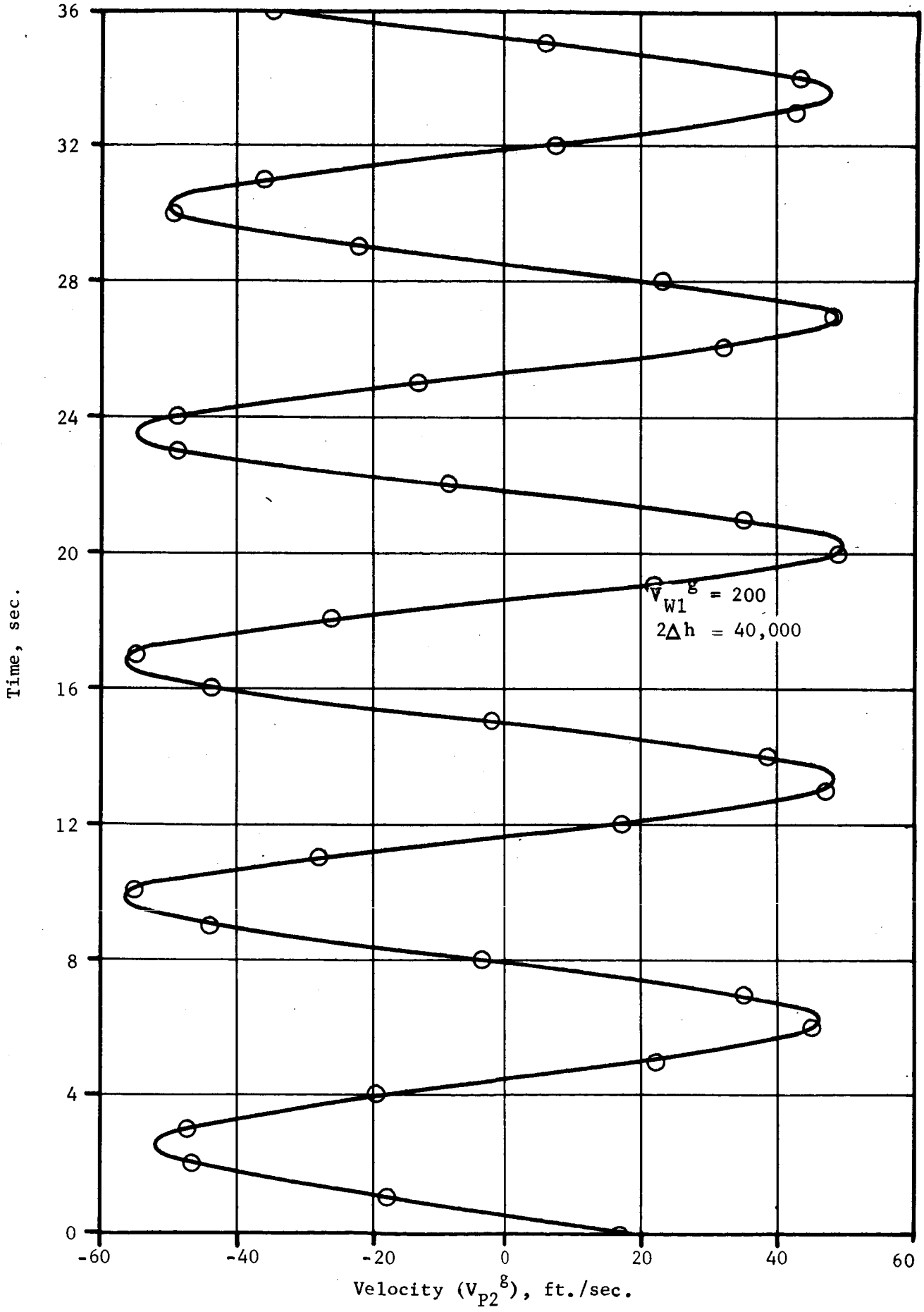

Figure 8g. Velocity vs. Time for Hemispherical Parachute

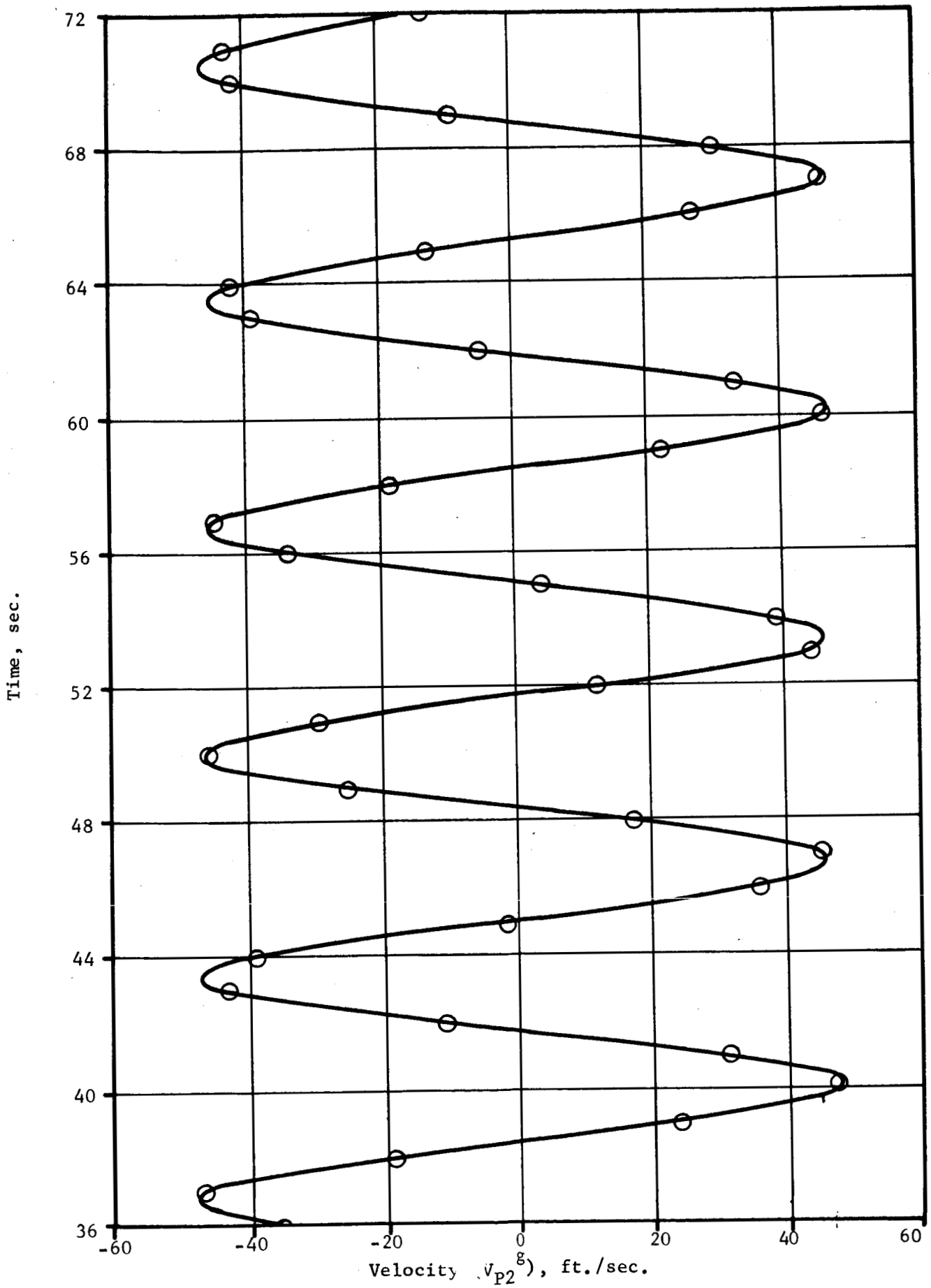

Figure 8g. (Page 2 of 9)

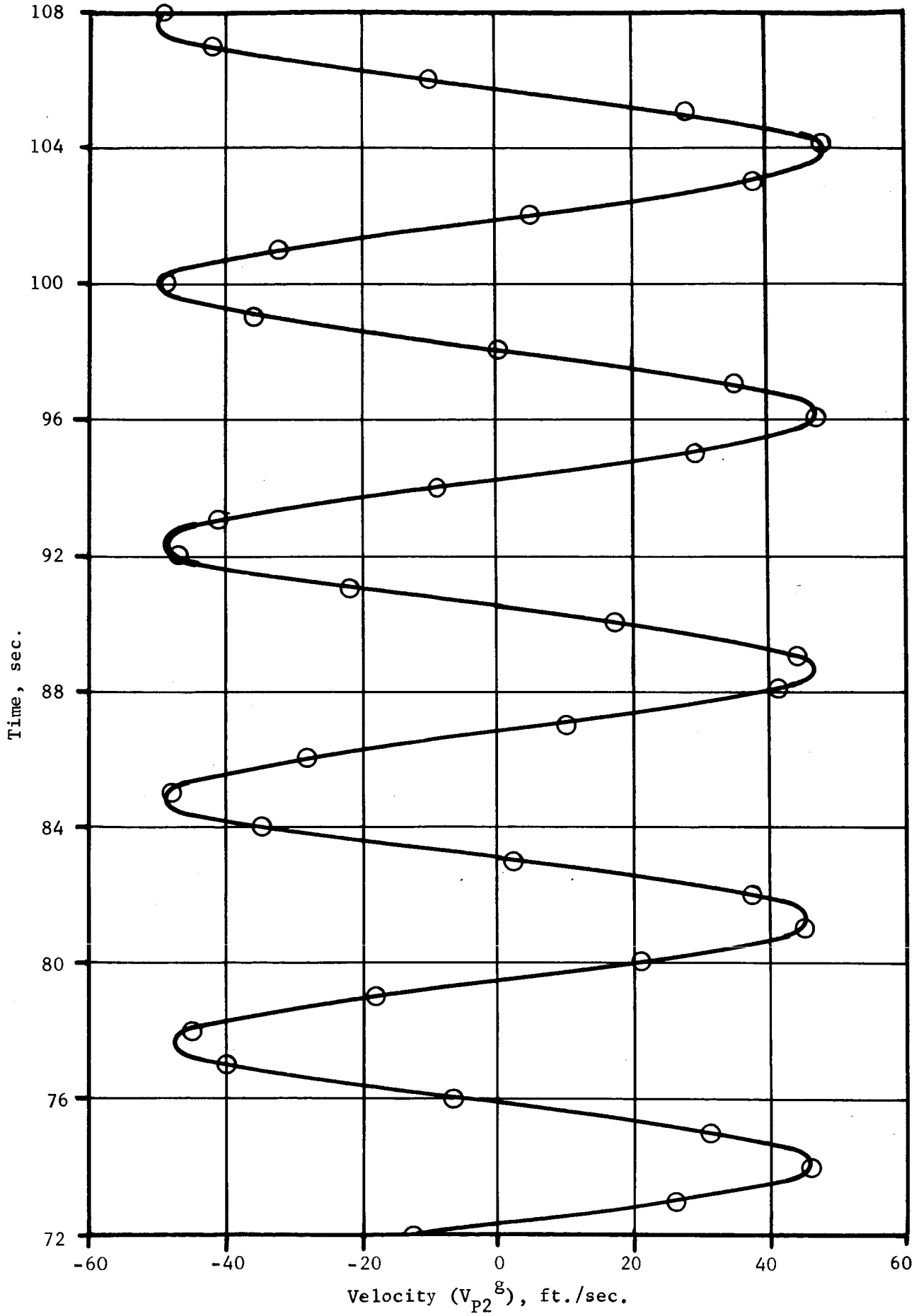

Figure 8g. (Page 3 of 9)

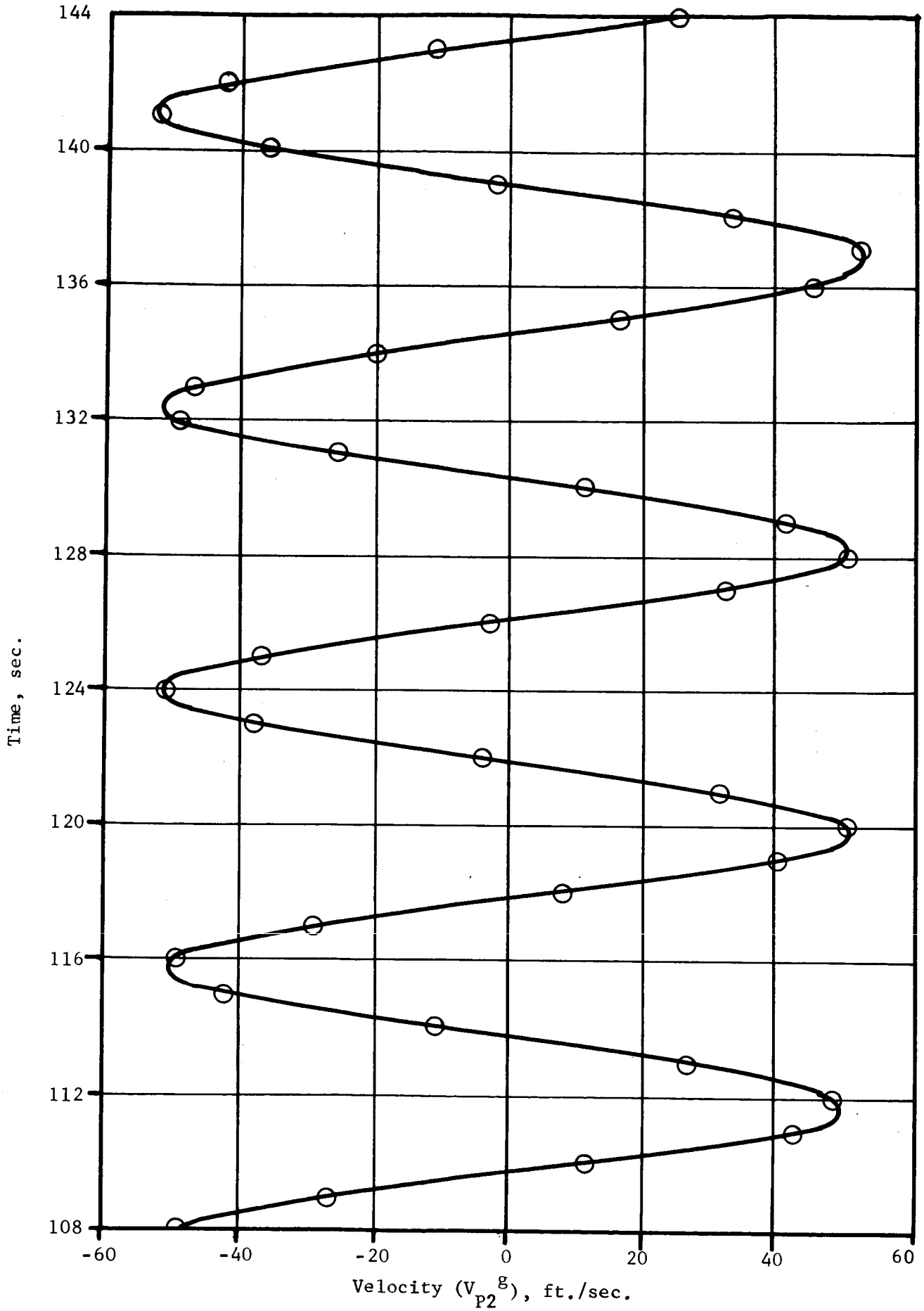

Figure 8g. (Page 4 of 9)

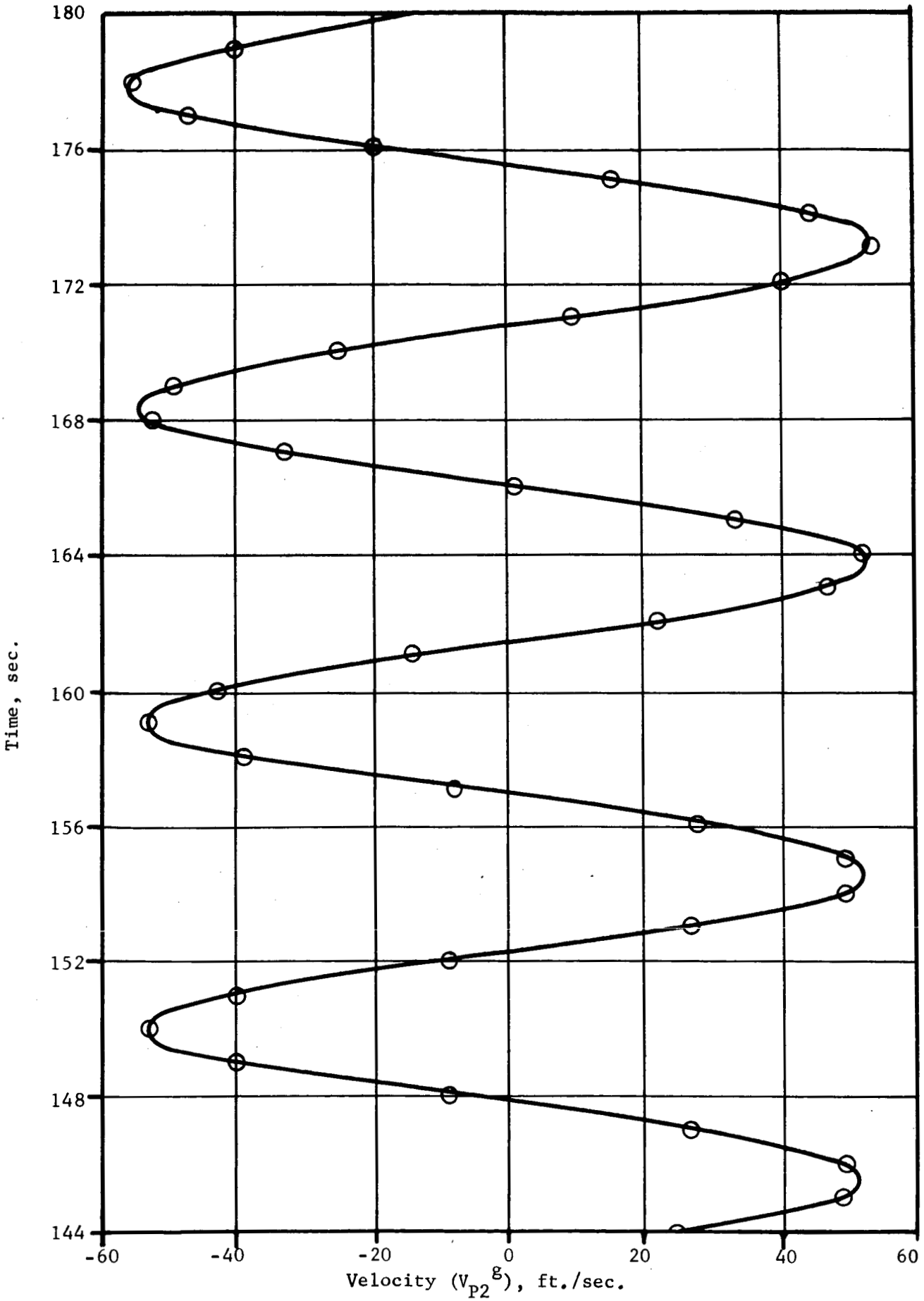

Figure 8g. (Page 5 of 9)

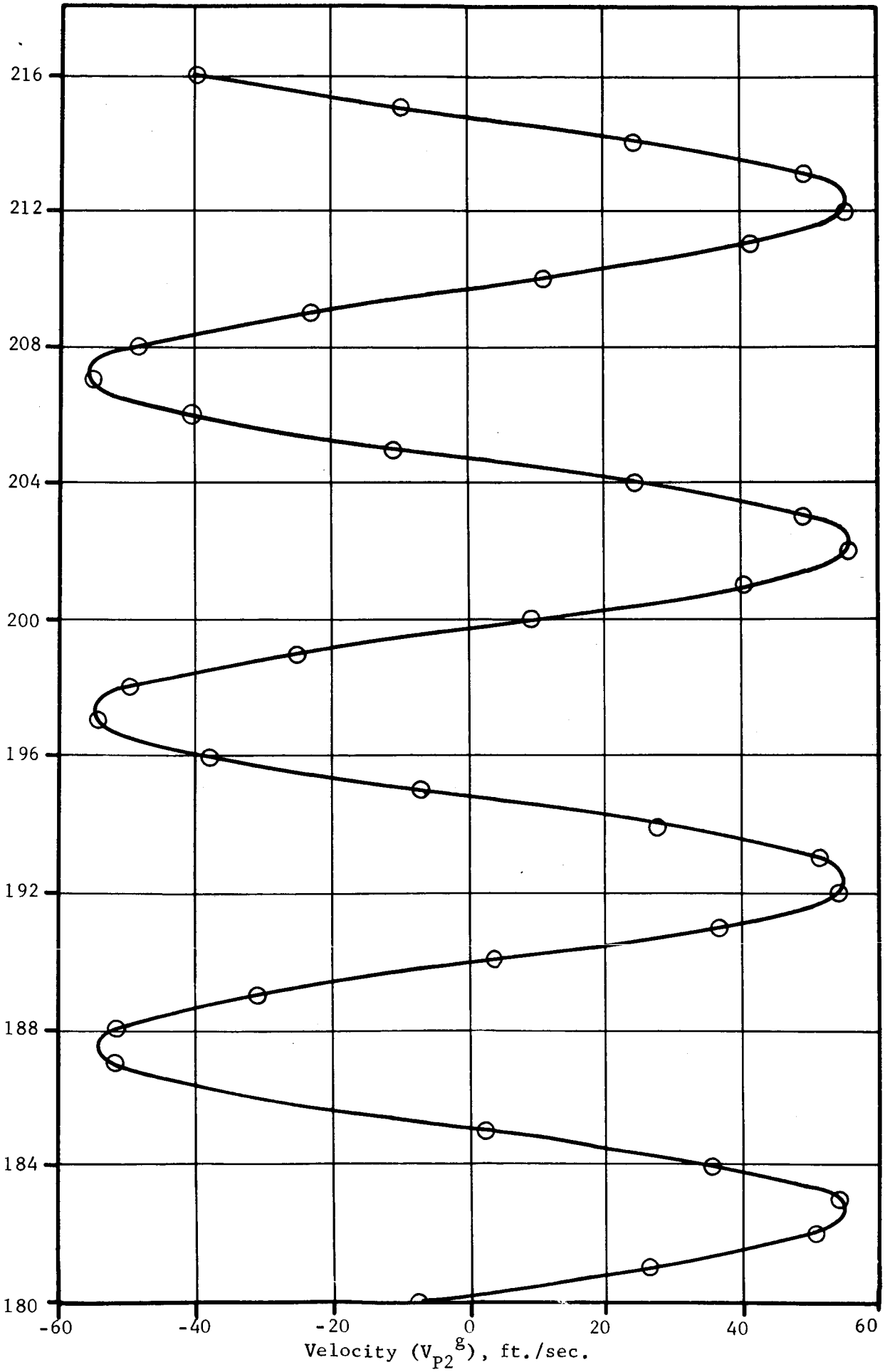

Figure 8g. (Page 6 of 9)

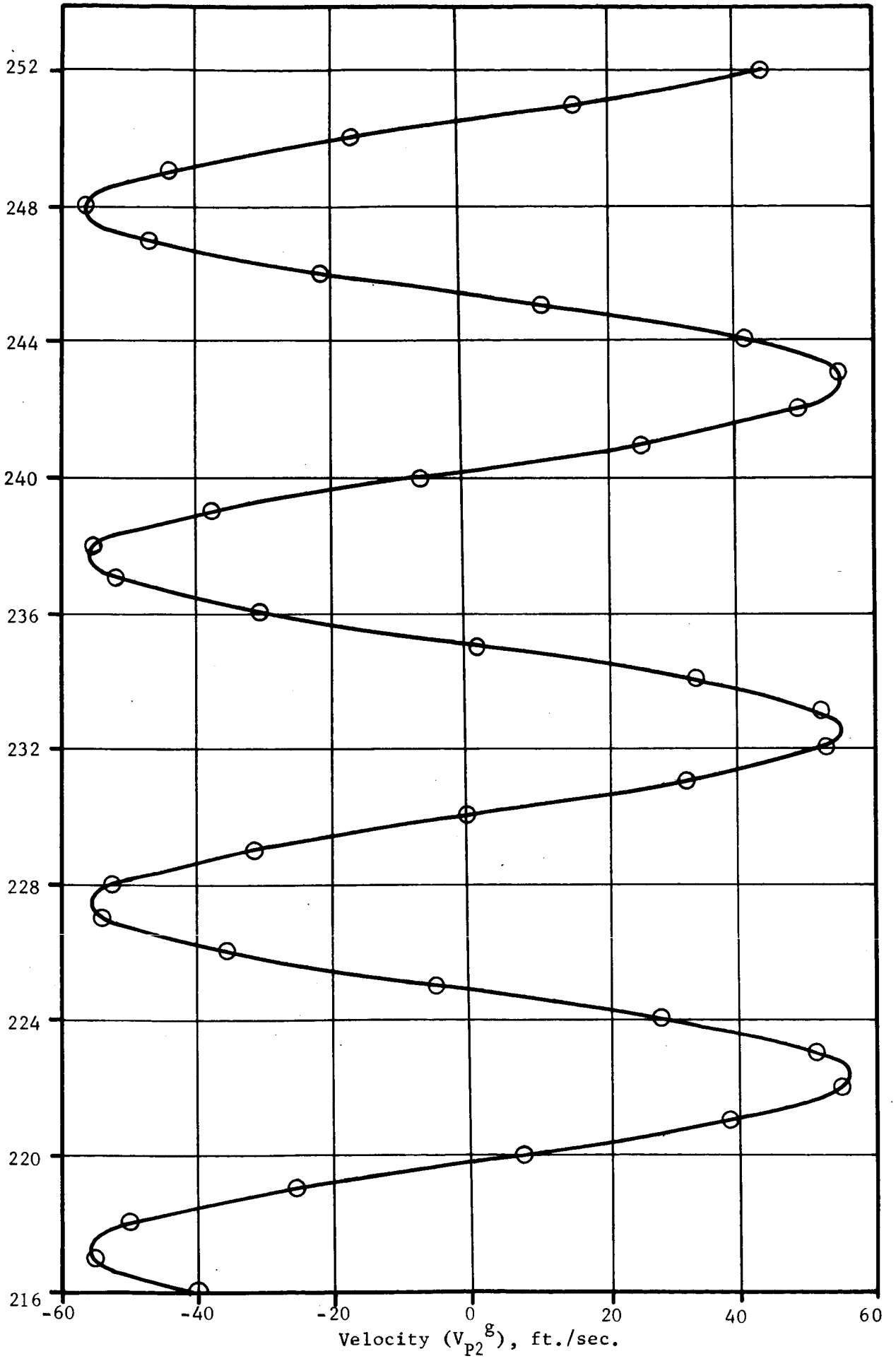

Figure 8g. (Page 7 of 9)

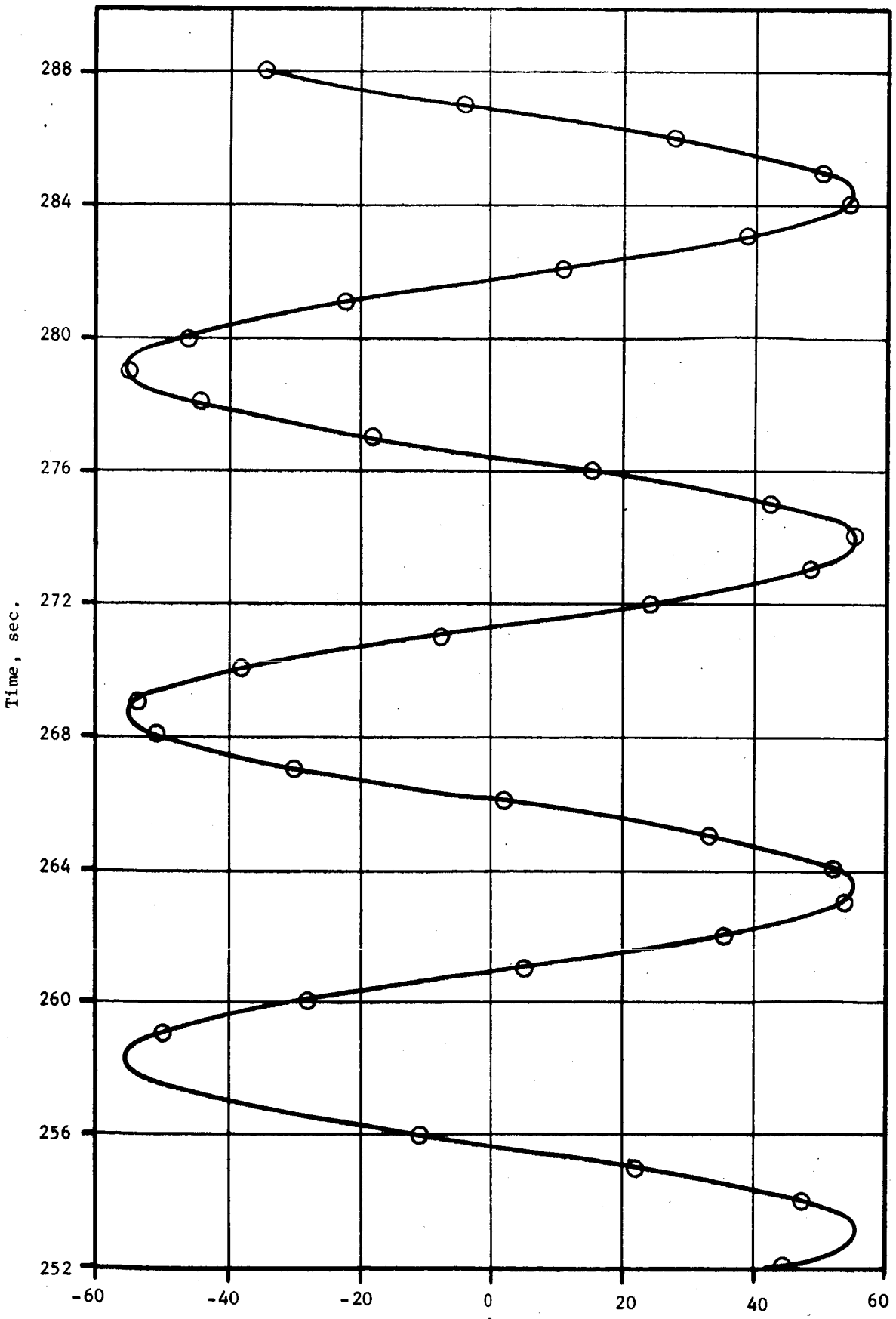

Figure 8g. (Page 8 of 9)

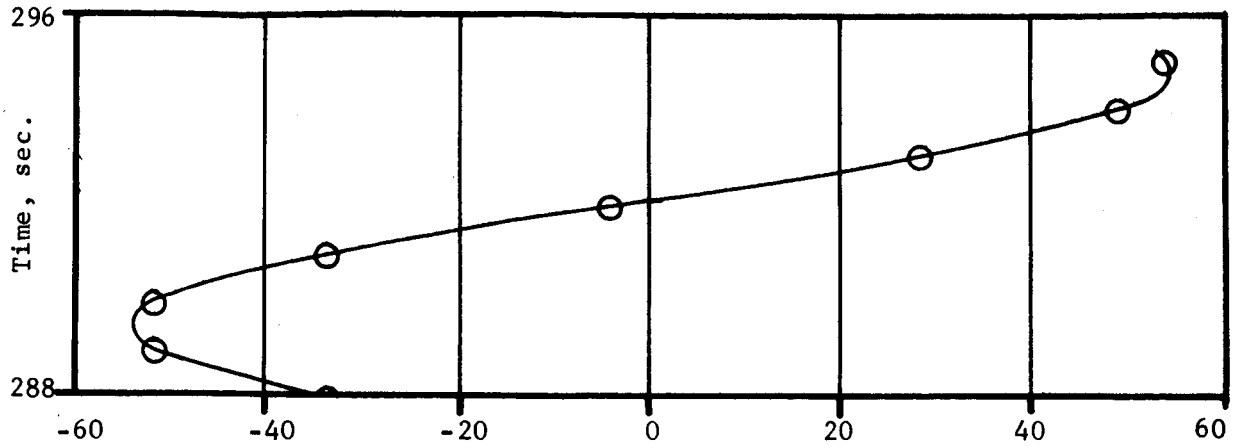

Figure 8g. (Page 9 of 9)

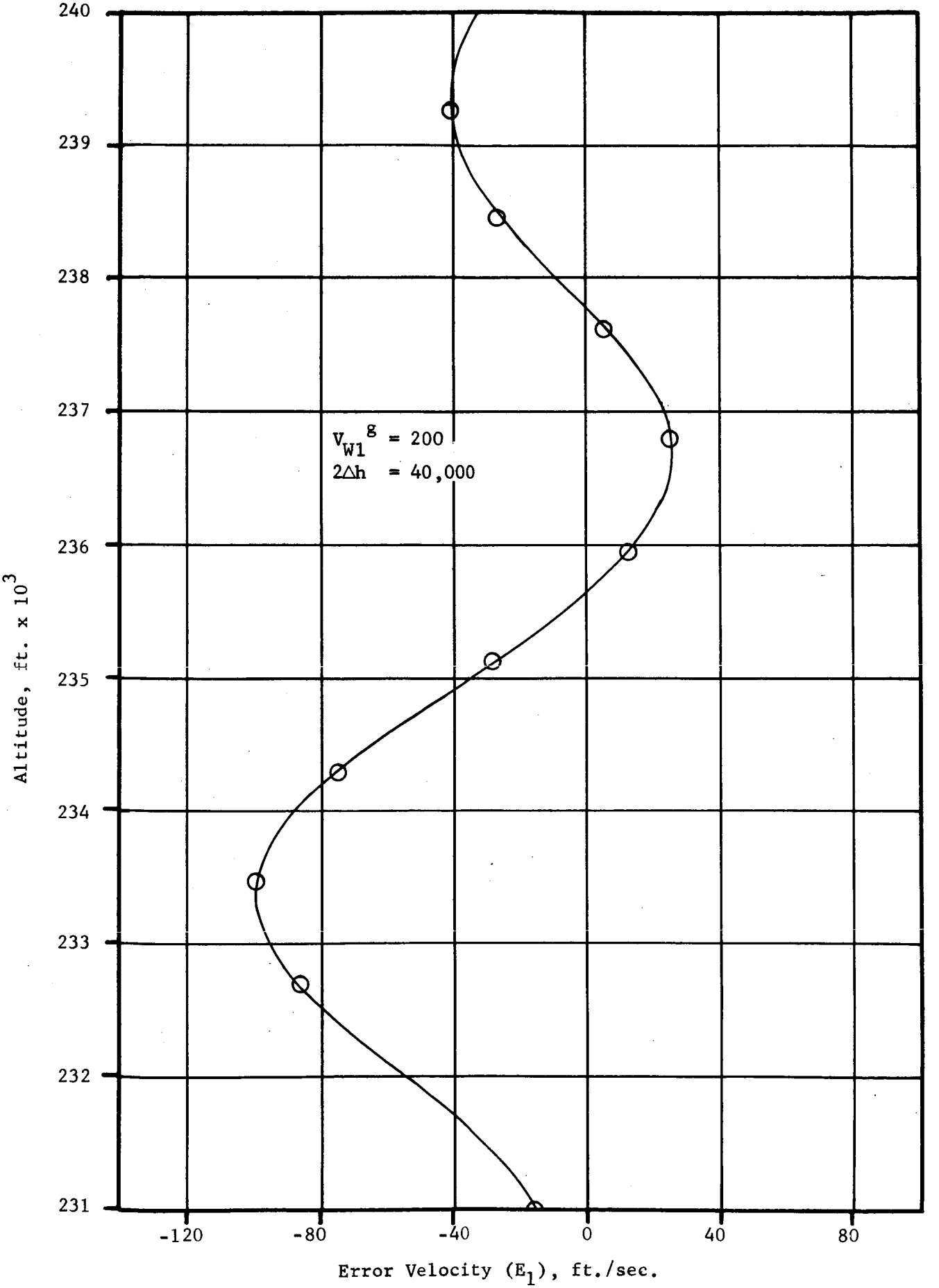

Figure 8h. Error Velocity vs. Altitude for Hemispherical Parachute

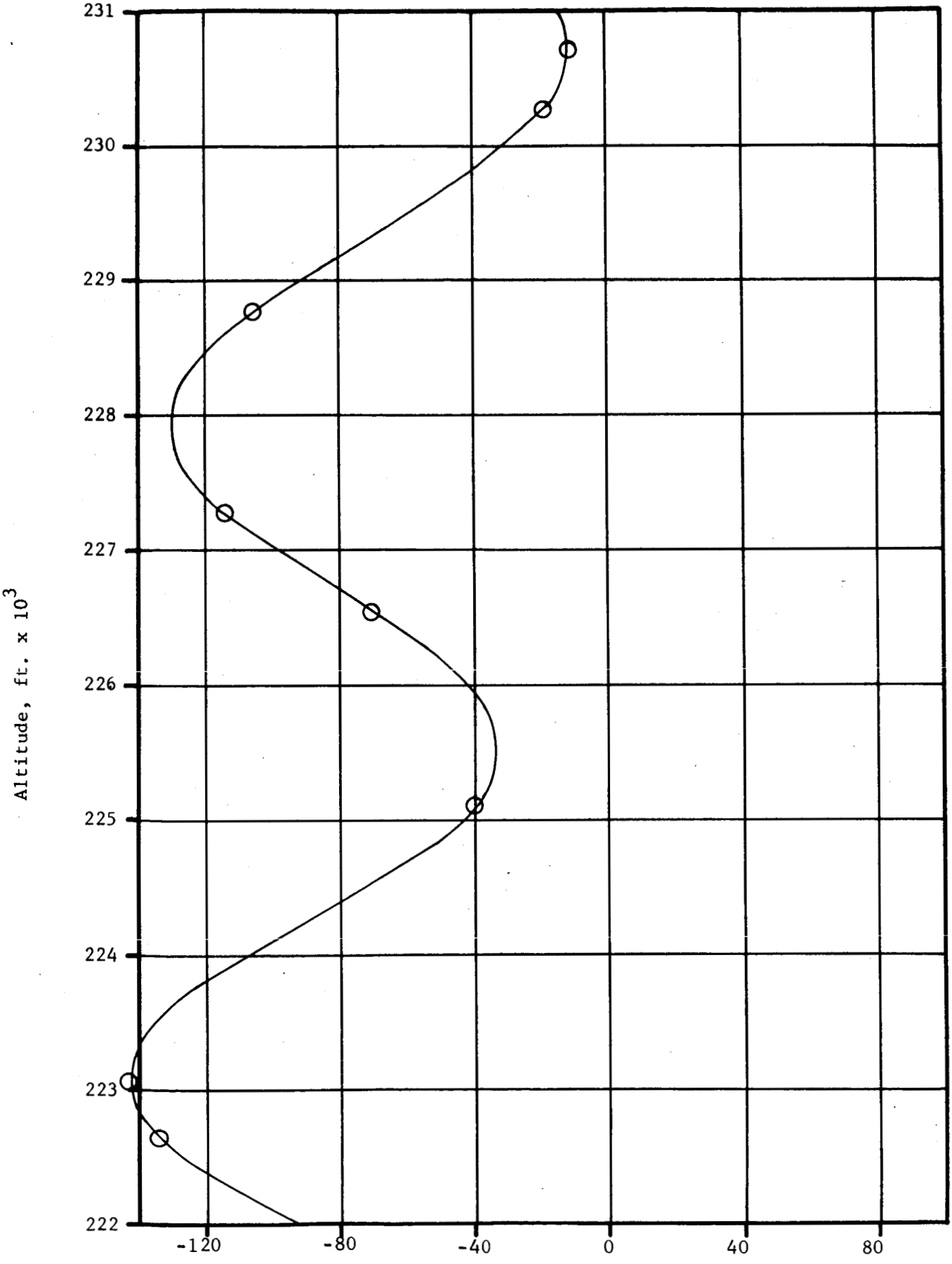

Figure 8h. (Page 2 of 10)

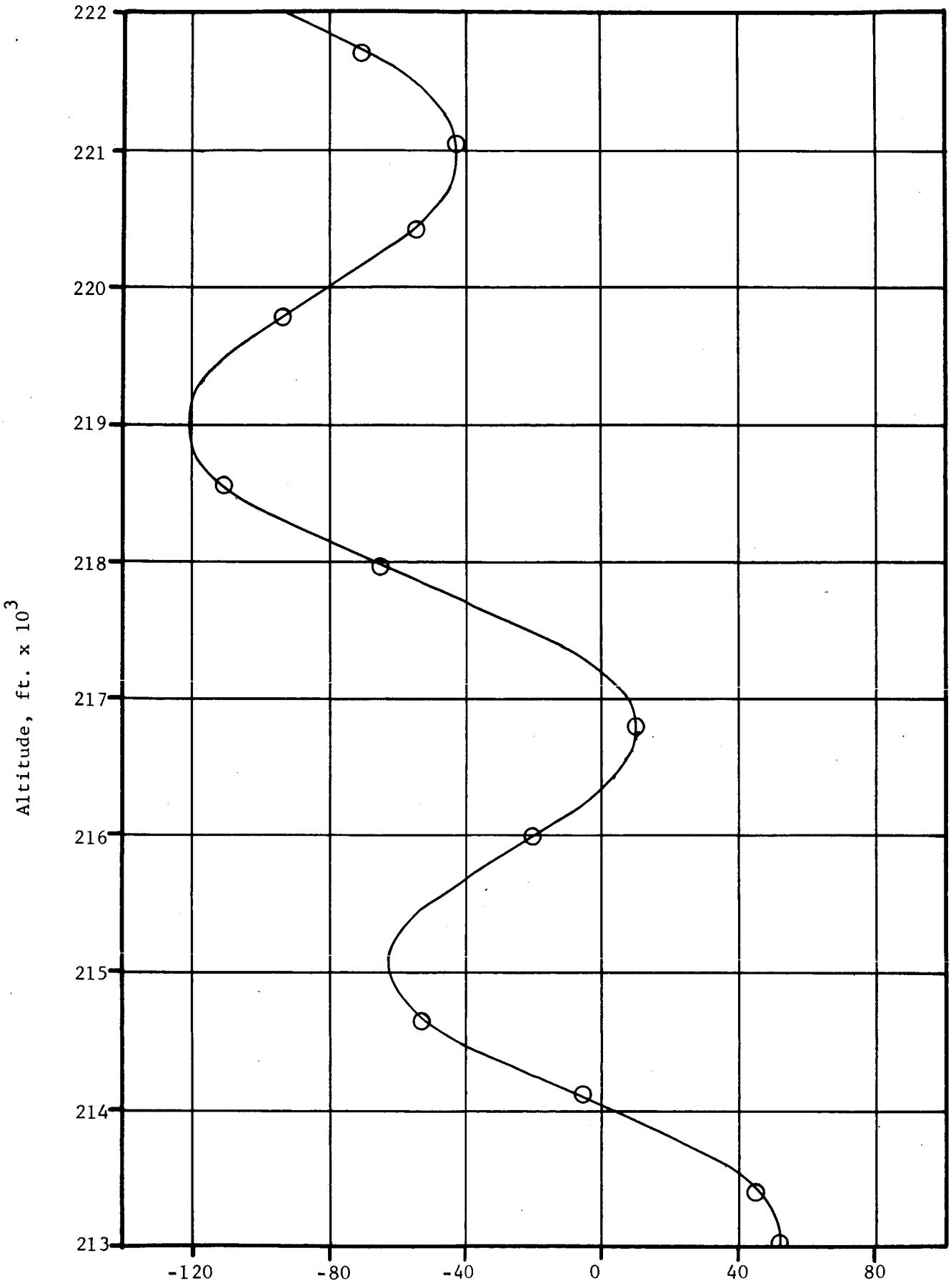

Figure 8h. (Page 3 of 10)

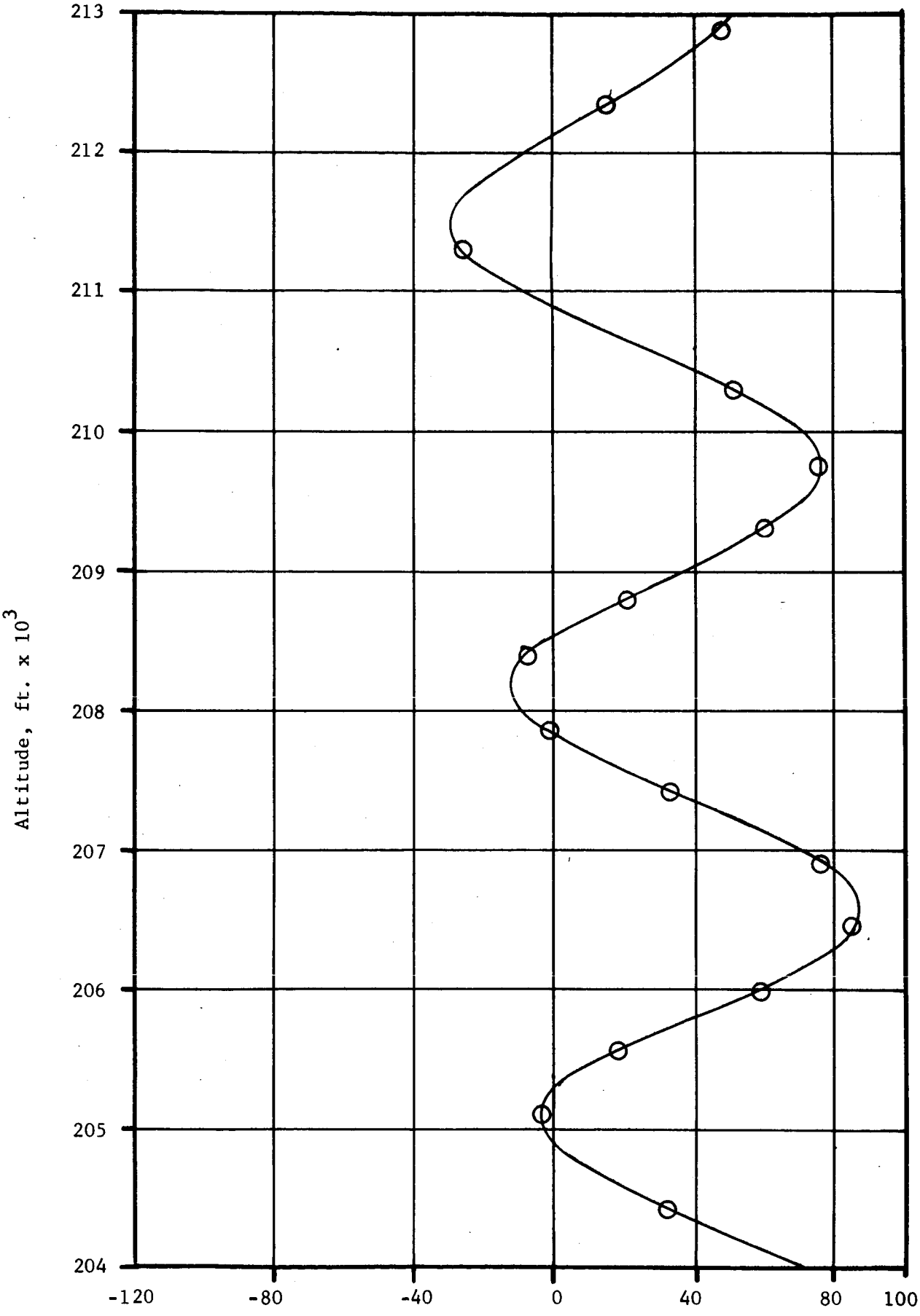

Figure 8h. (Page 4 of 10)

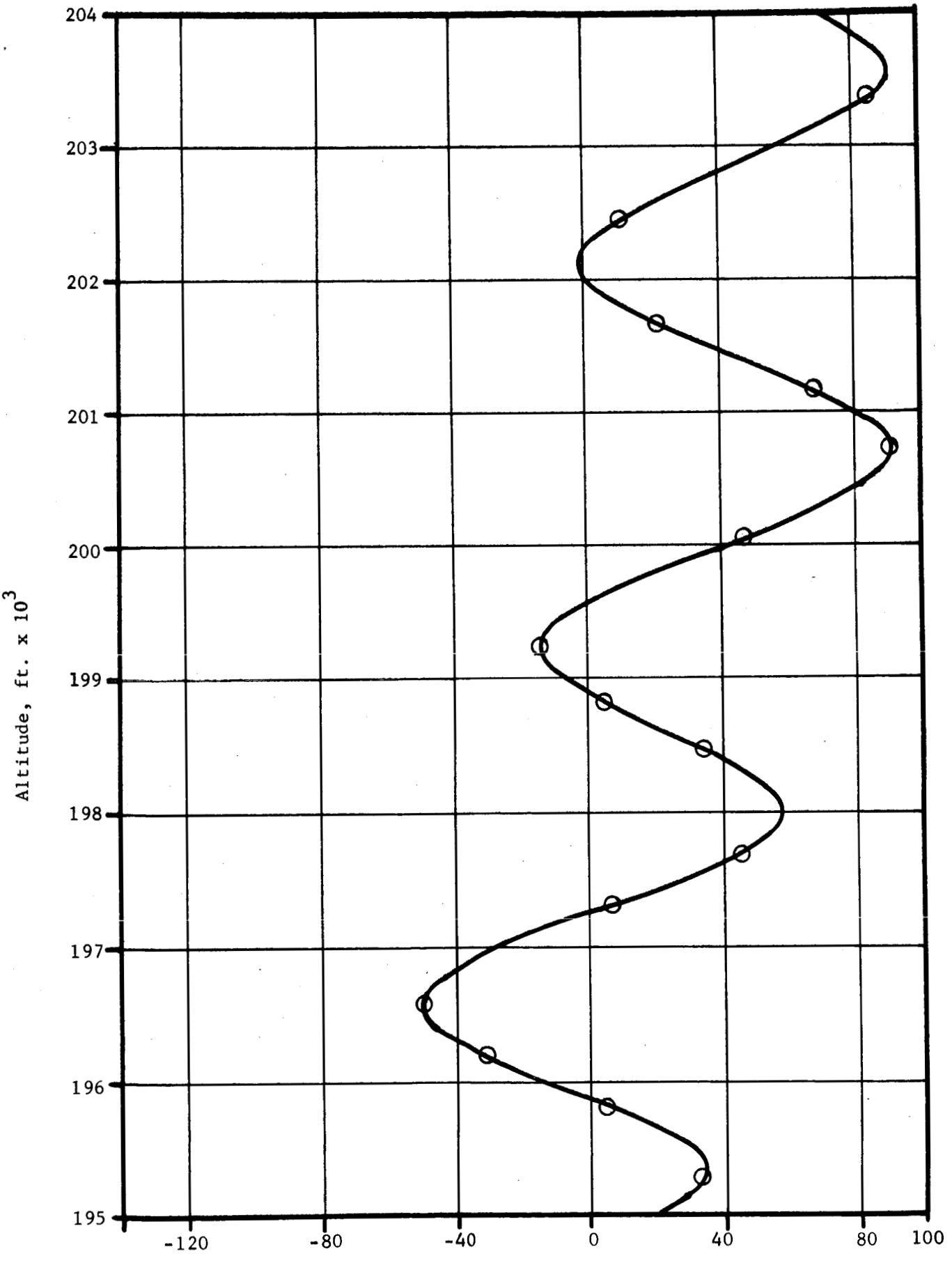

Figure 8h. (Page 5 of 10)

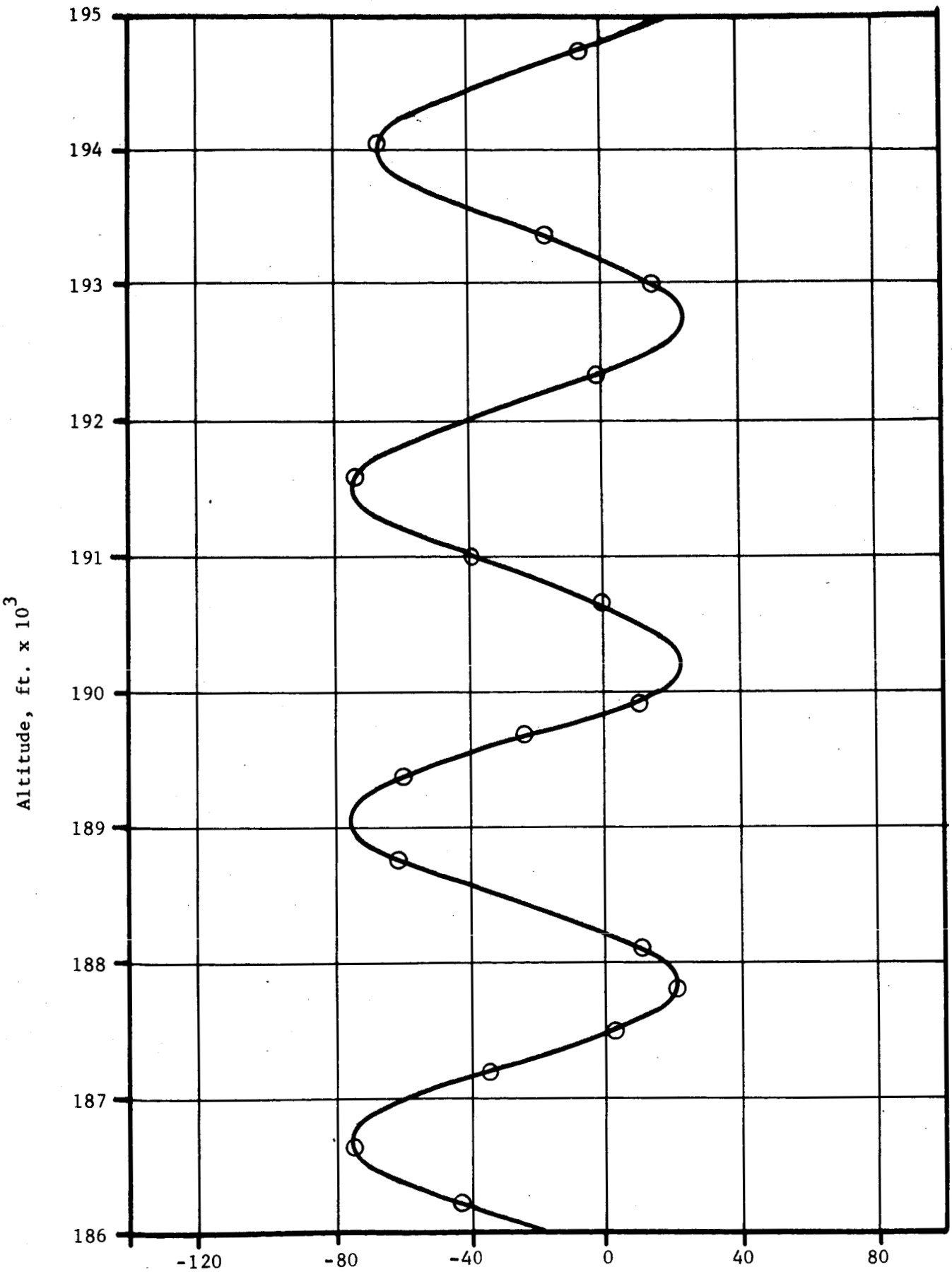

Figure 8h. (Page 6 of 10)

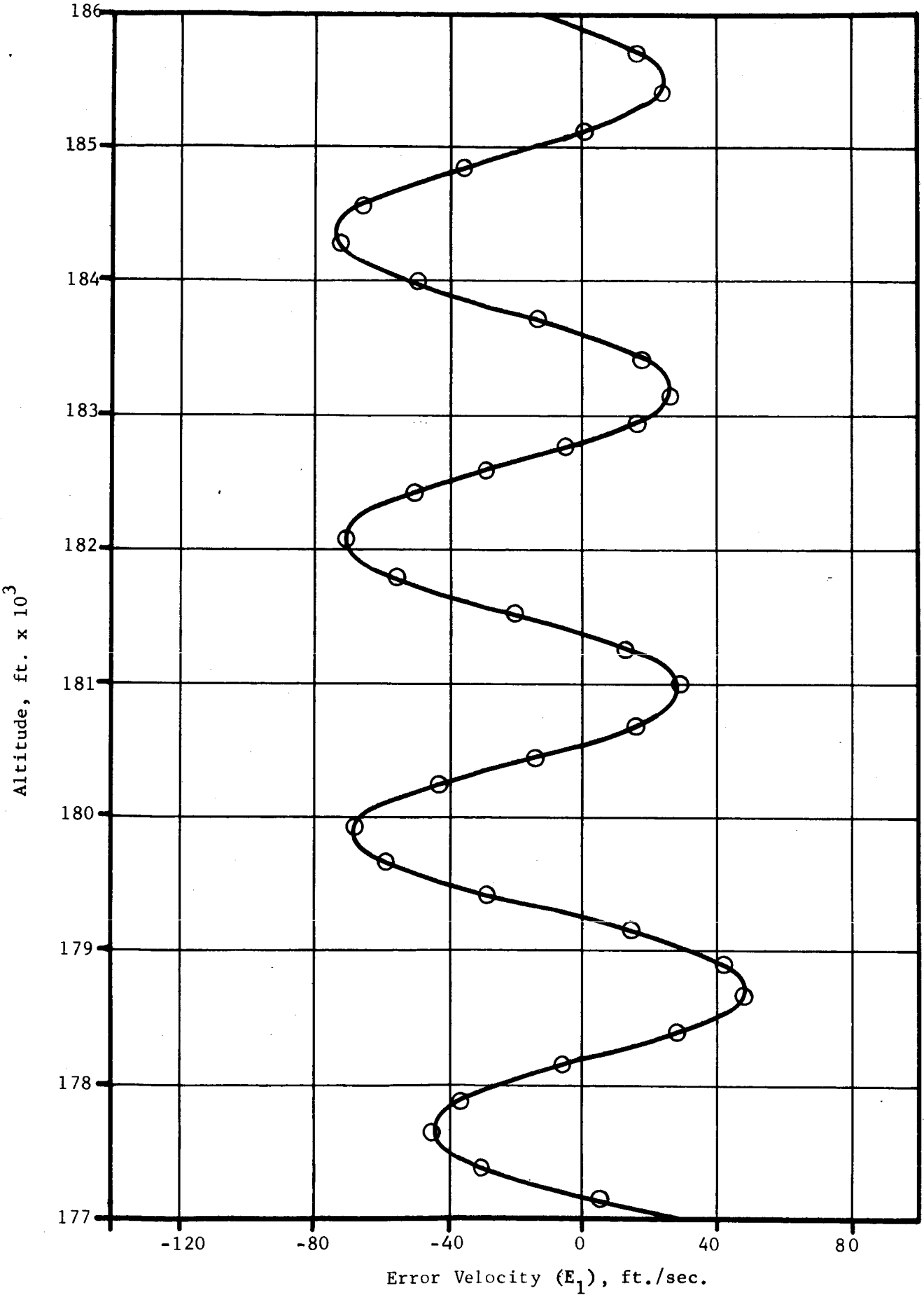

Figure 8h. (Page 7 of 10)

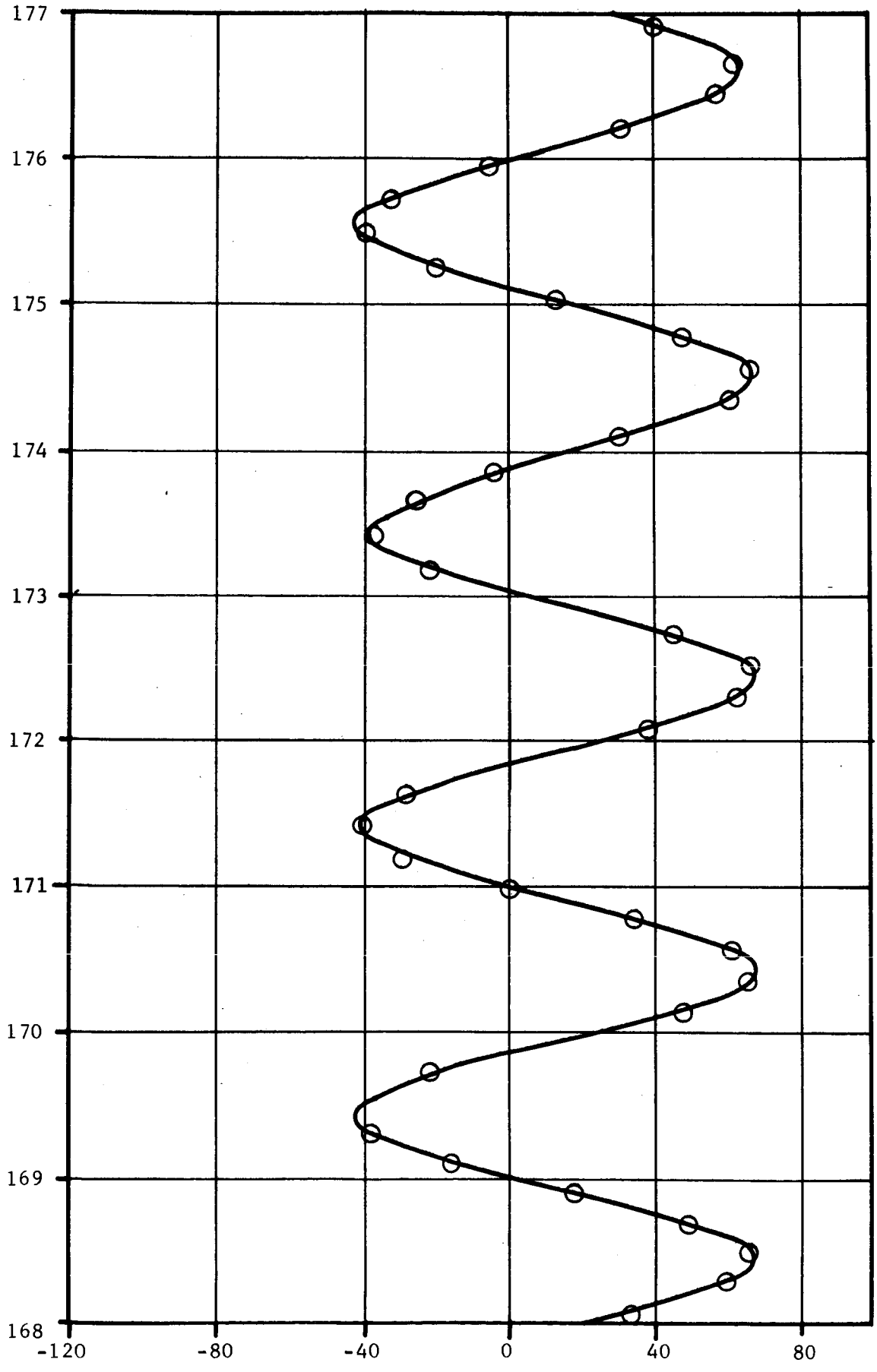

Figure 8h. (Page 8 of 10)

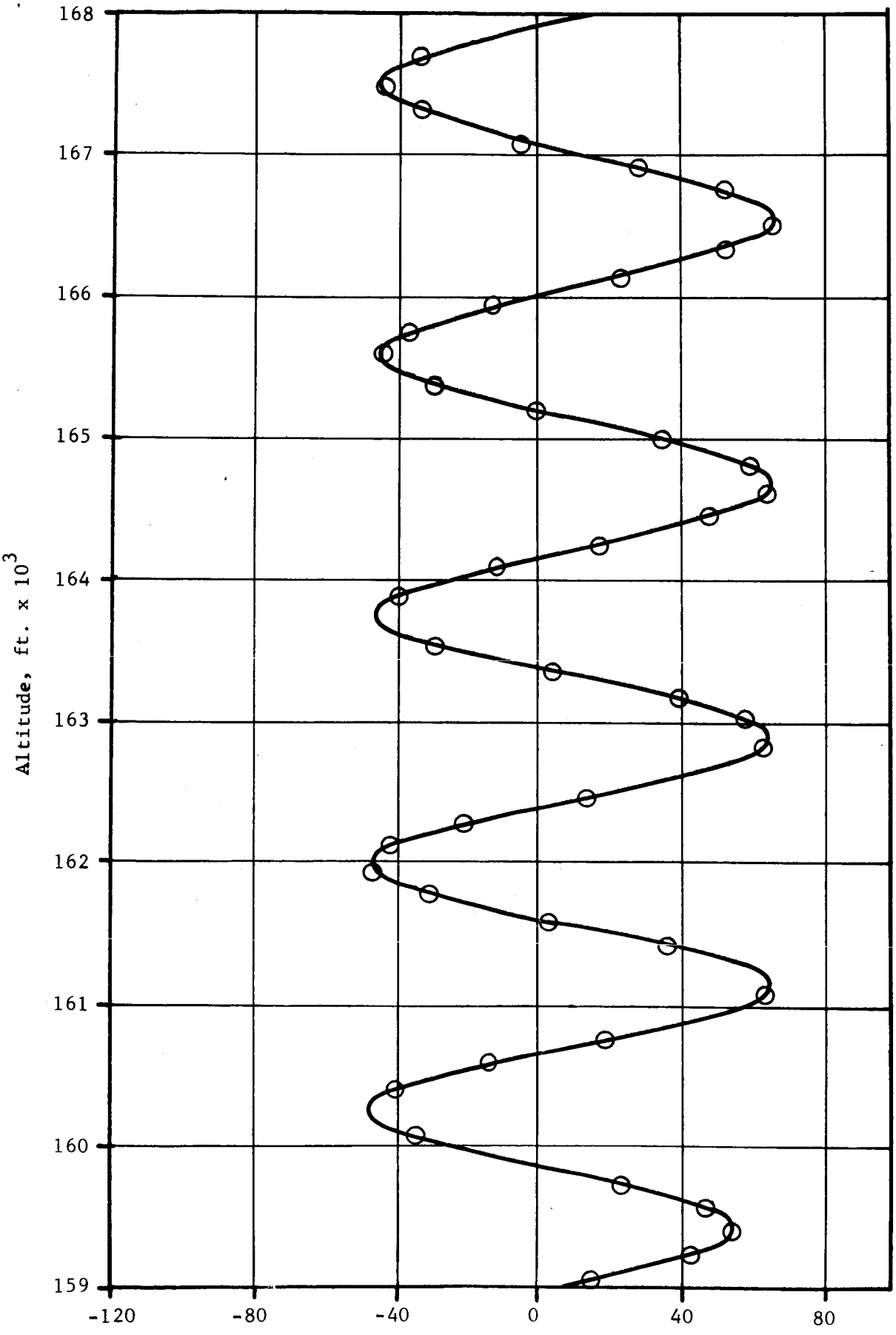

Figure 8h. (Page 9 of 10)

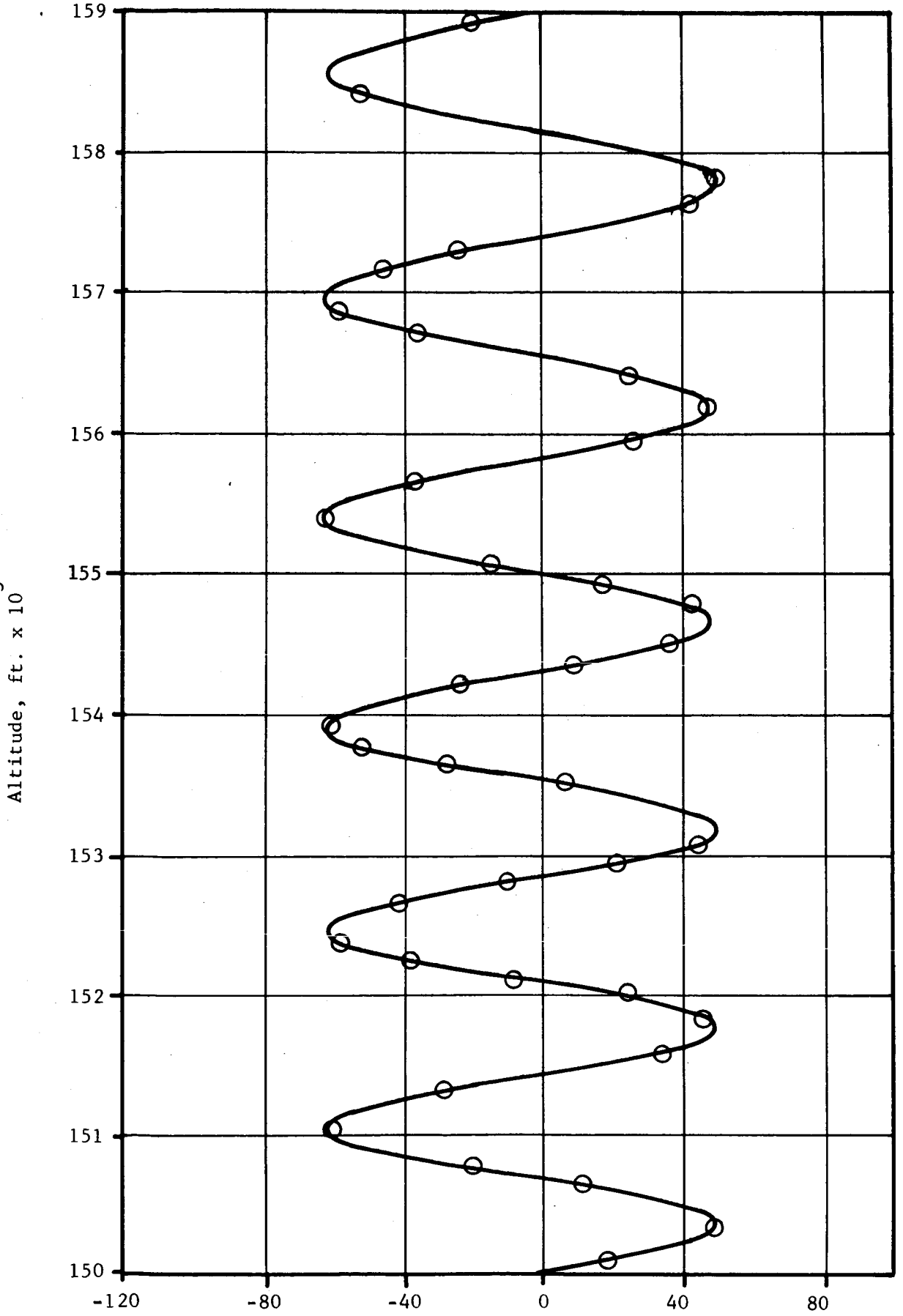

Figure 8h. (Page 10 of 10)

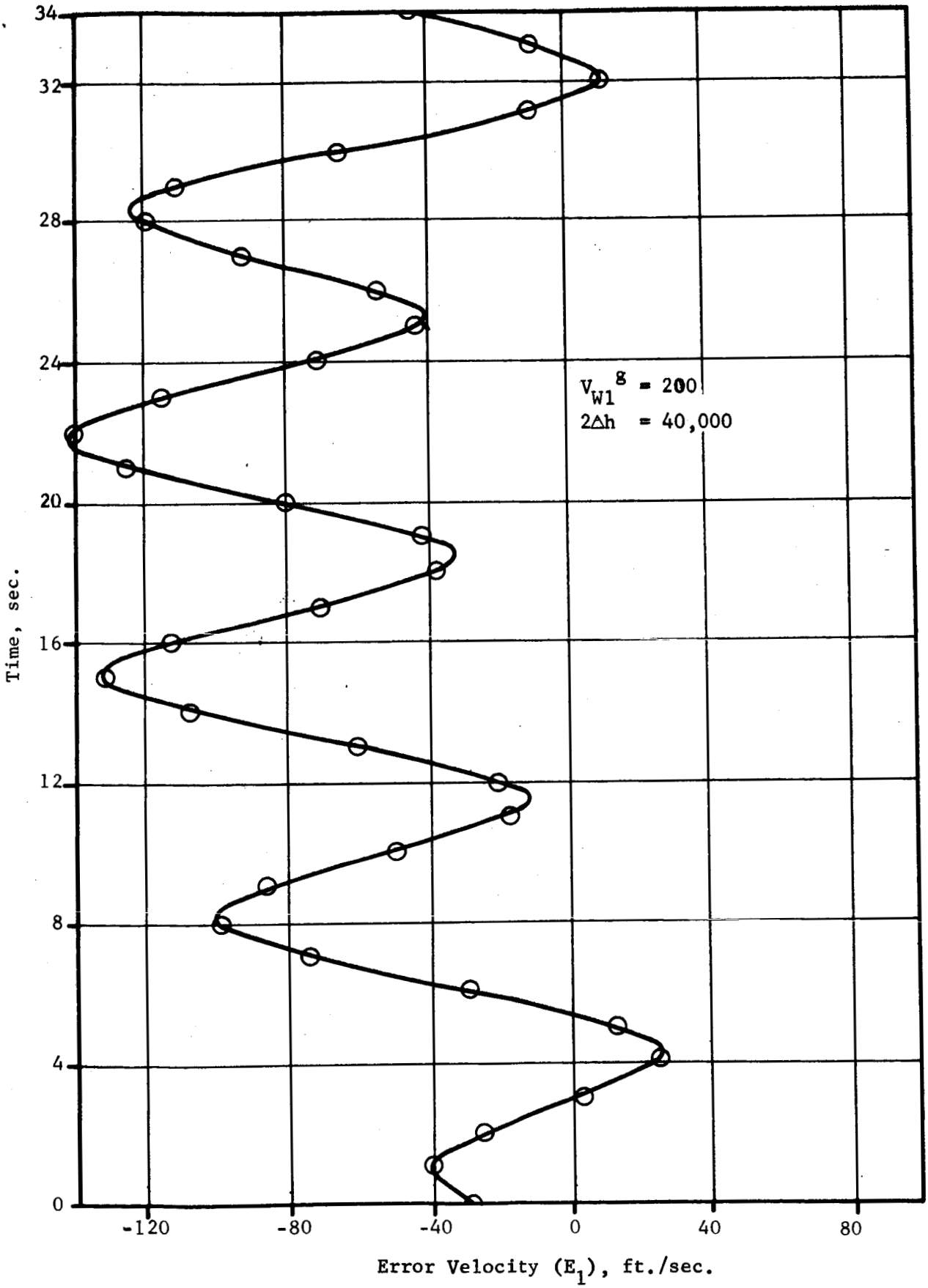

Figure 8i. Error Velocity vs. Time for Hemispherical Parachute

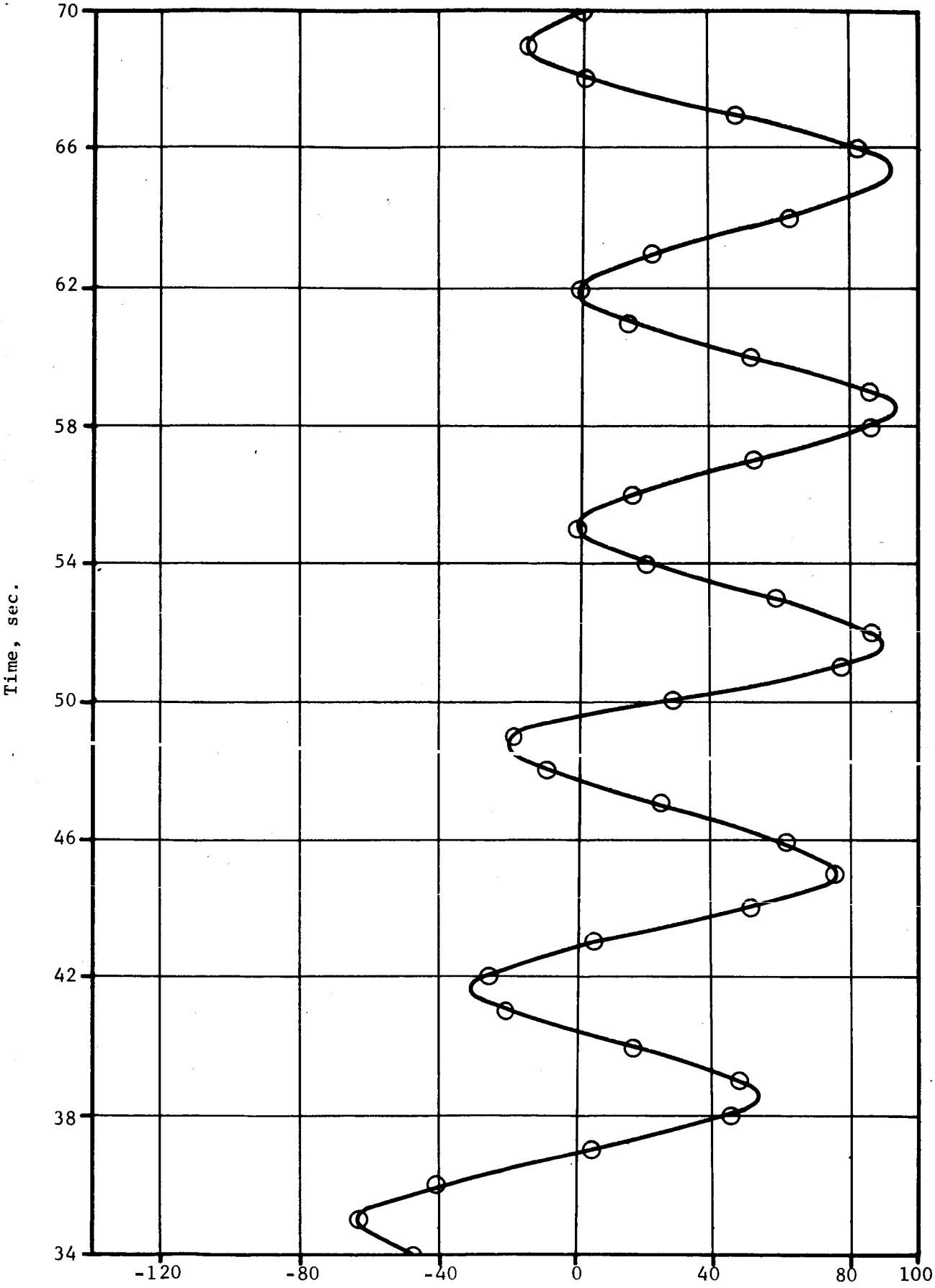

Figure 8i. (Page 2 of 9)

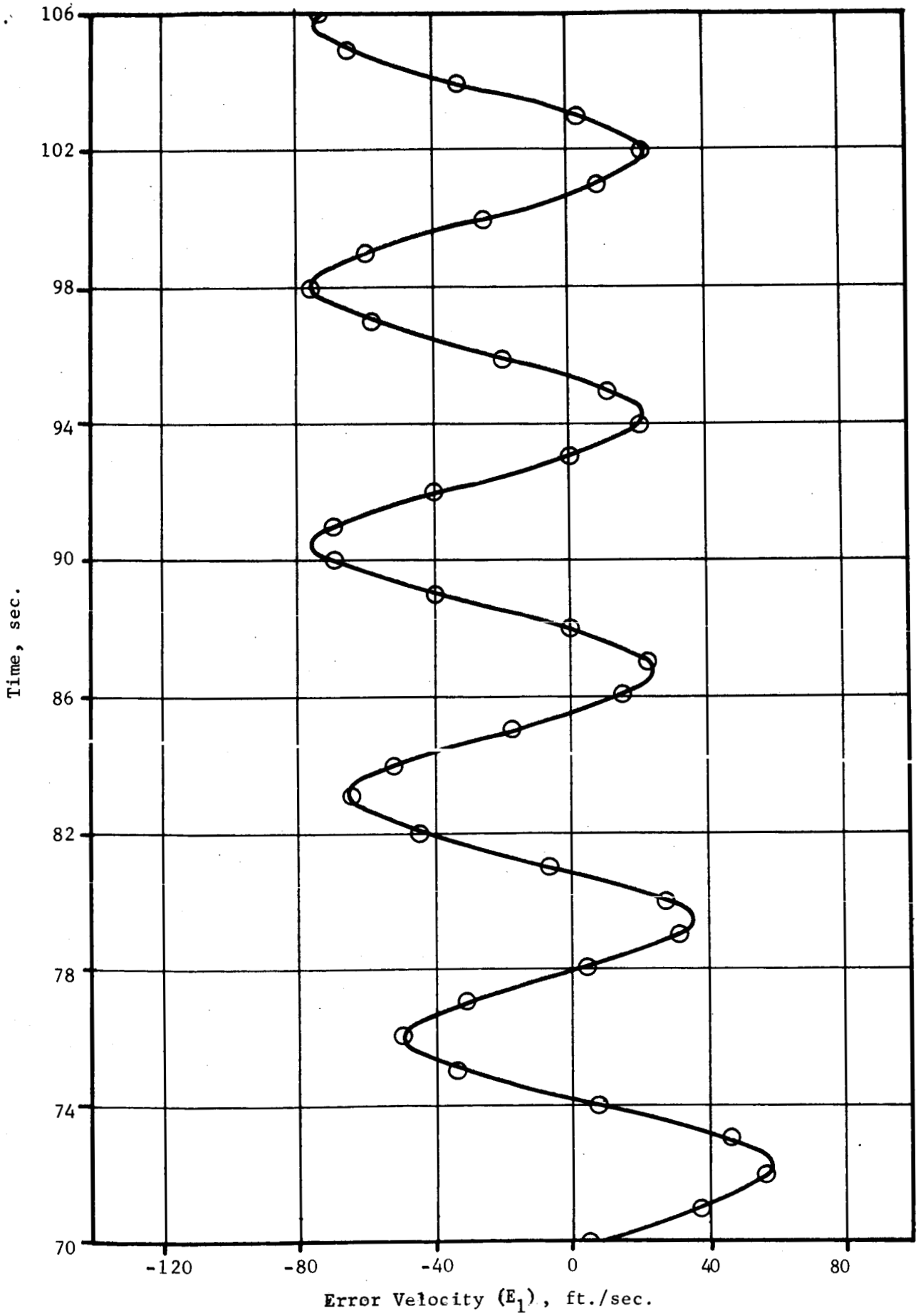

Figure 8i. (Page 3 of 9)

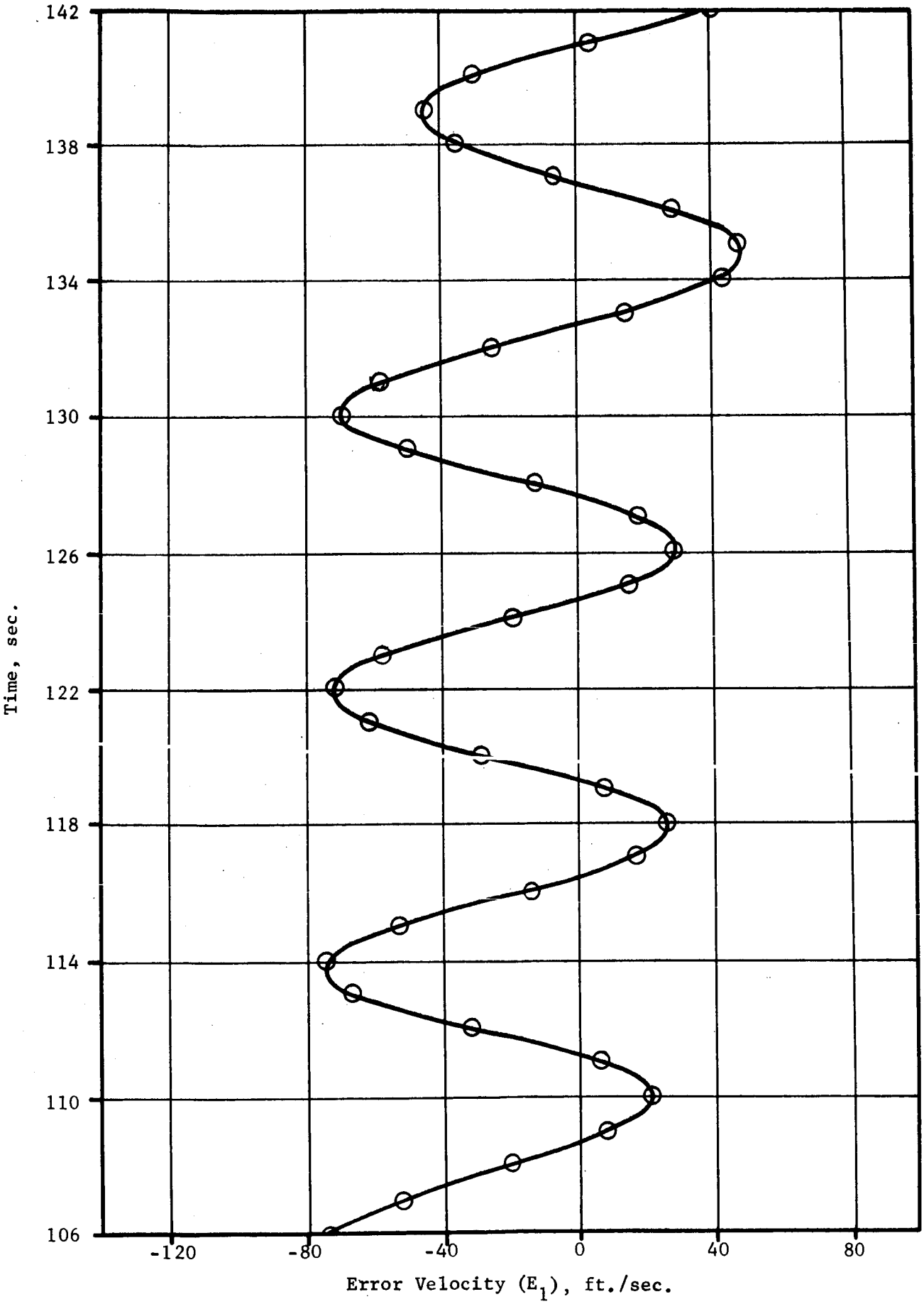

Figure 8i. (Page 4 of 9)

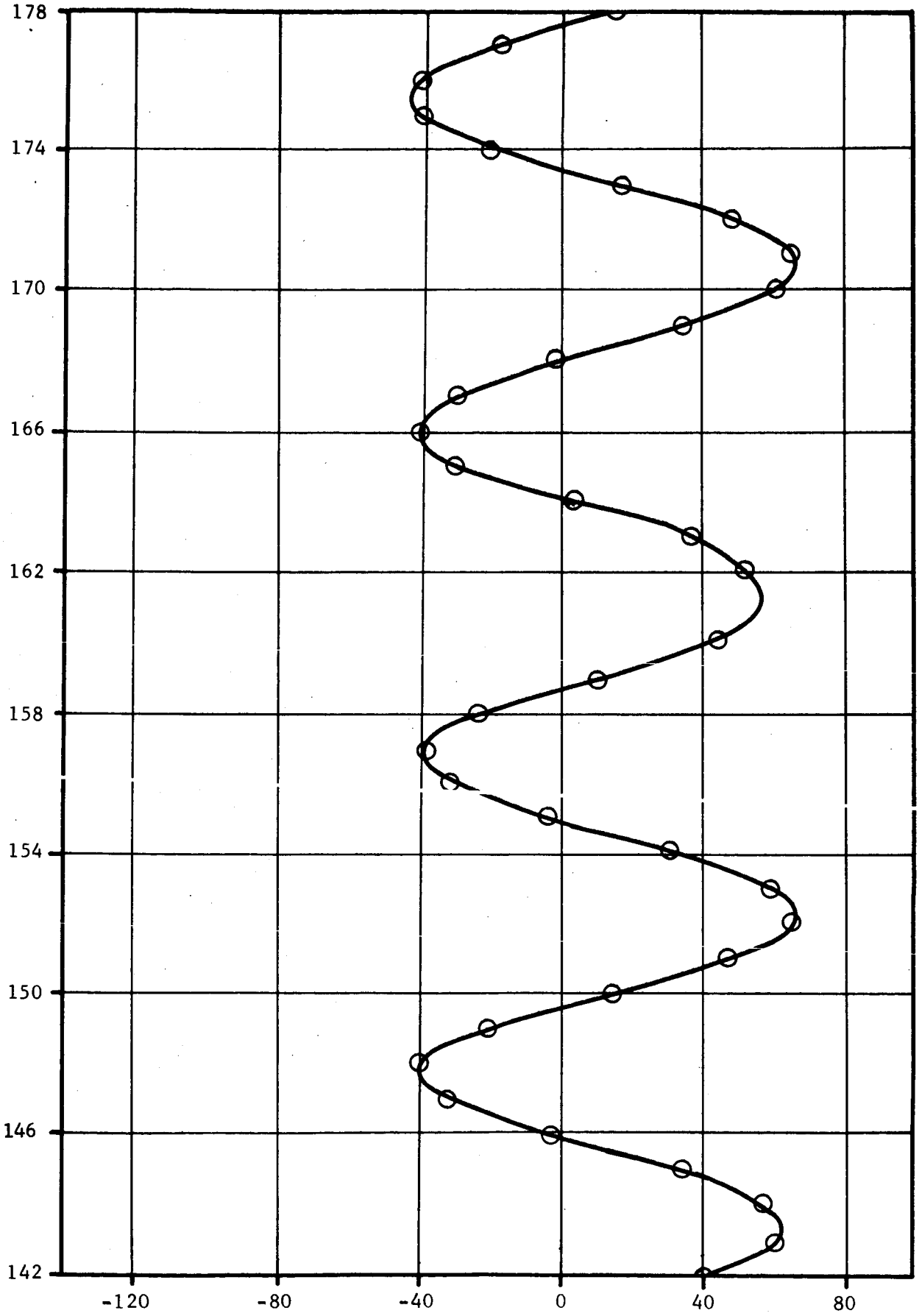

Figure 8i. (Page 5 of 9)

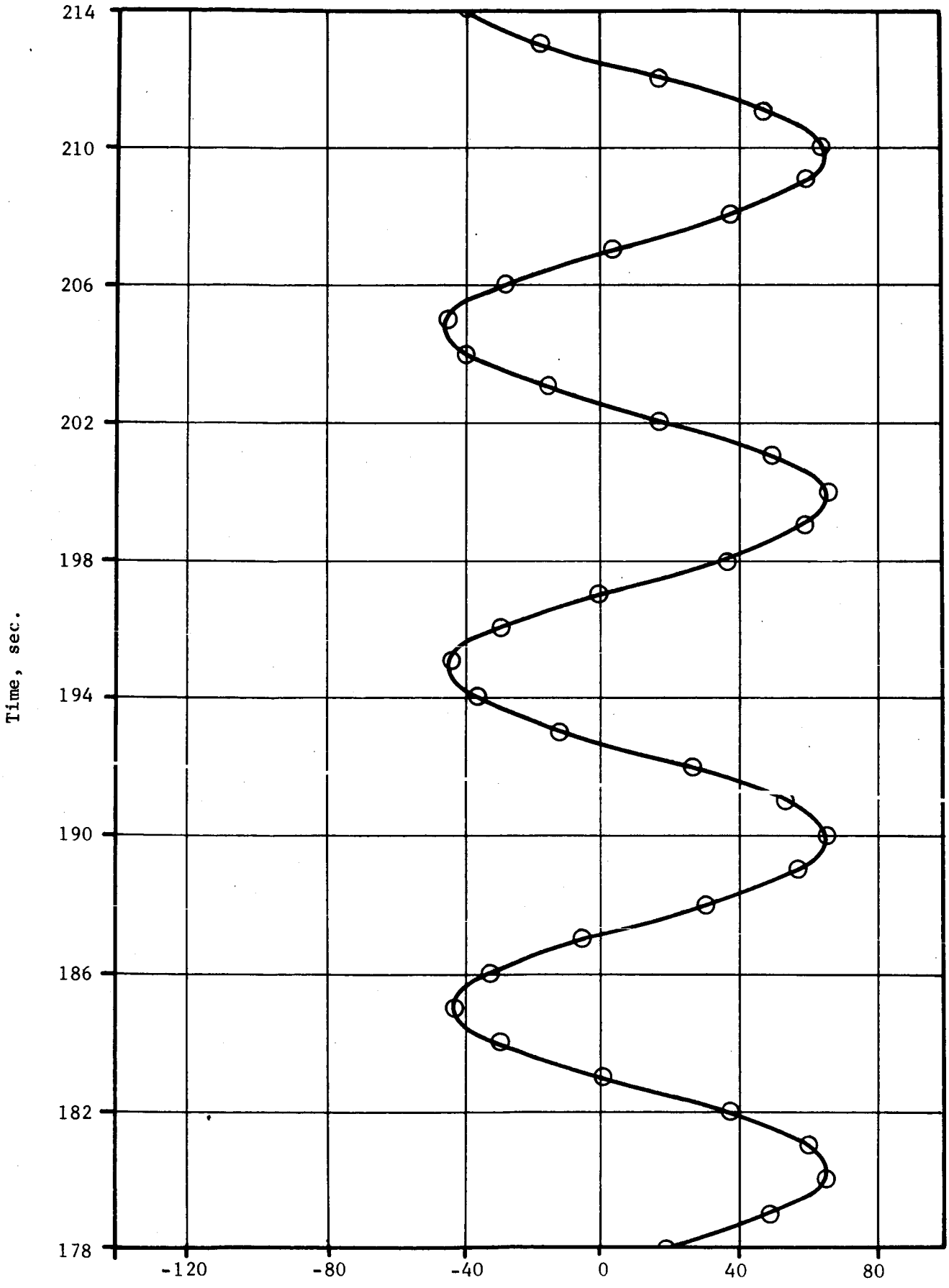

Figure 8i. (Page 6 of 9)

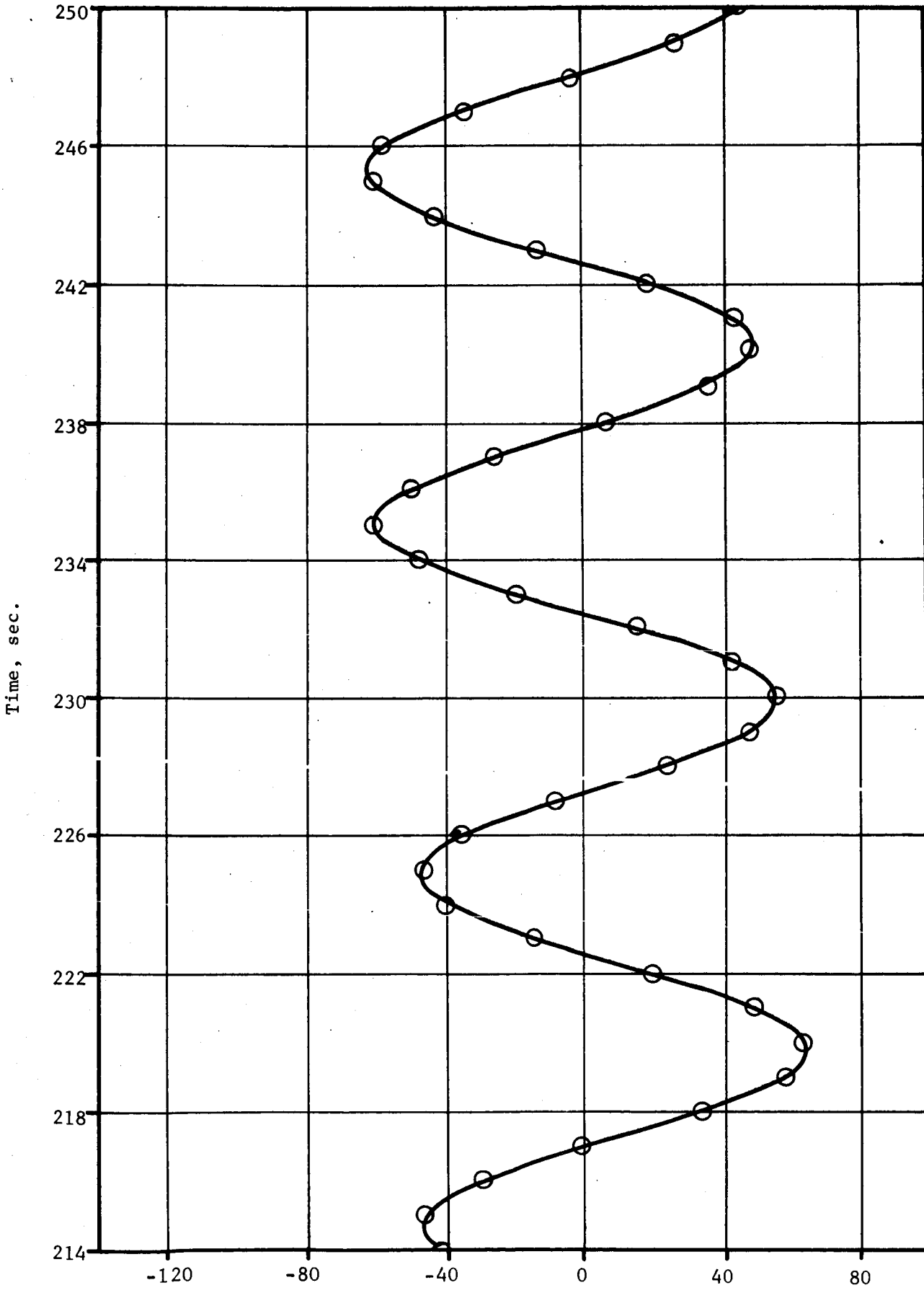

Figure 8i. (Page 7 of 9)

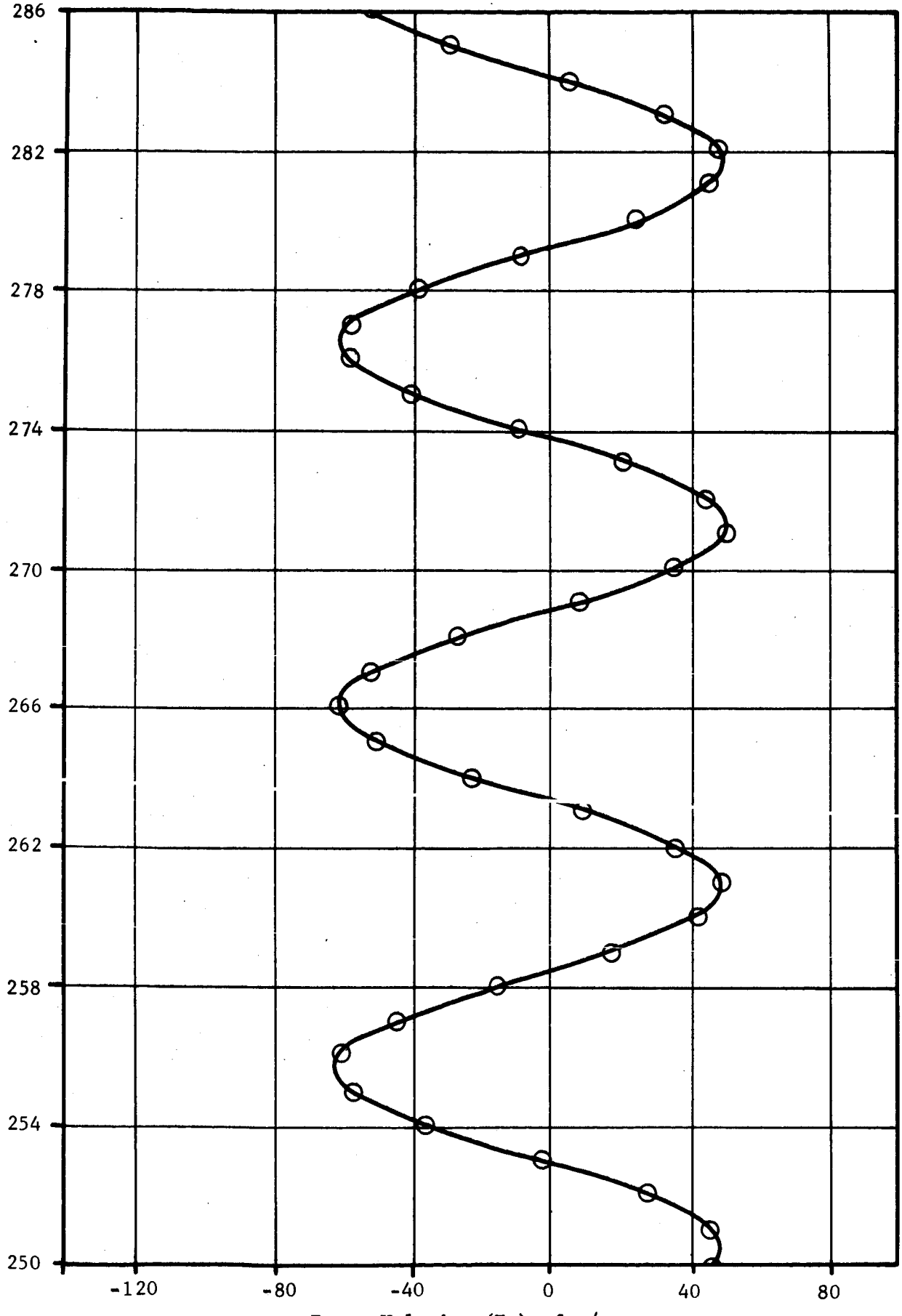

Figure 8i. (Page 8 of 9)

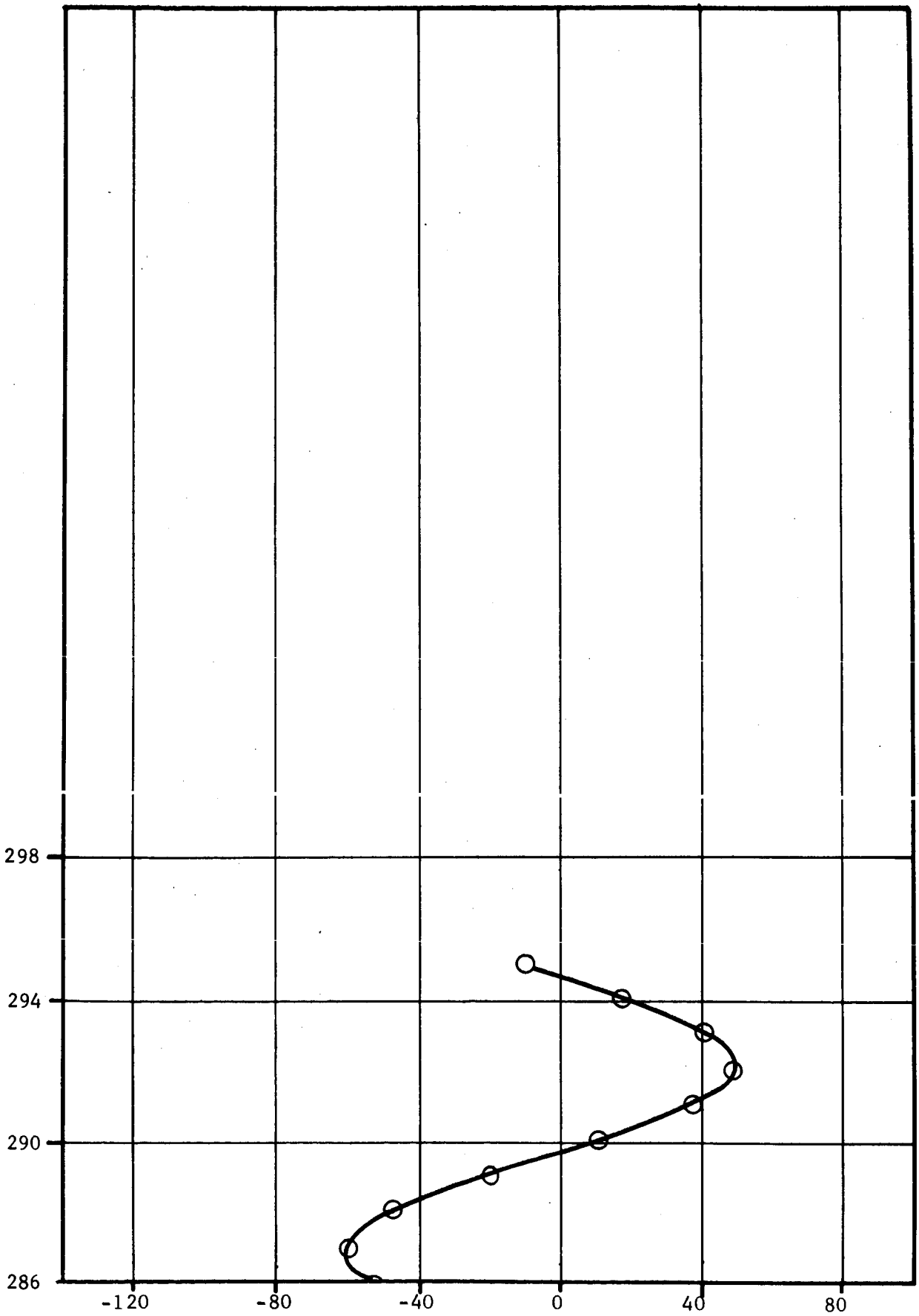

Figure 8i. (Page 9 of 9)

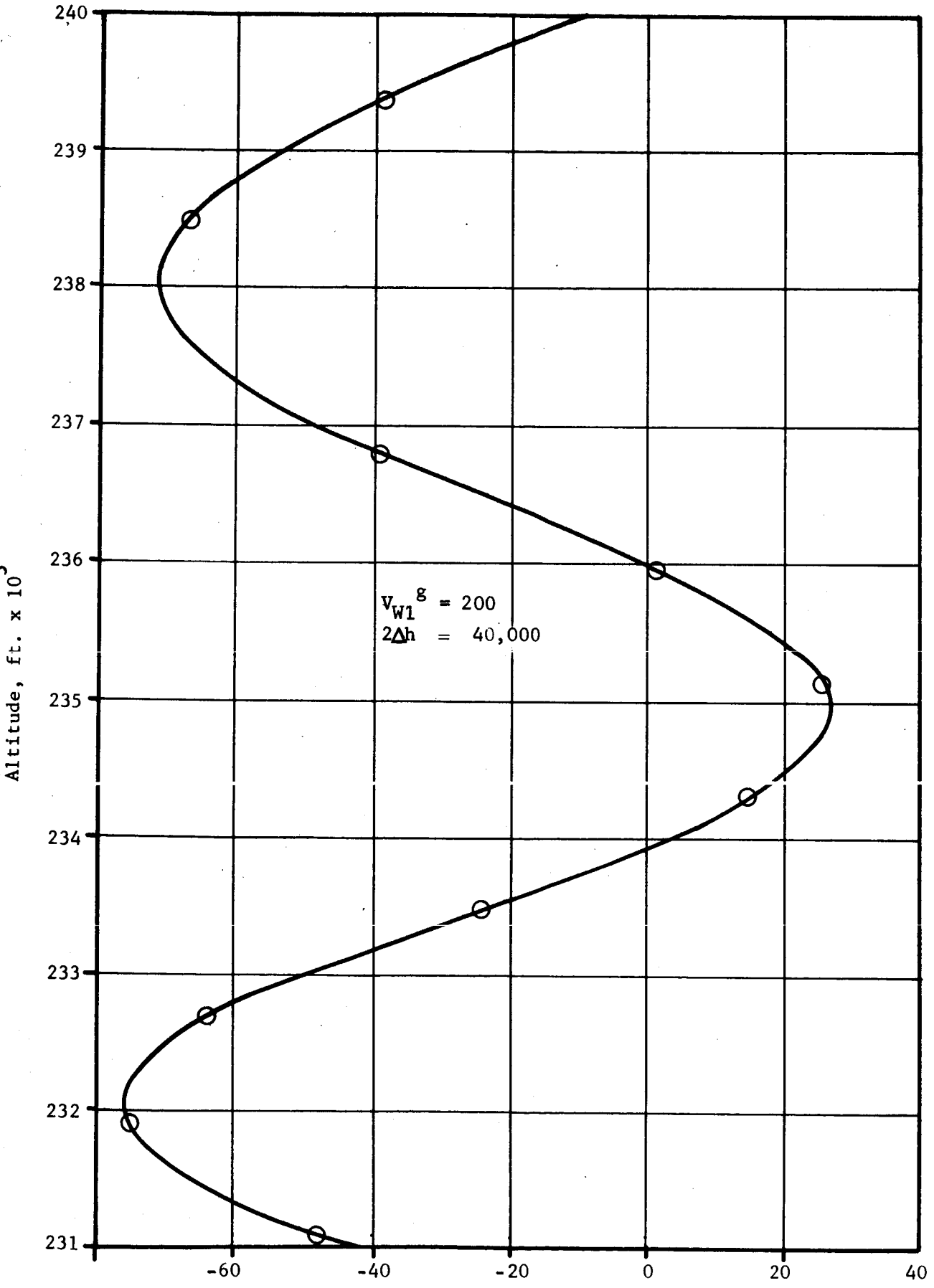

Figure 8j. Error Velocity vs. Altitude for Hemispherical Parachute

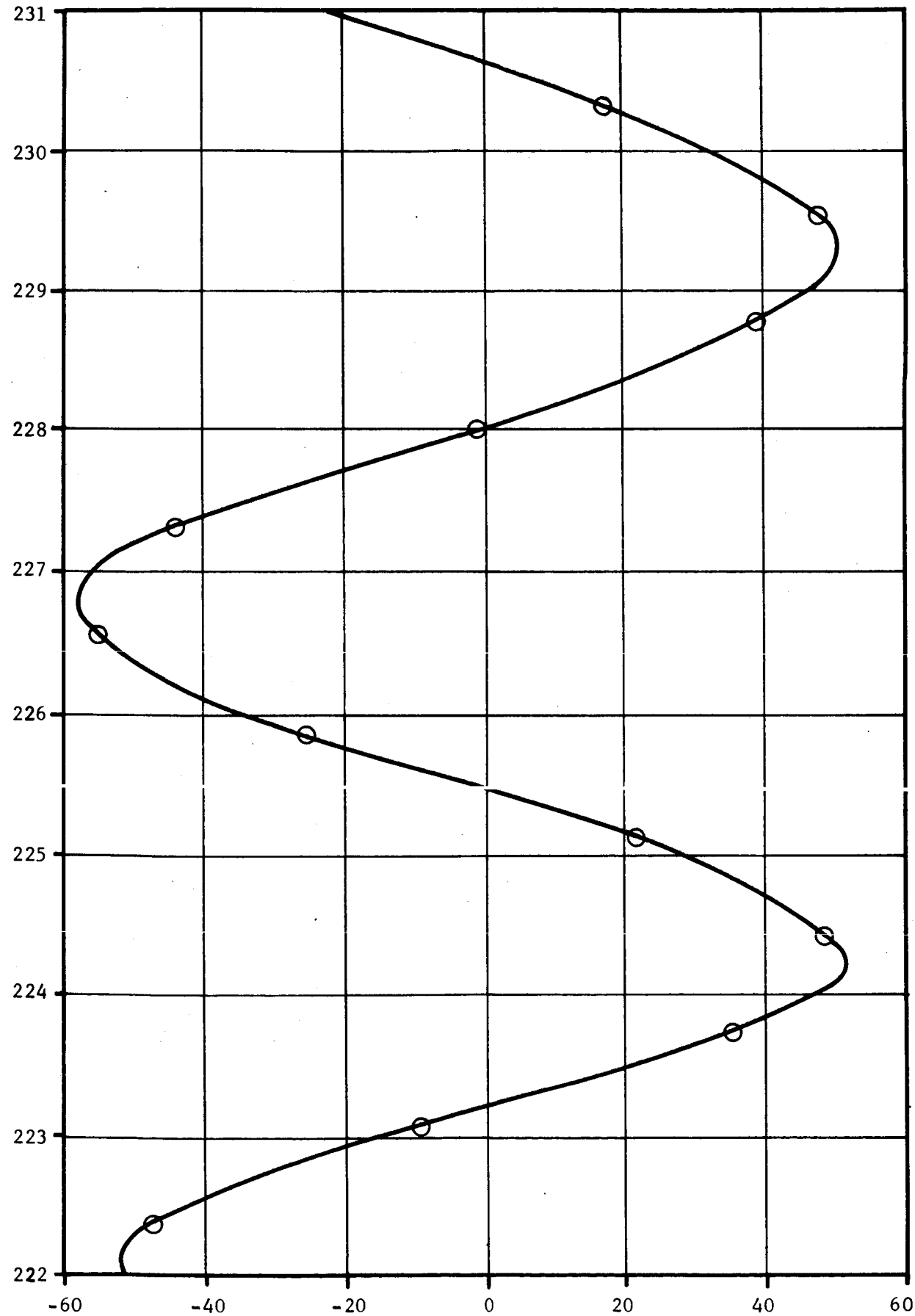

Figure 8j. (Page 2 of 10)

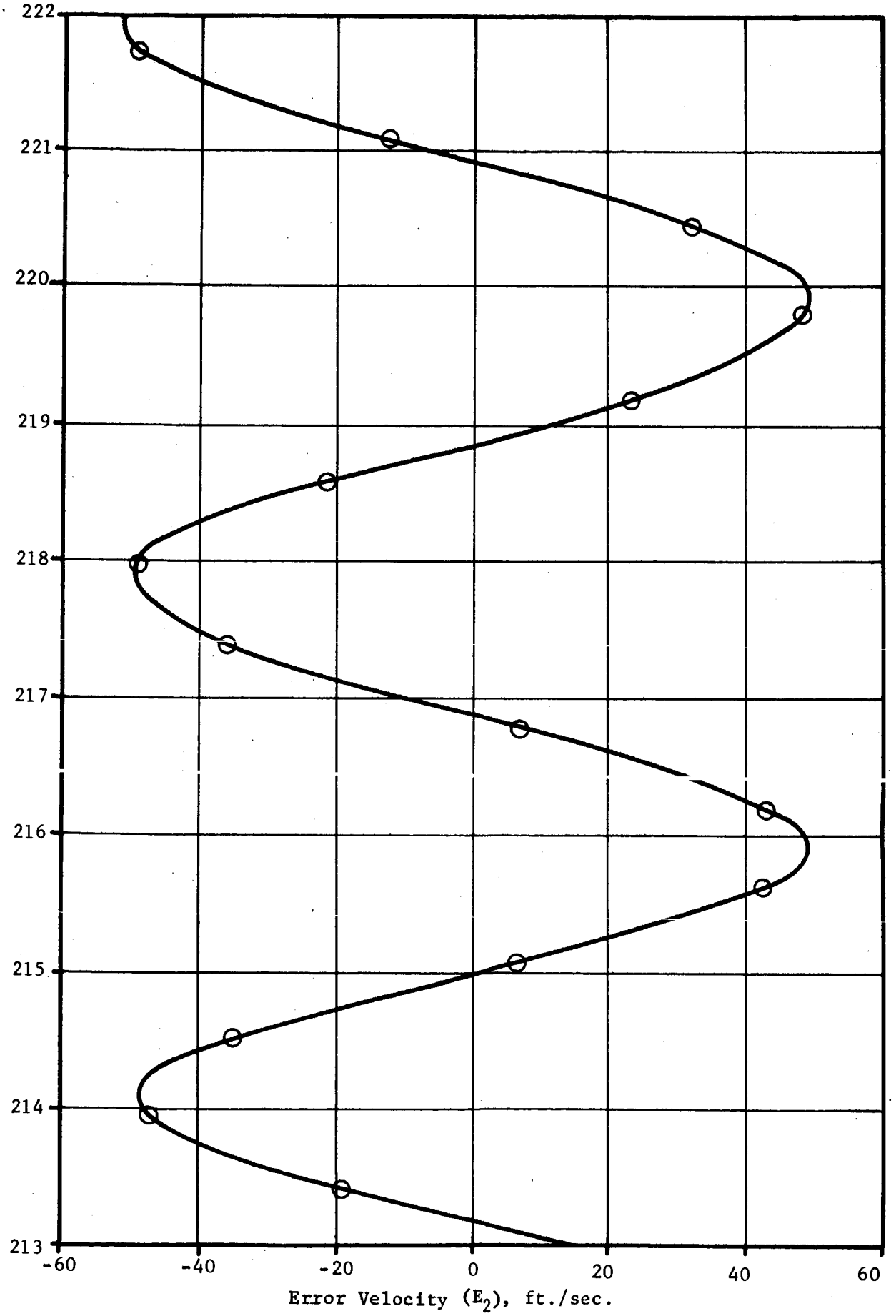

Figure 8j. (Page 3 of 10)

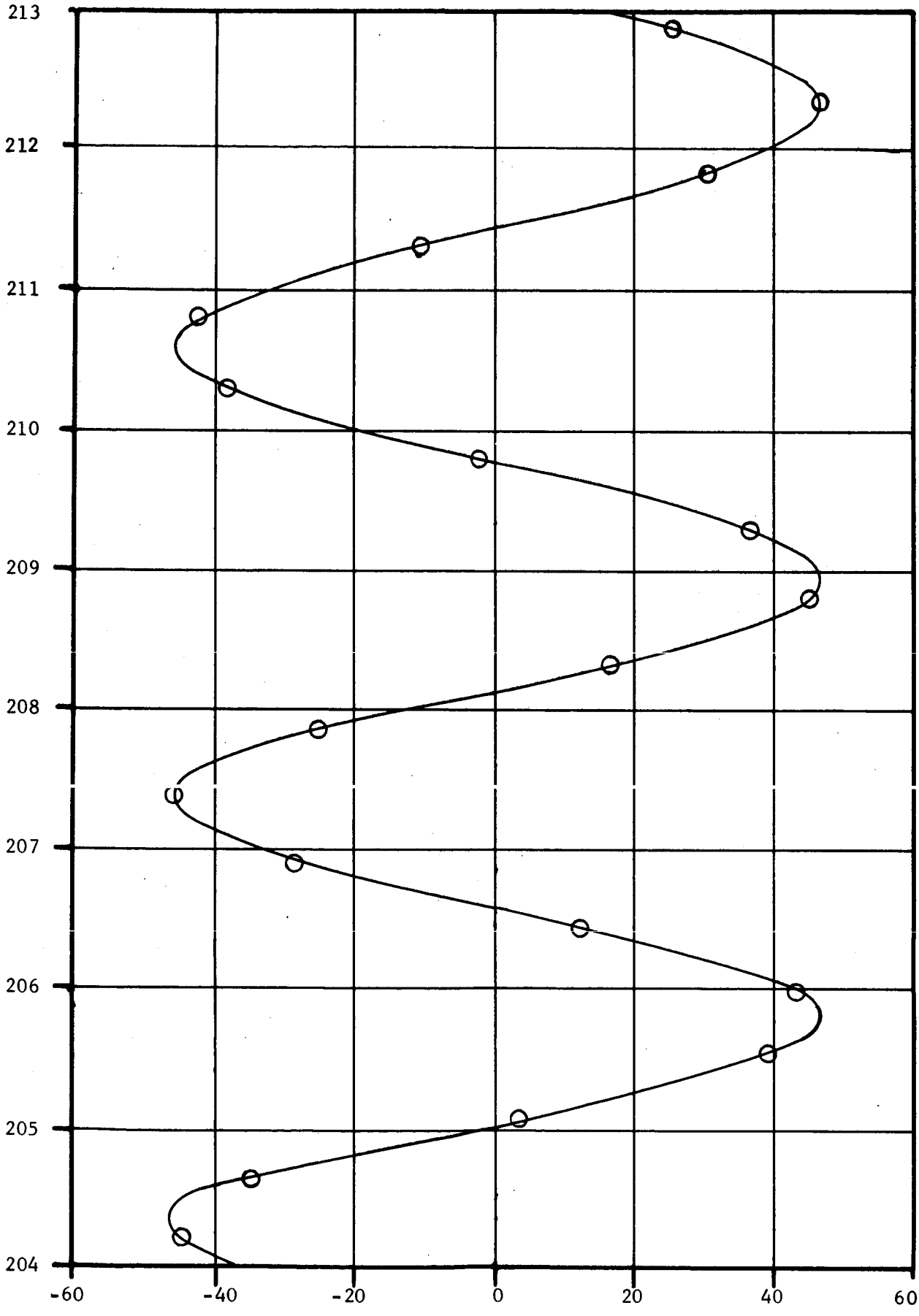

Figure 8j. (Page 4 of 10)

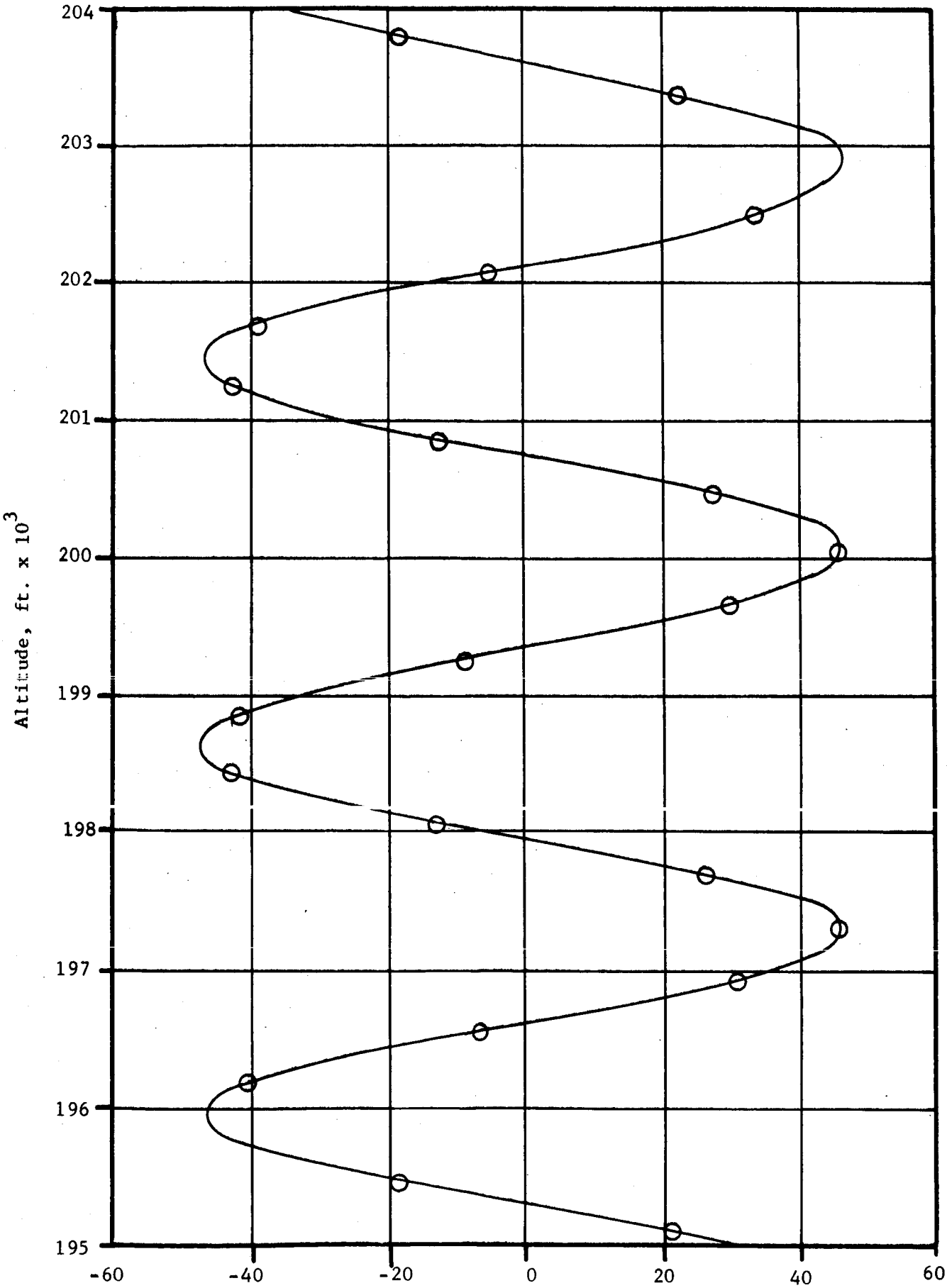

Figure 8j. (Page 5 of 10)

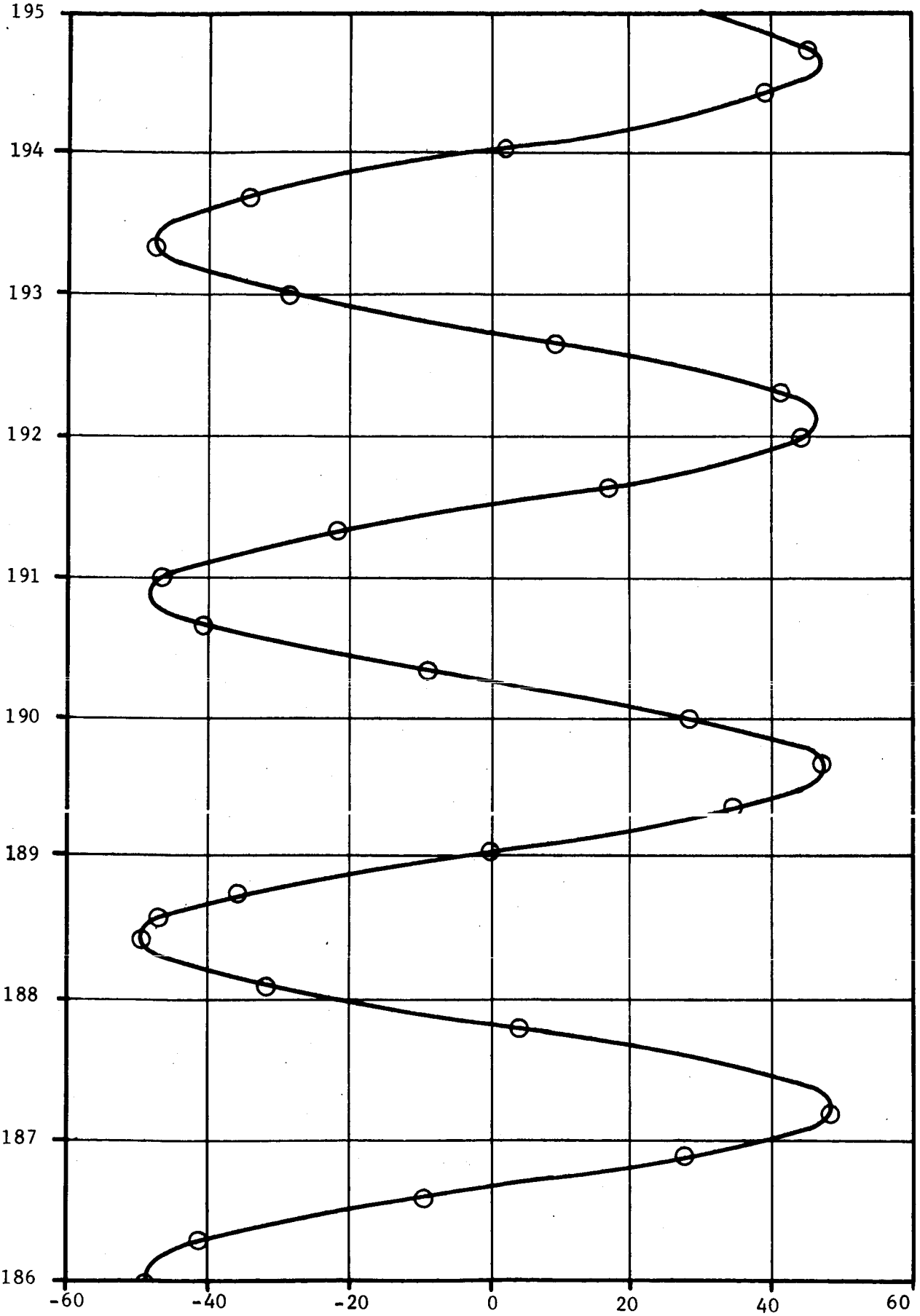

Figure 8j. (Page 6 of 10)

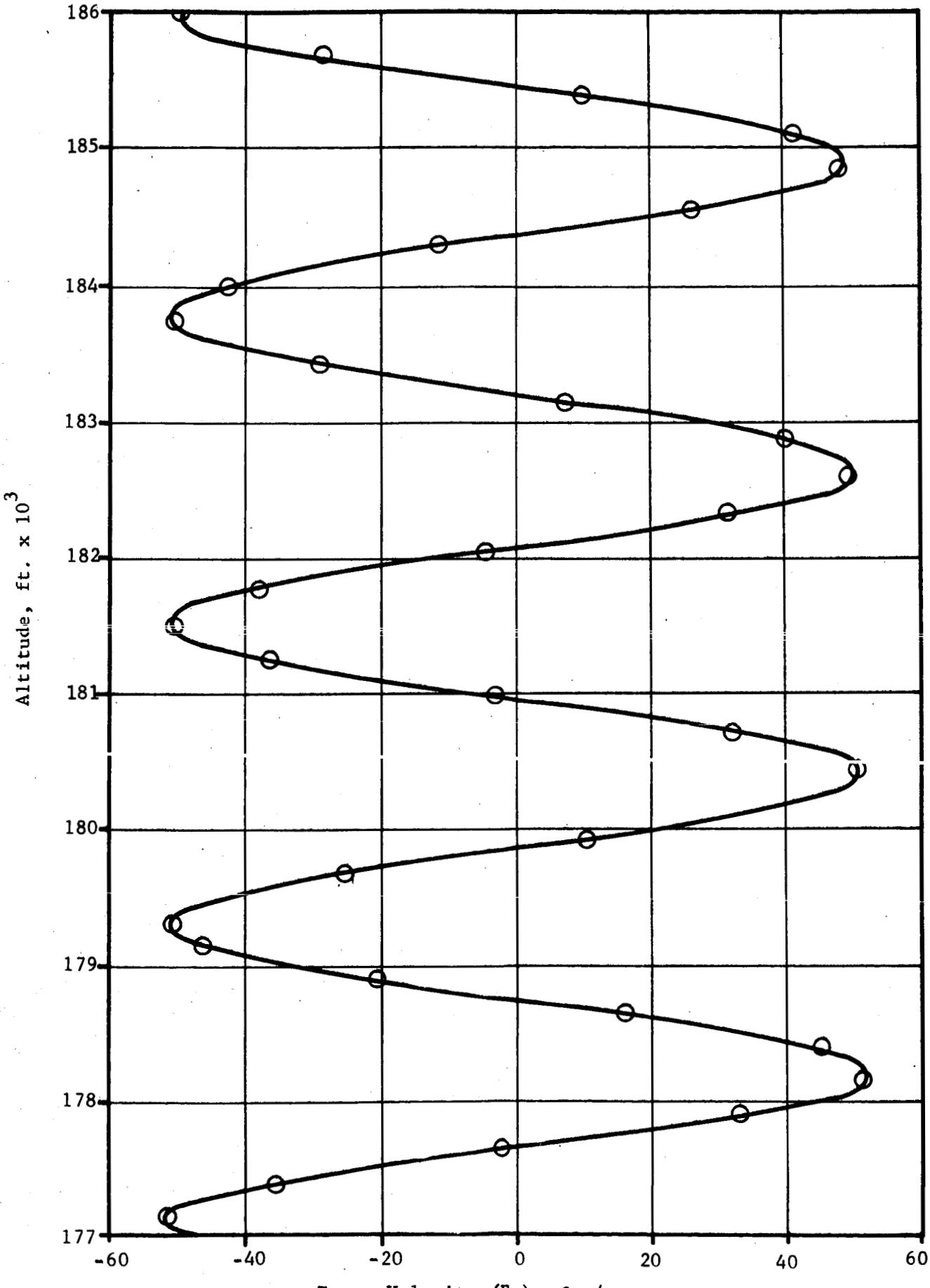

Figure 8j. (Page 7 of 10)

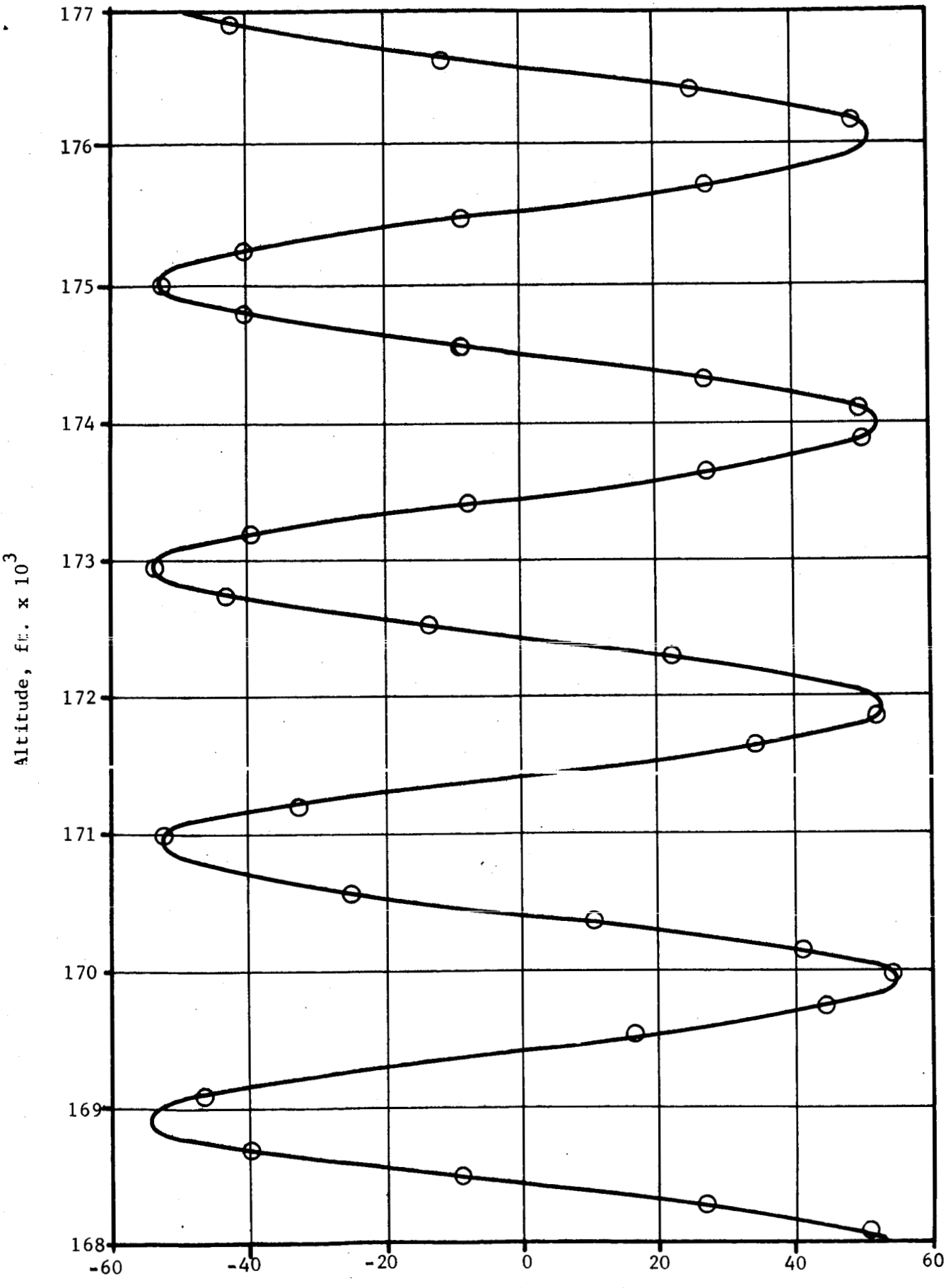

Figure 8j. (Page 8 of 10)

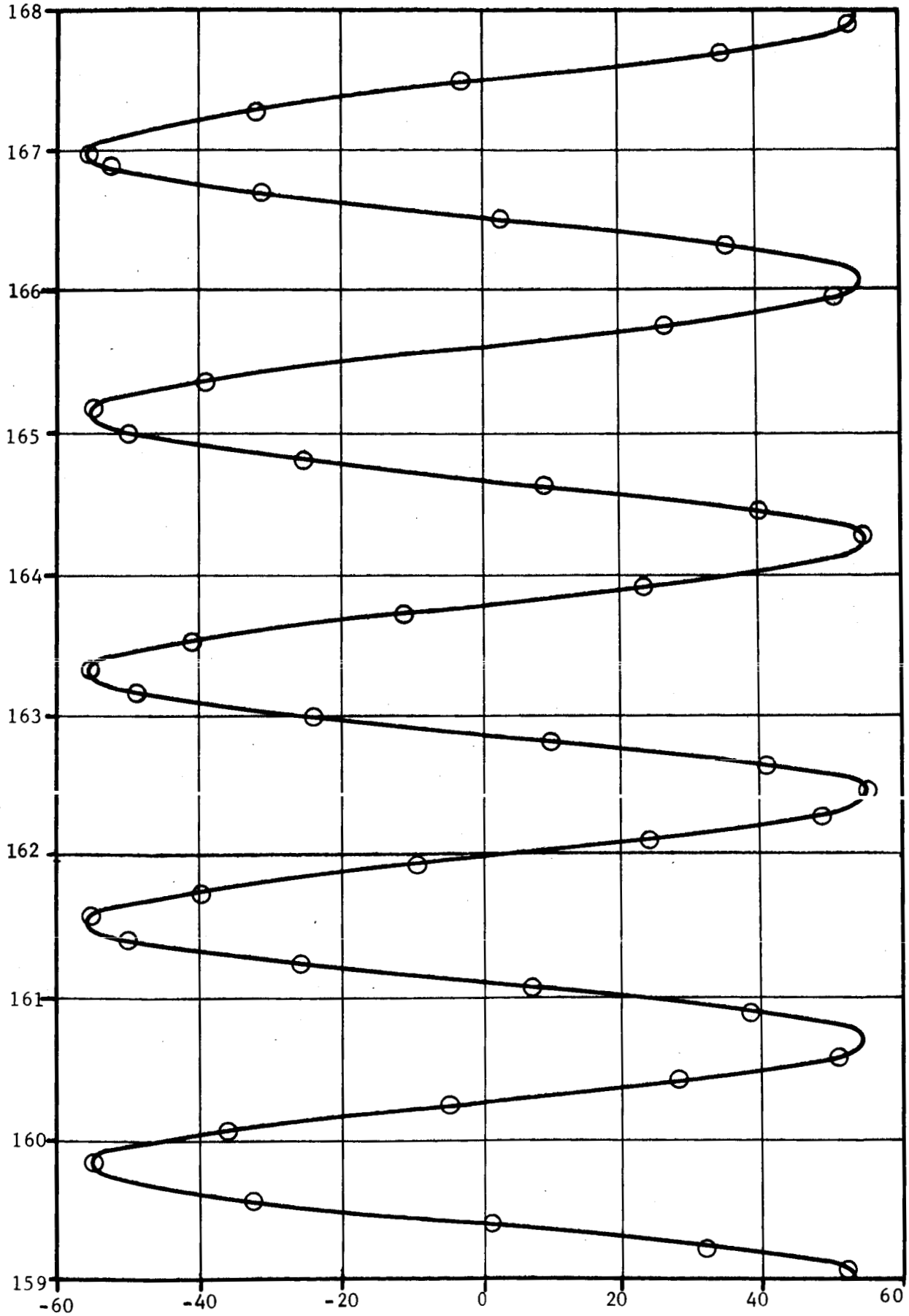

Figure 8j. (Page 9 of 10)

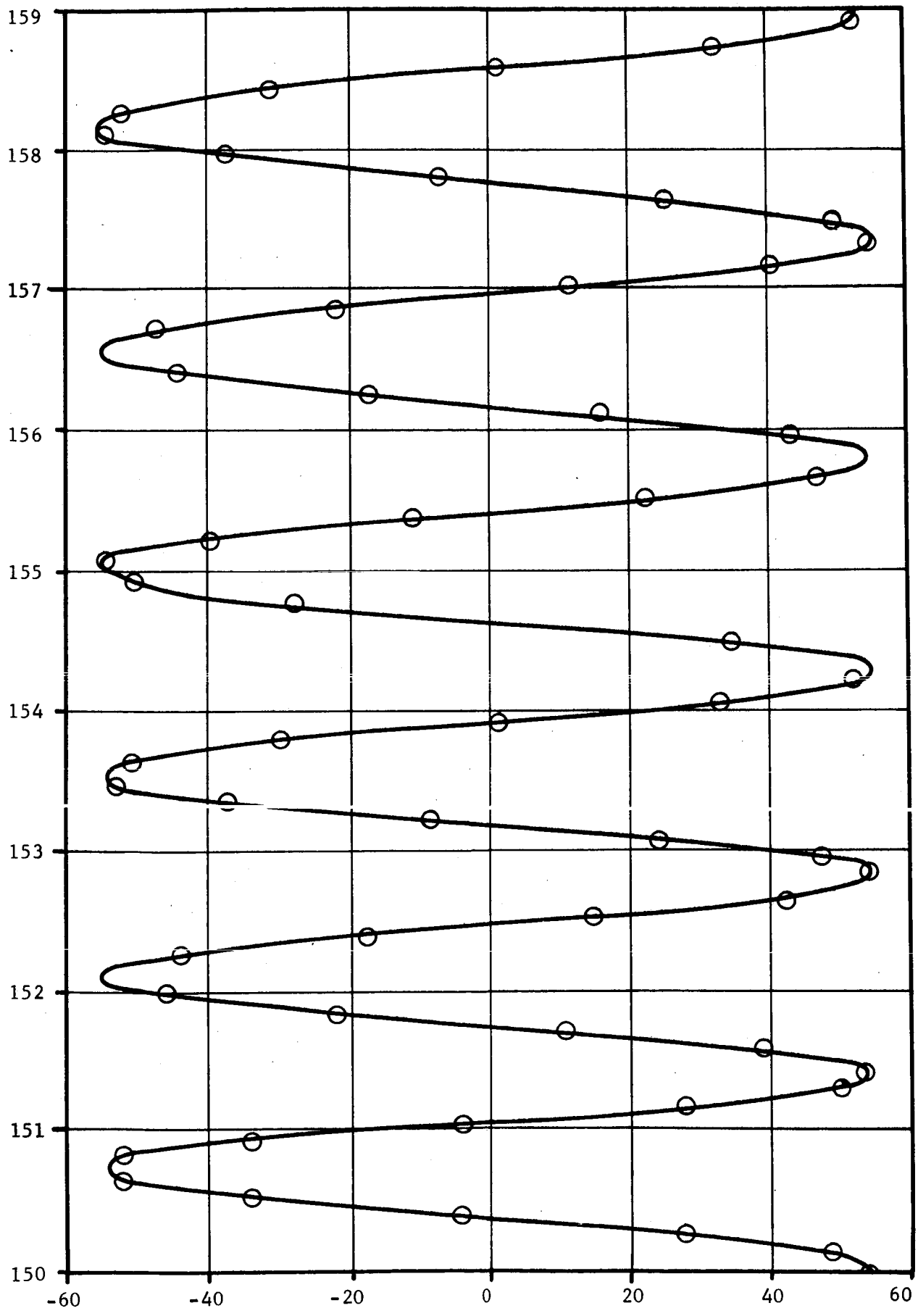

Figure 8j. (Page 10 of 10)

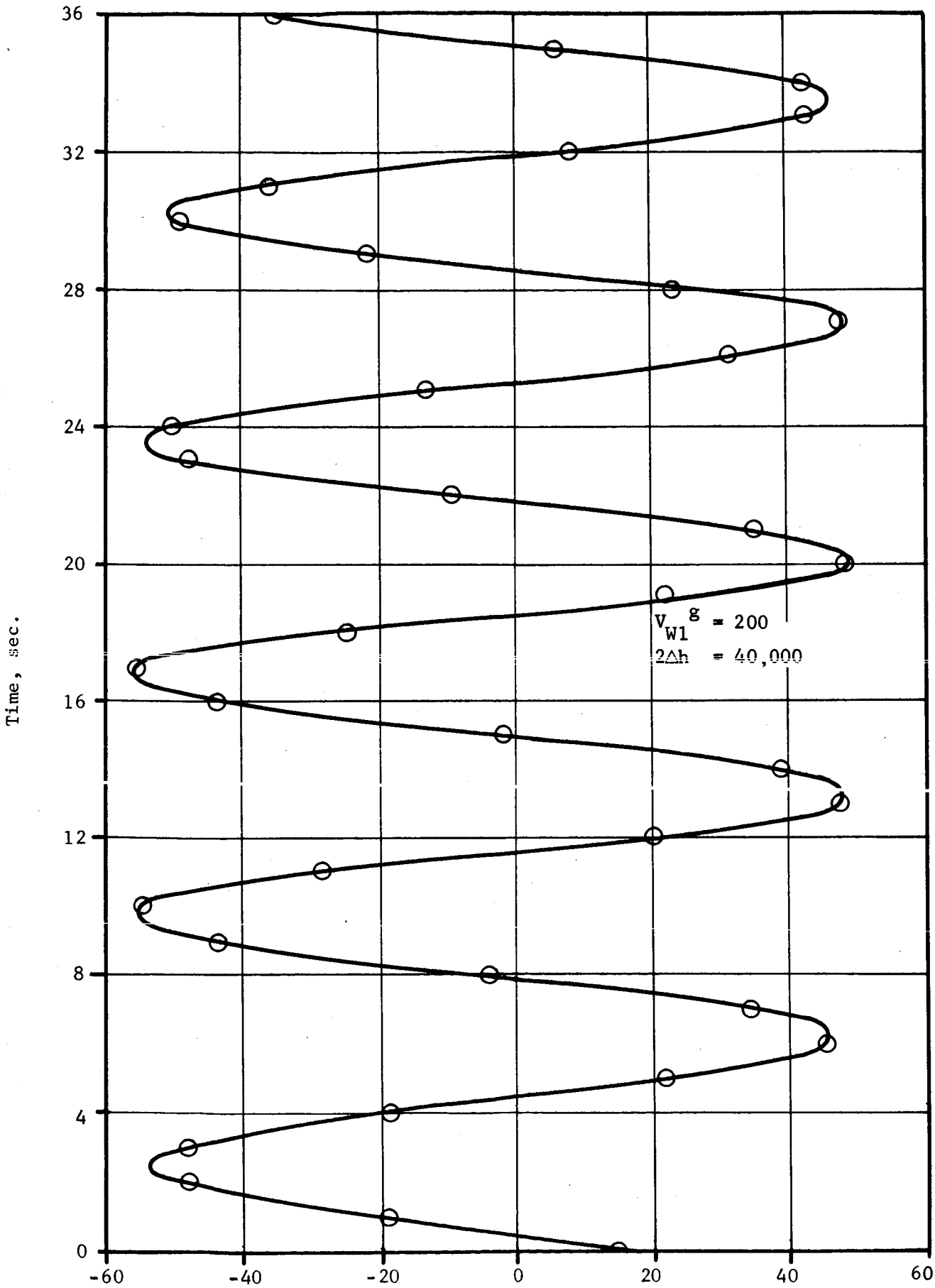

Figure 8k. Error Velocity vs. Time for Hemispherical Parachute

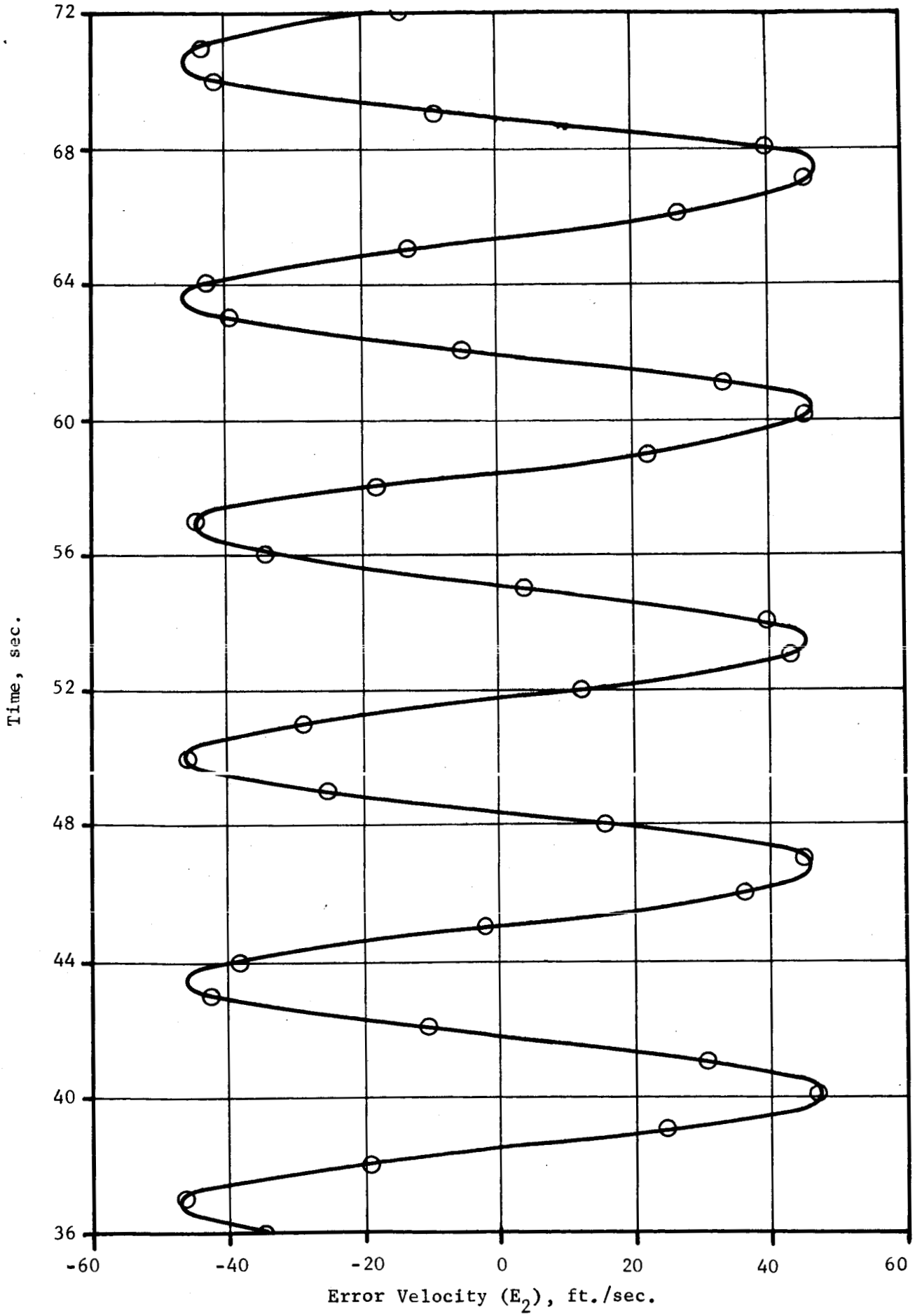

Figure 8k. (Page 2 of 9)

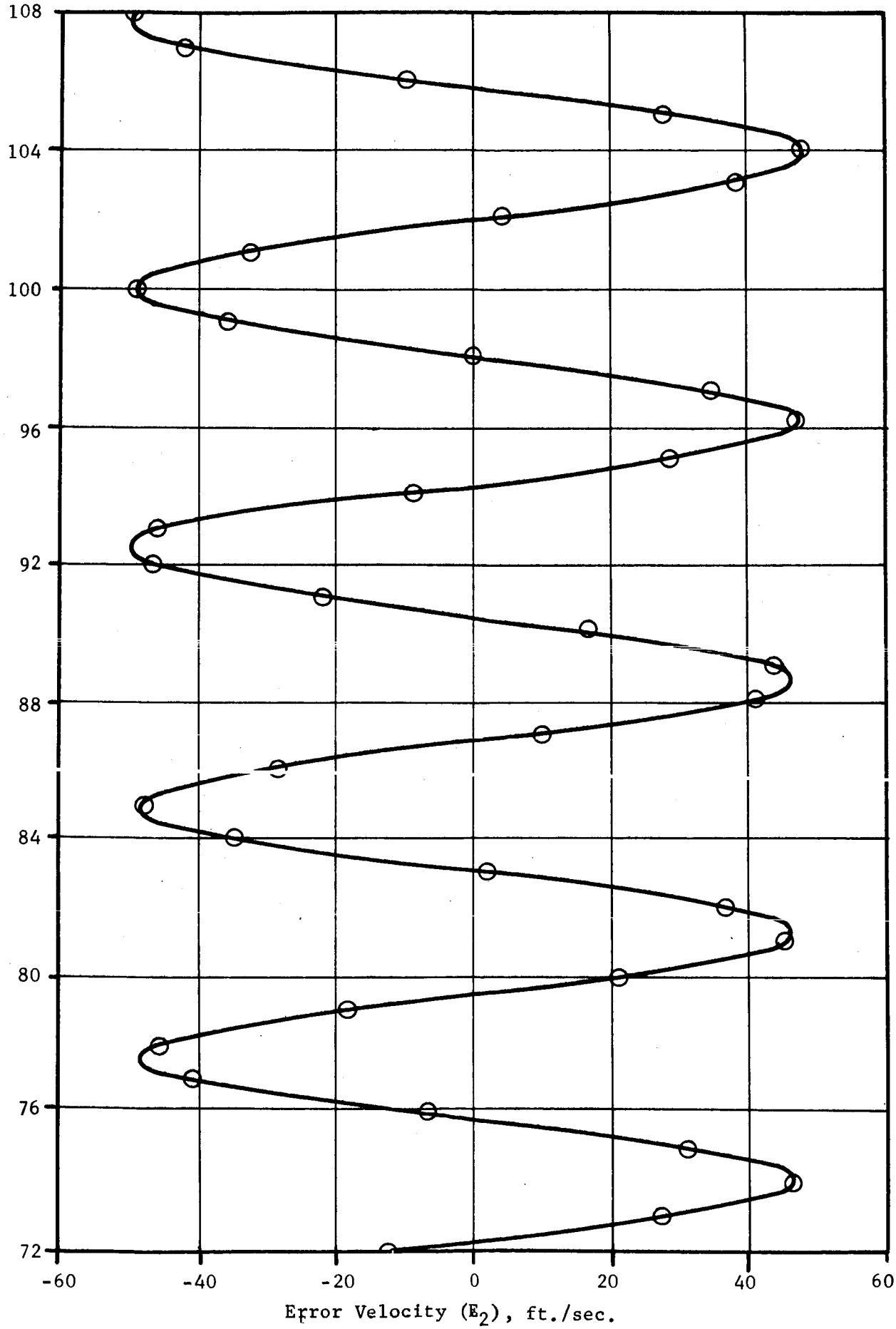

Figure 8k. (Page 3 of 9)

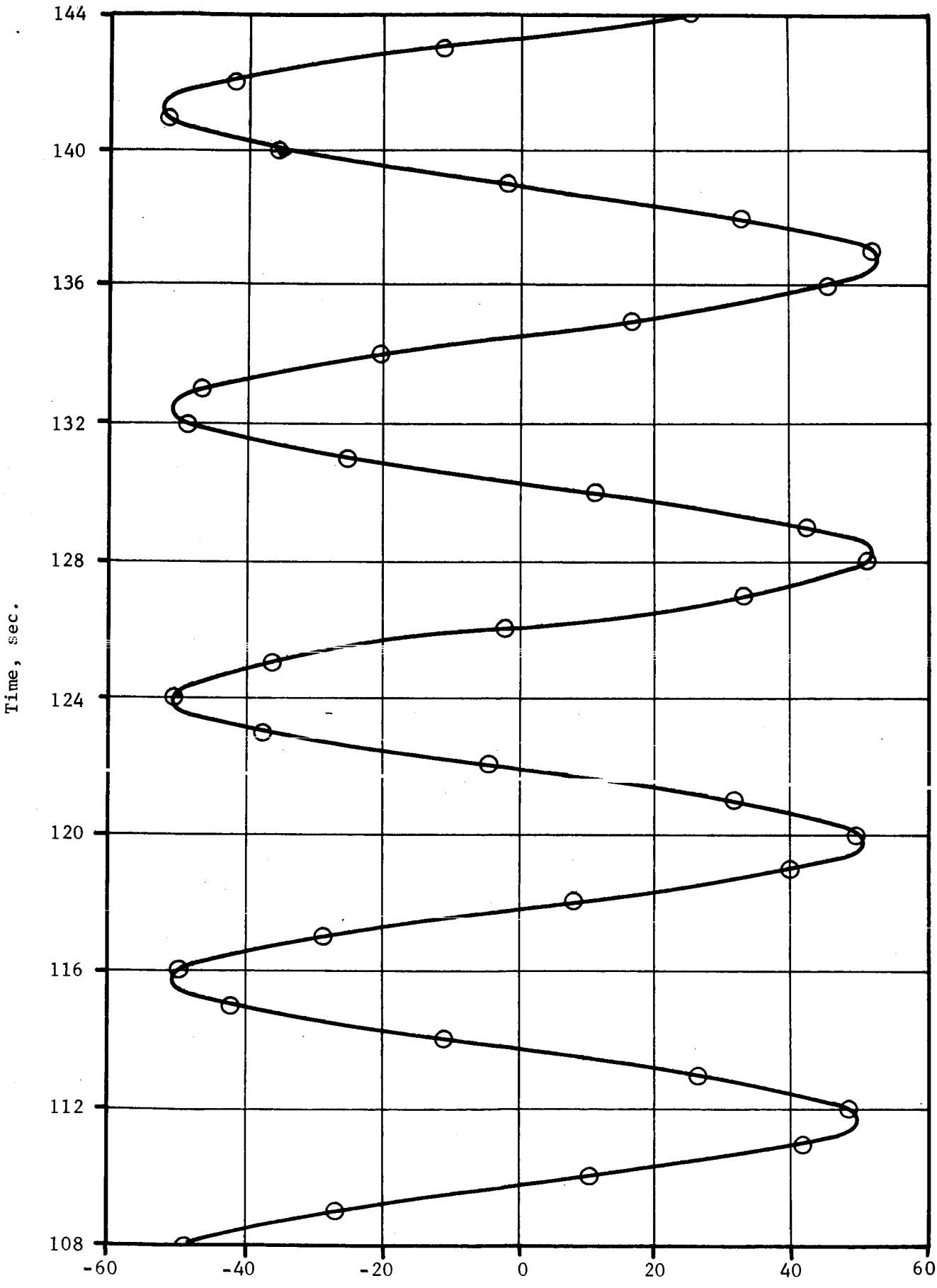

Figure 8k. (Page 4 of 9)

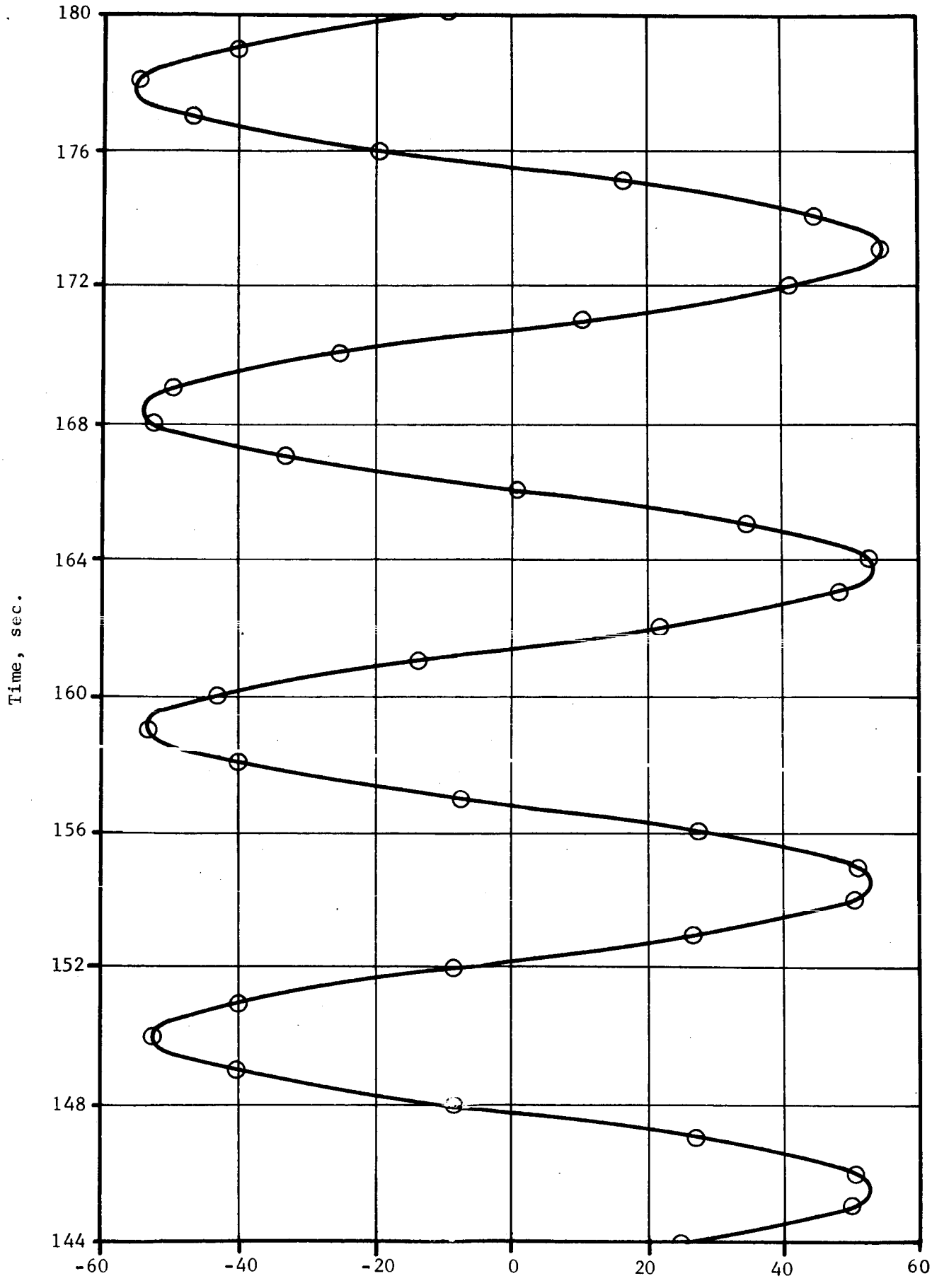

Figure 8k. (Page 5 of 9)

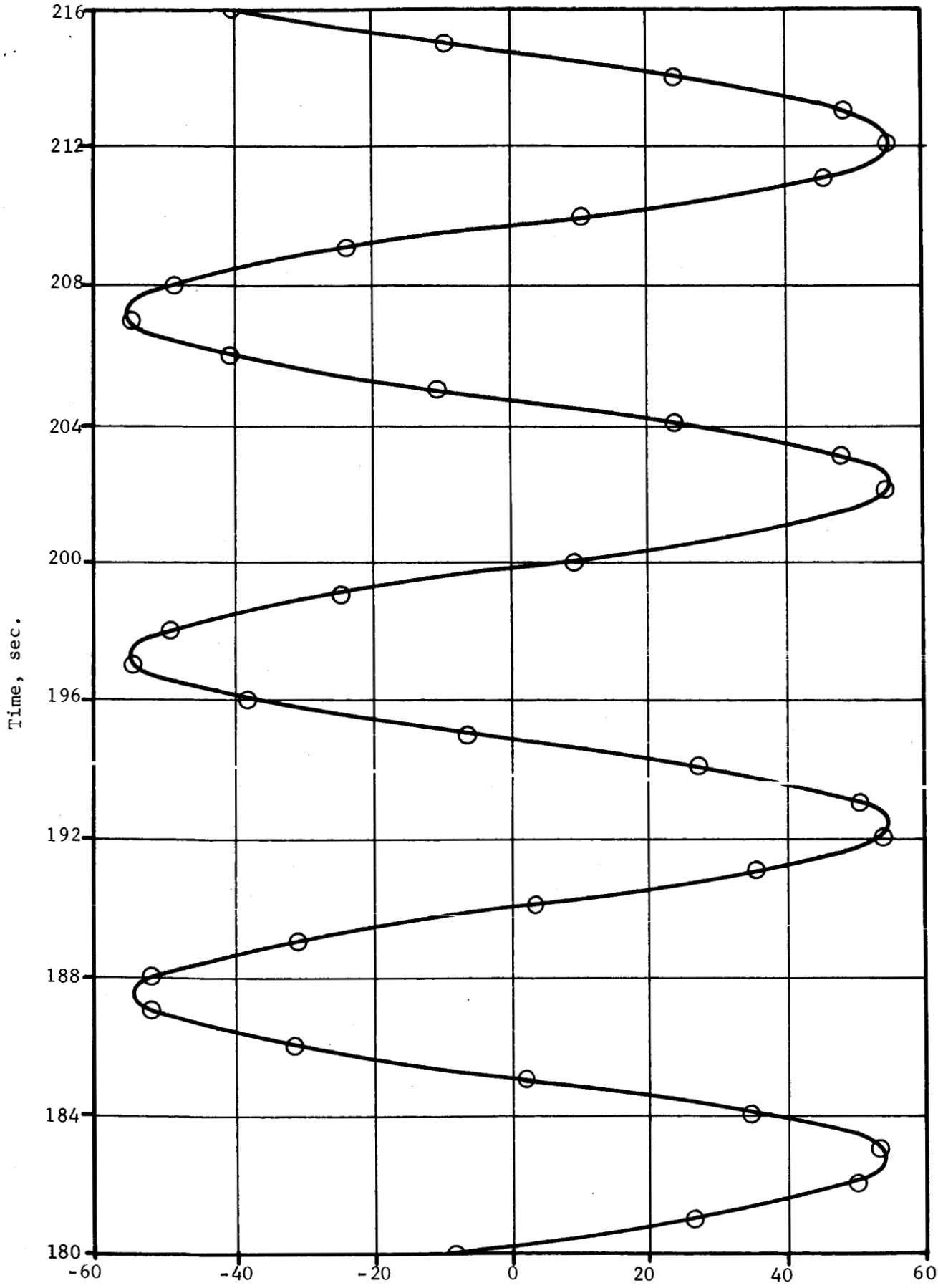

Figure 8k. (Page 6 of 9)

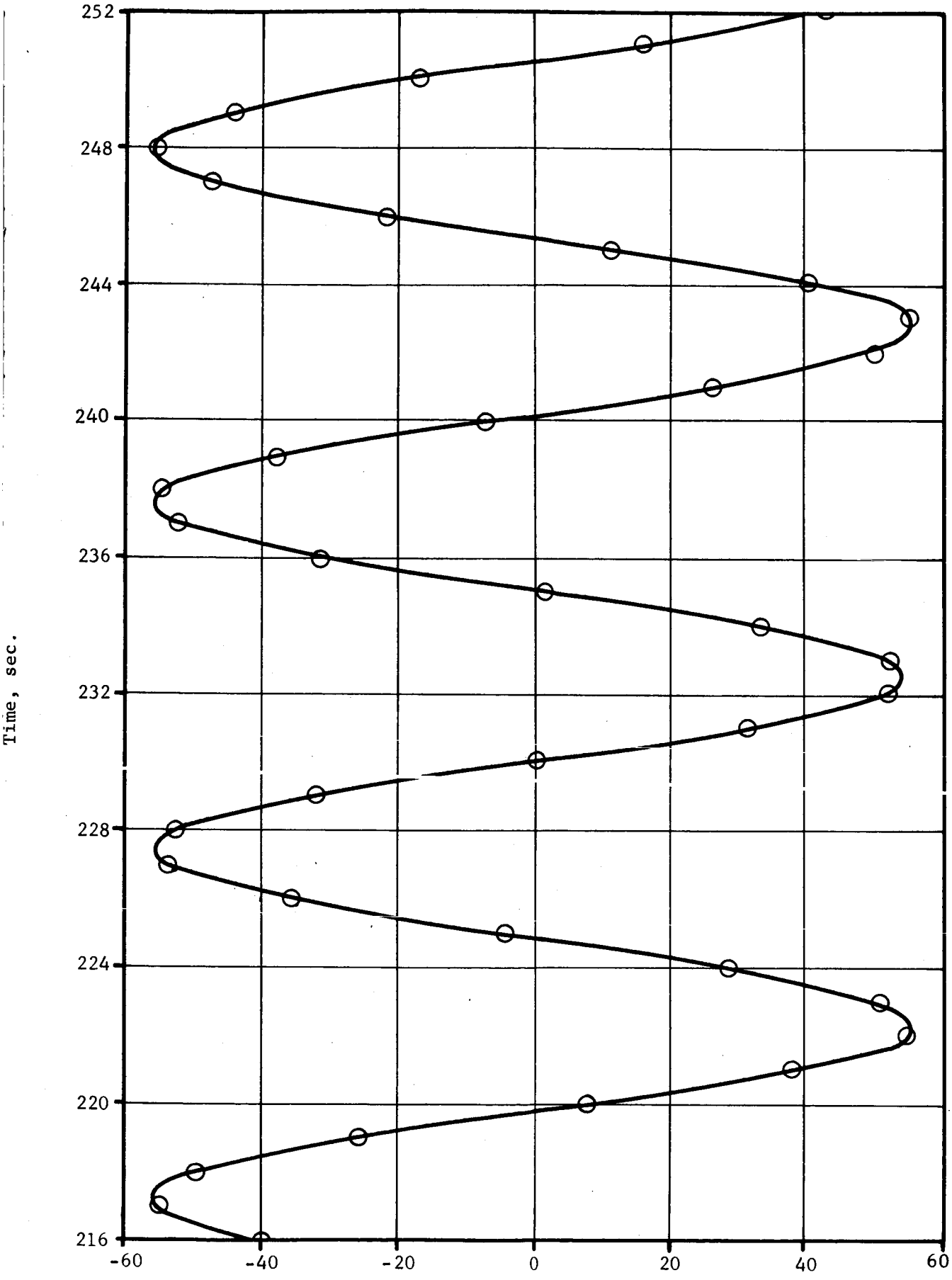

Figure 8k. (Page 7 of 9)

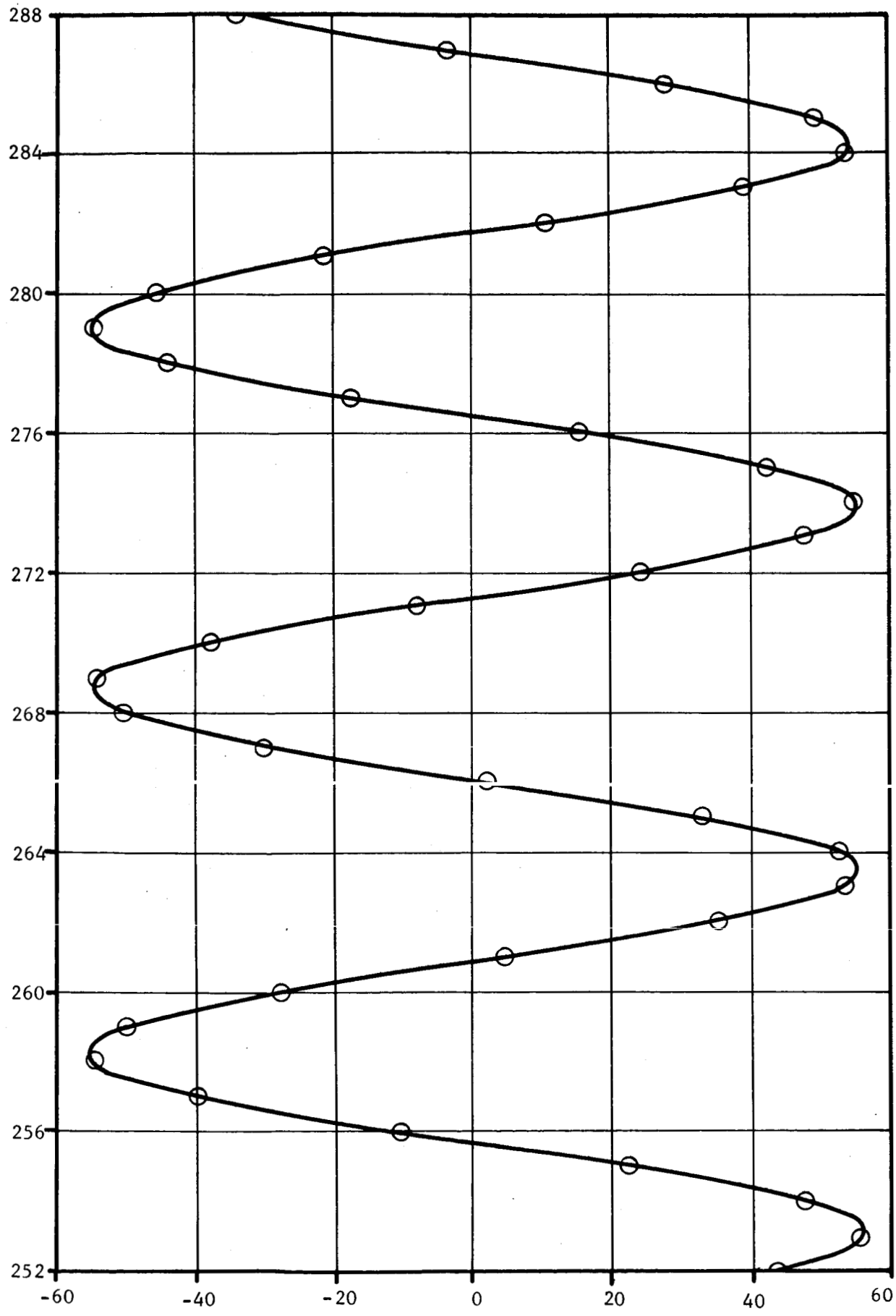

Figure 8k. (Page 8 of 9)

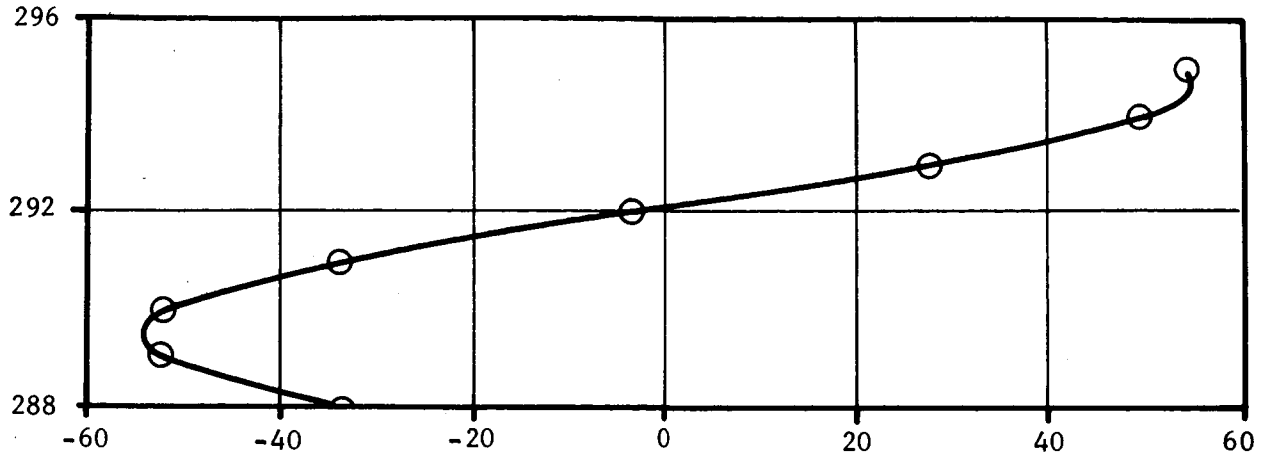

Error Velocity (E_2), ft./sec.

Figure 8k. (Page 9 of 9)

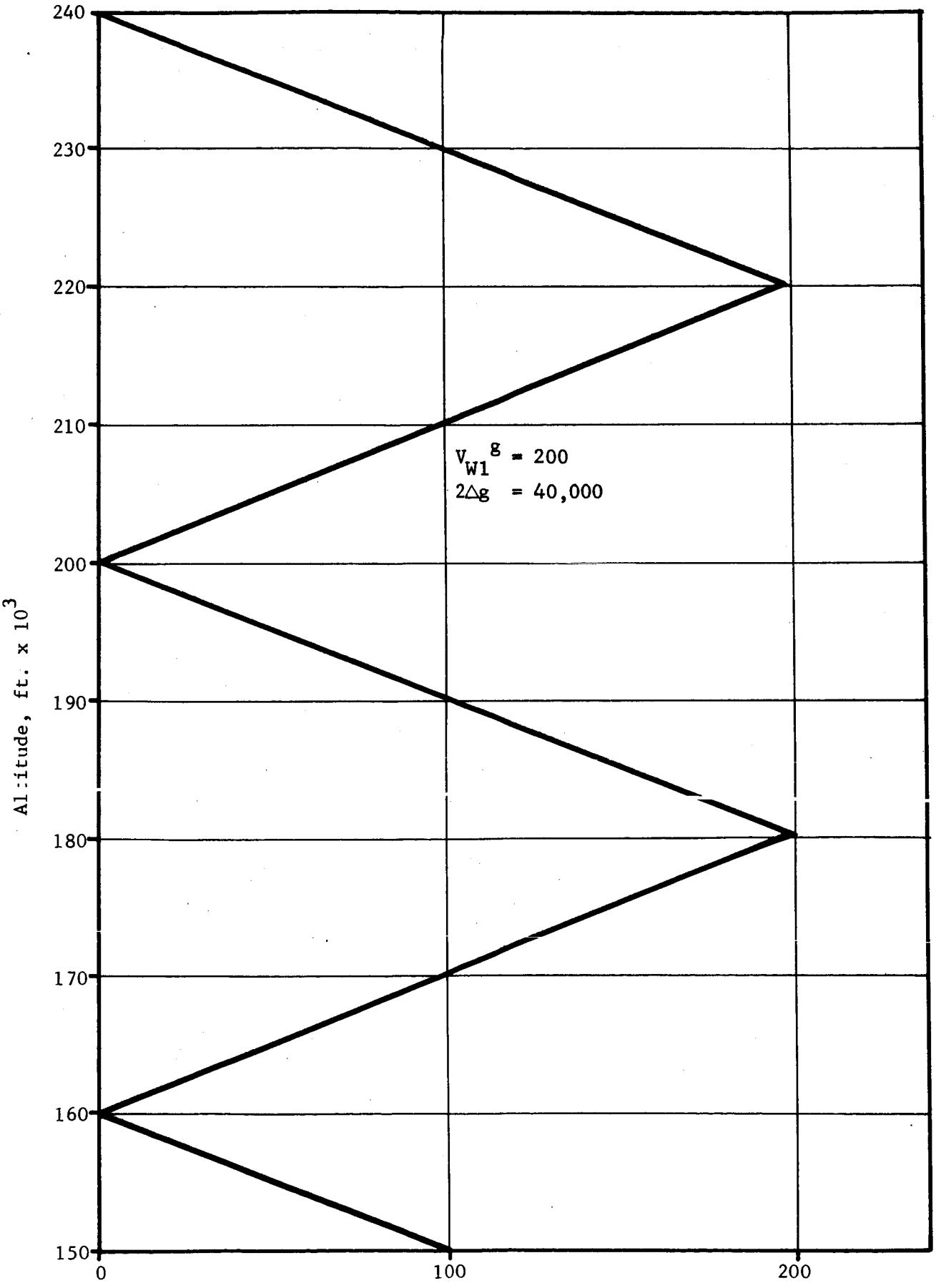

Figure 8ℓ. Wind Velocity vs. Altitude for Hemispherical Parachute

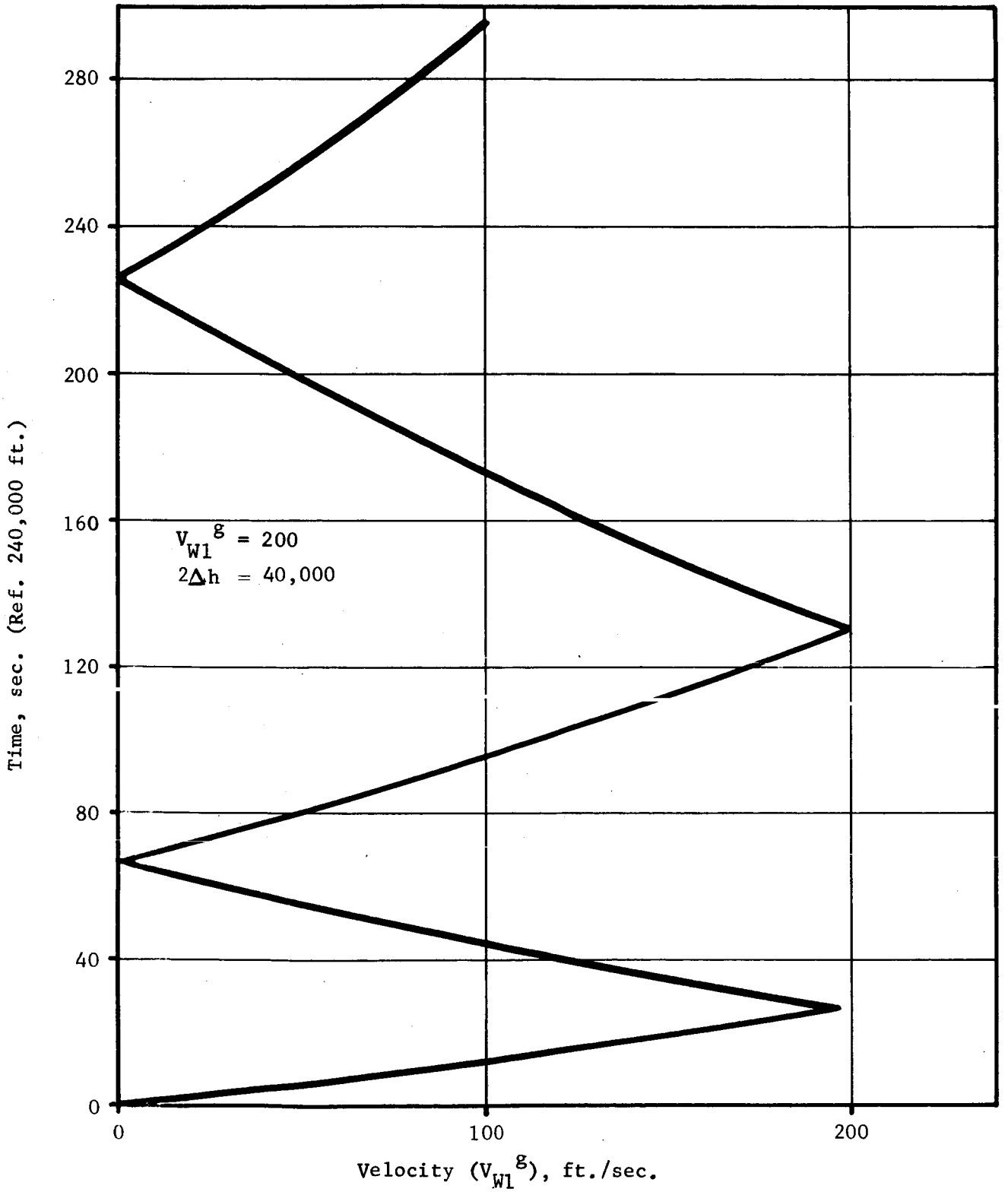

Figure 8m. Wind Velocity vs. Time For Hemispherical Parachute

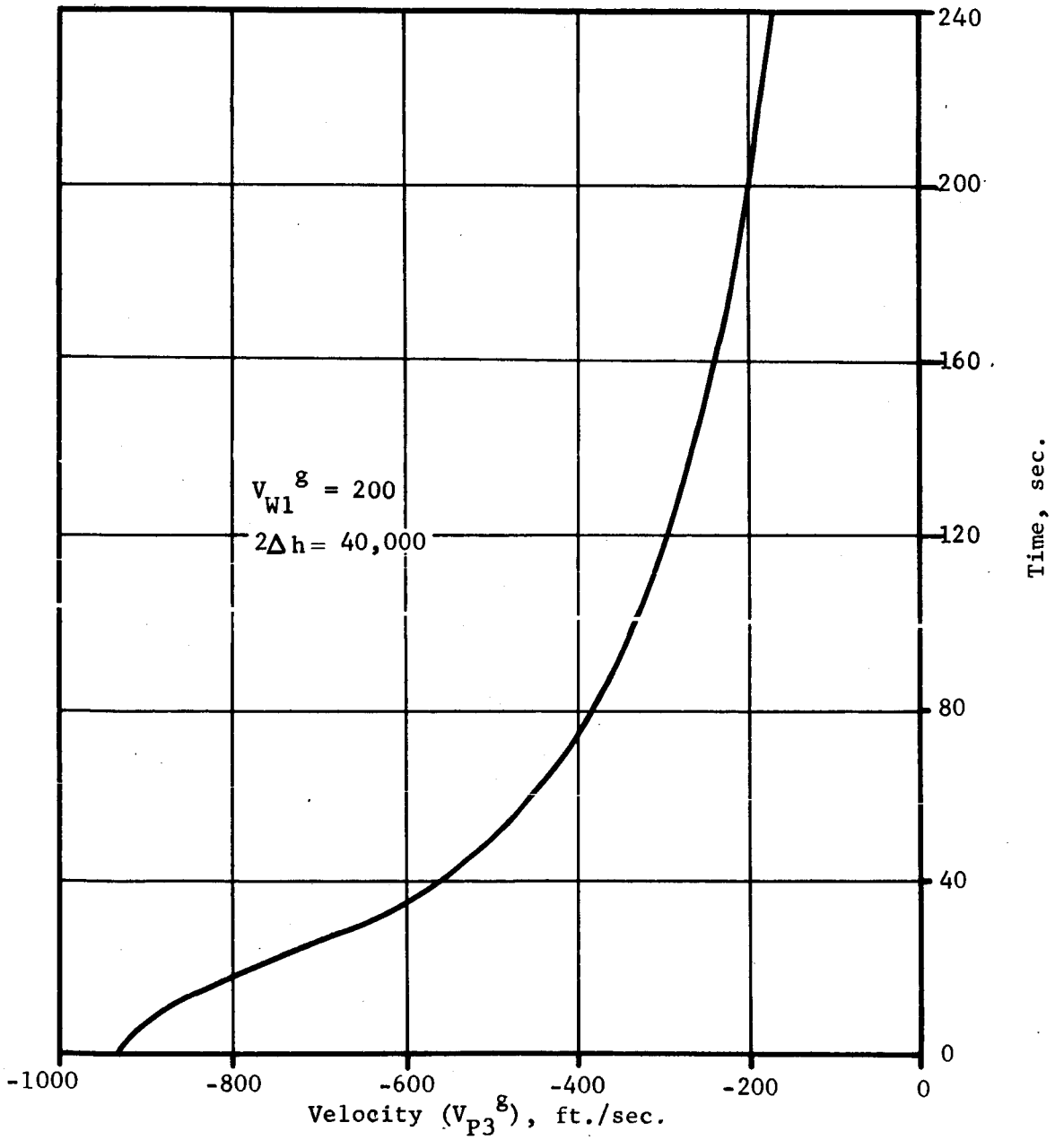

Figure 9a. Velocity vs. Time for Disc-Gap-Band Parachute

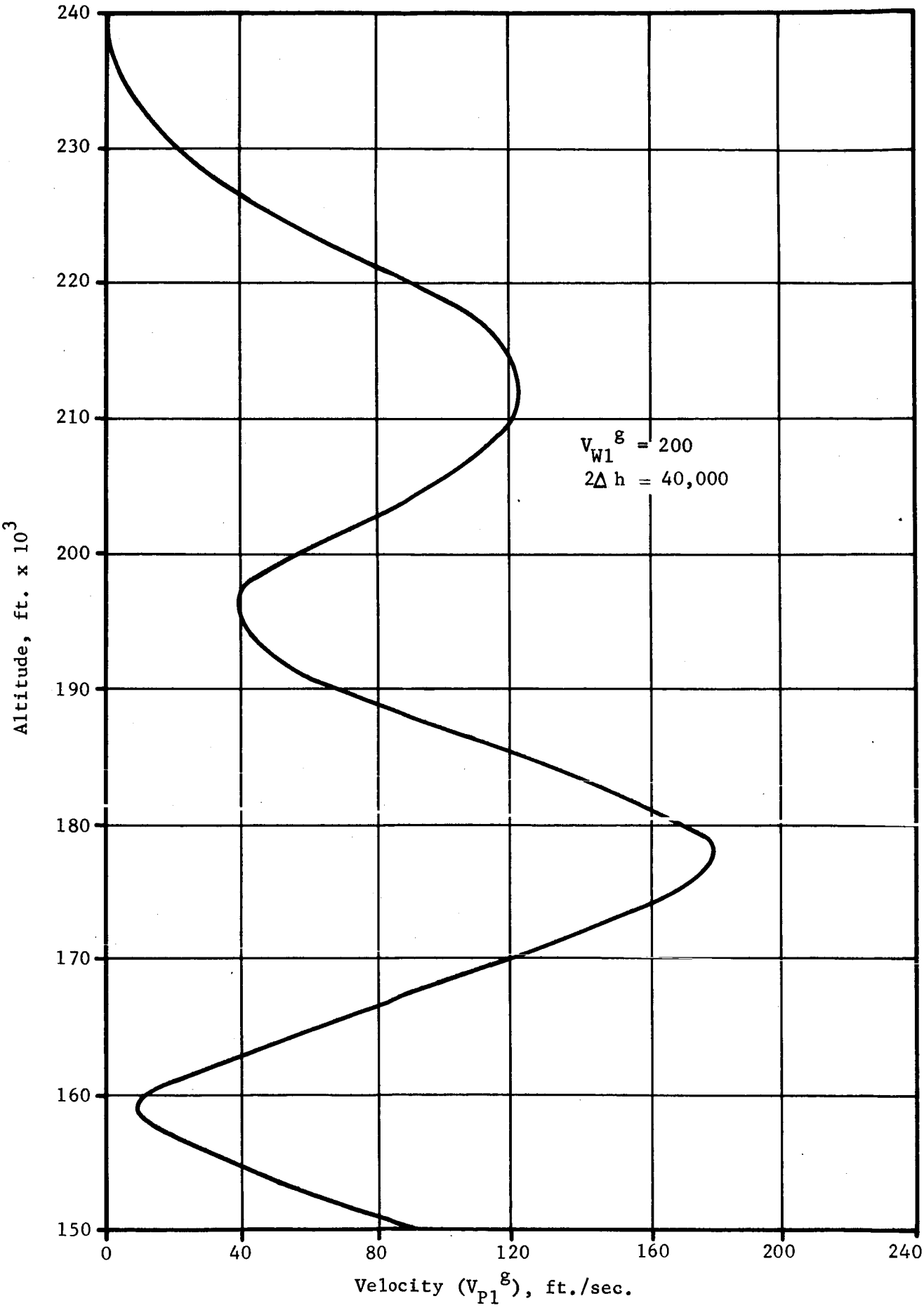

Figure 9b. Velocity vs. Altitude for Disc-Gap-Band Parachute

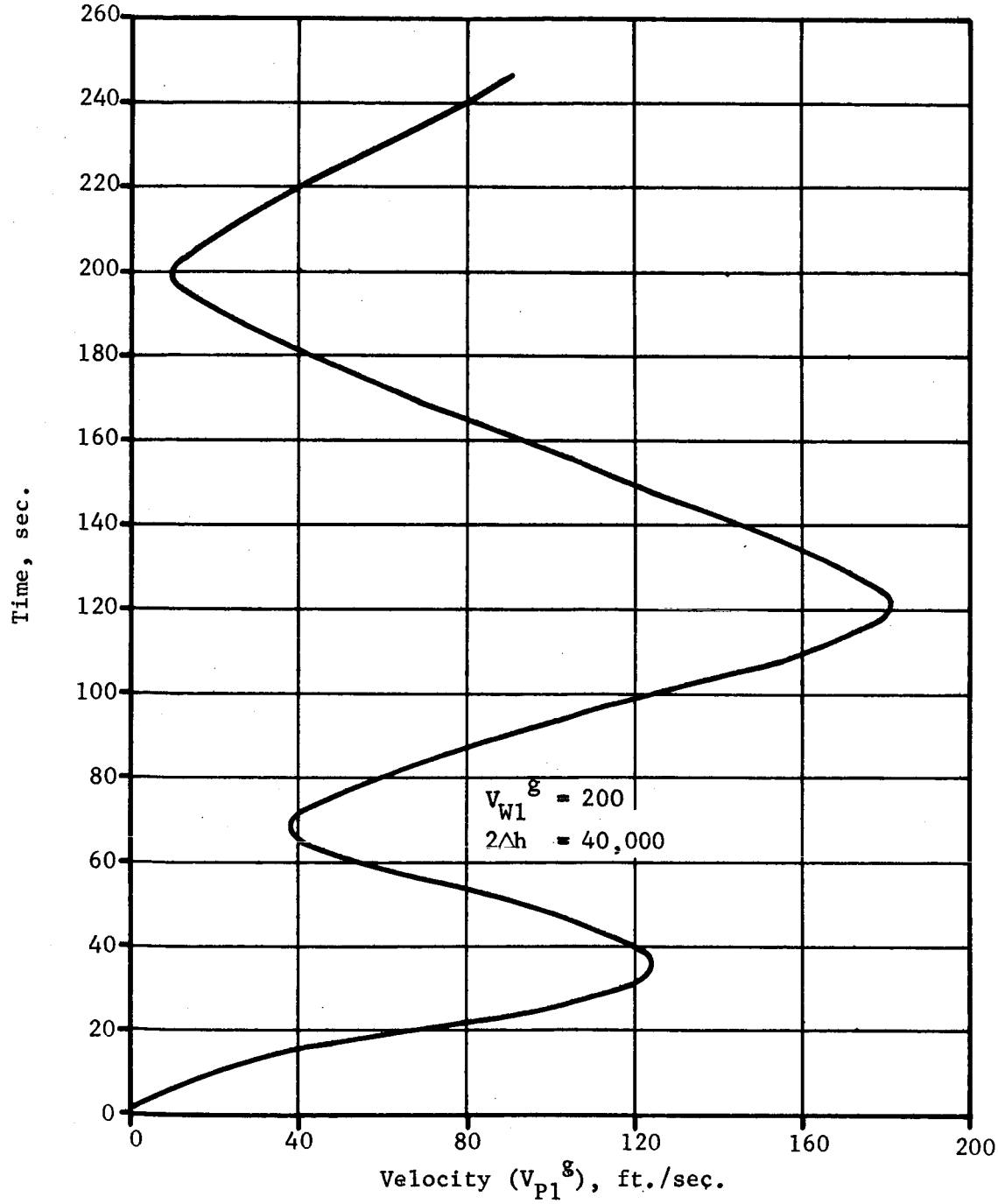

Figure 9c. Velocity vs. Time for Disc-Gap-Band Parachute

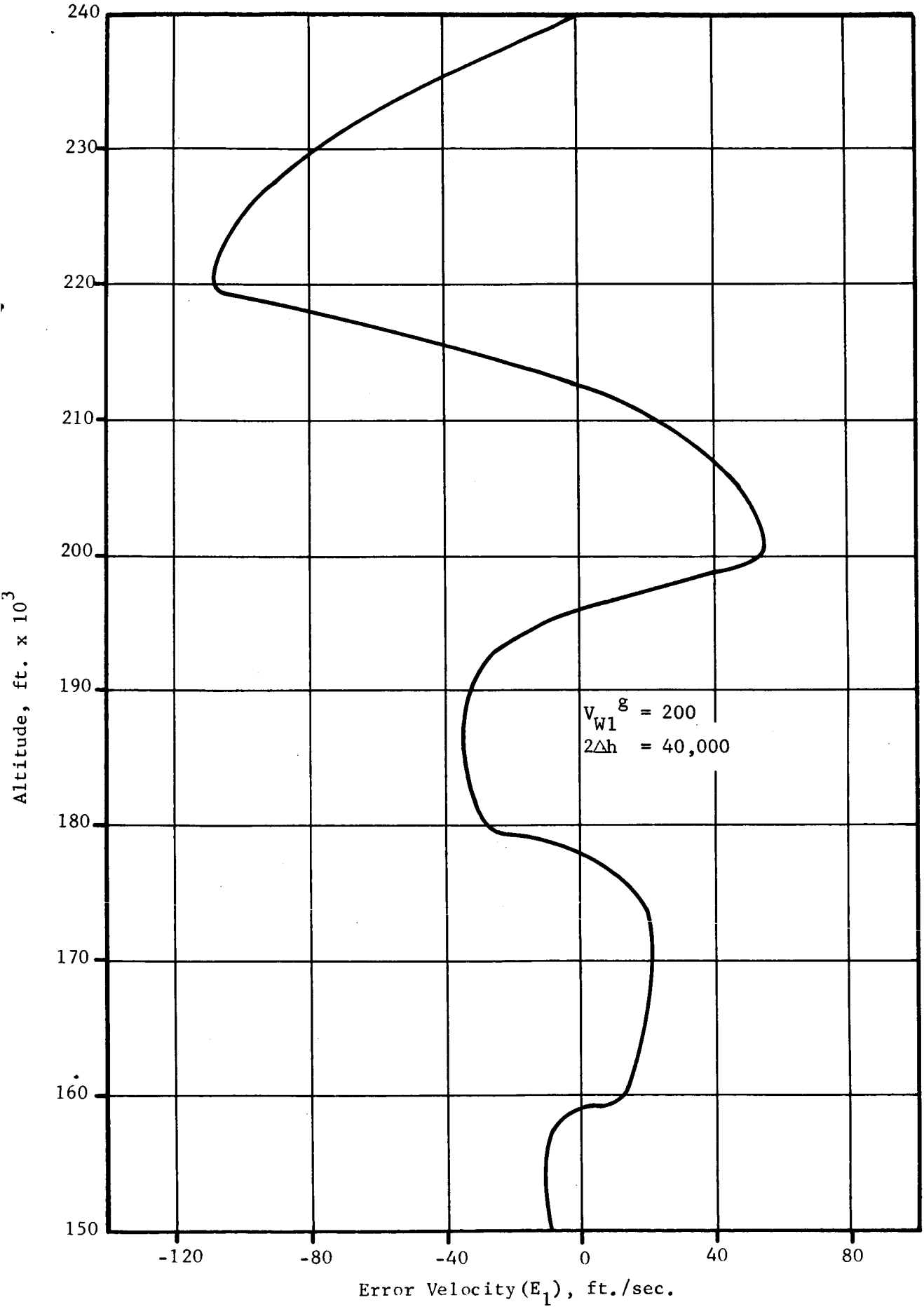

Figure 9d. Error Velocity vs. Altitude for Disc-Gap-Band Parachute

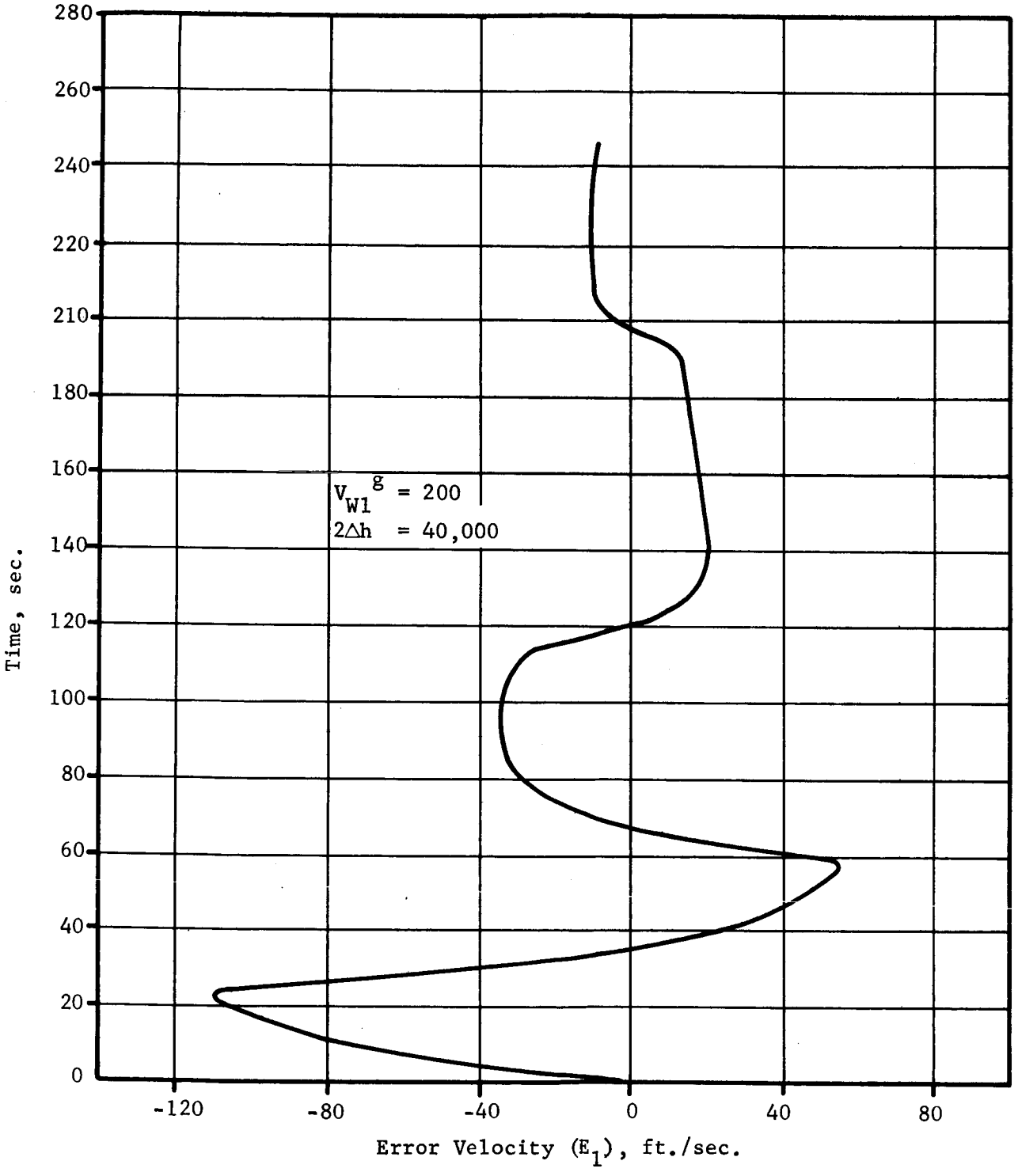

Figure 9e. Error Velocity vs. Time for Disc-Gap-Band Parachute

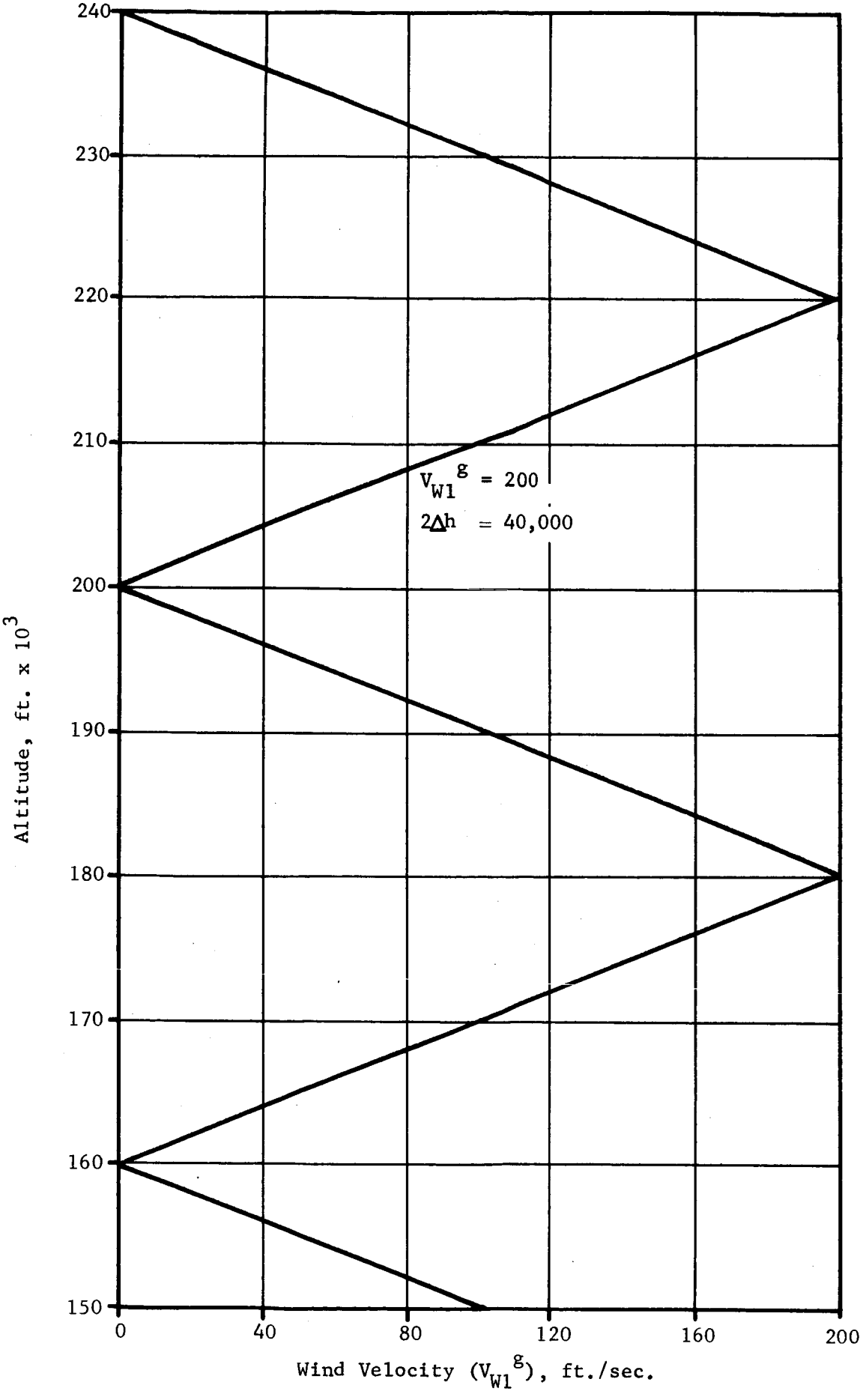

Figure 9f. Wind Velocity vs. Altitude for Disc-Gap-Band Altitude

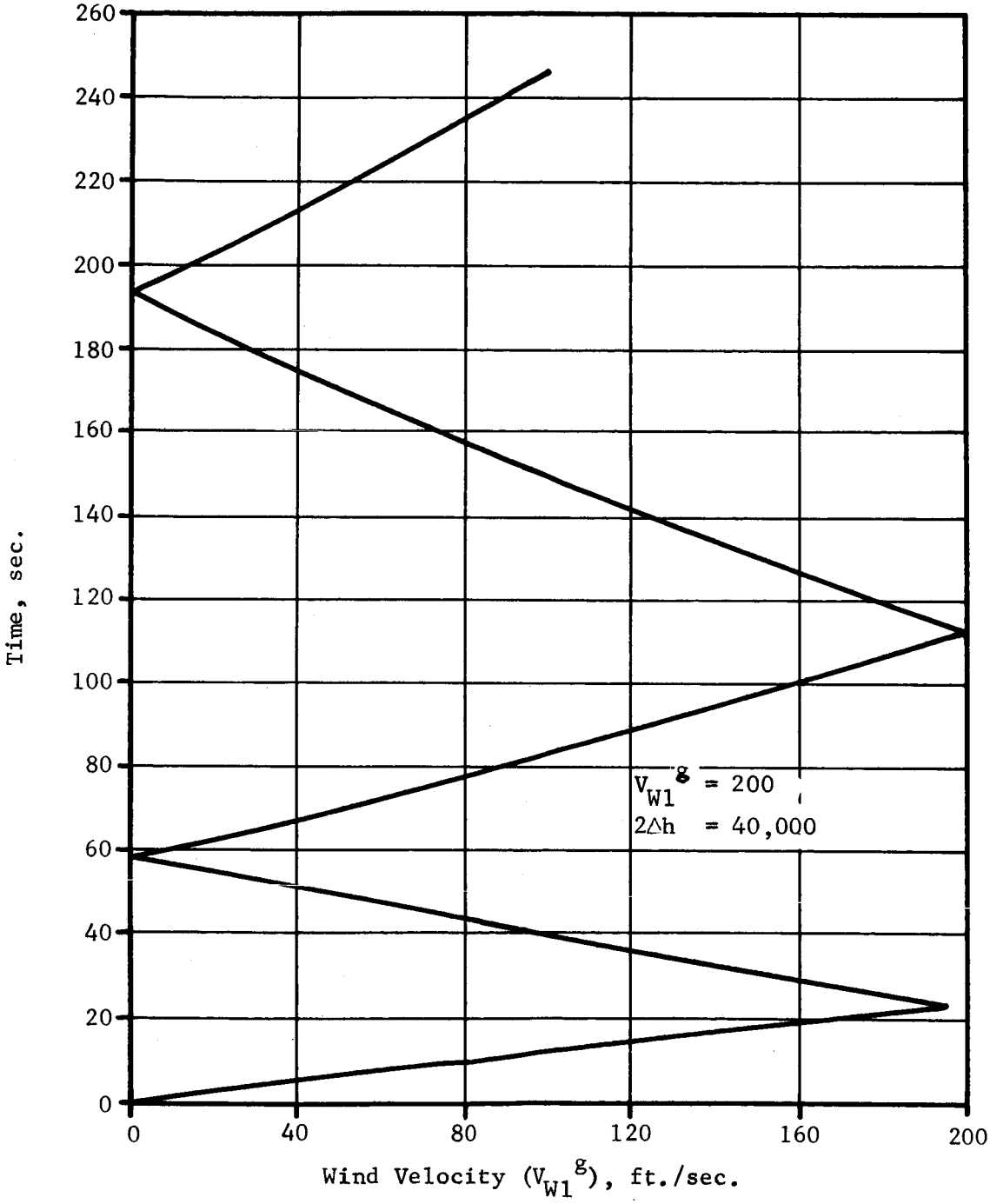

Figure 9g. Wind Velocity vs. Time for Disc-Gap-Band Parachute

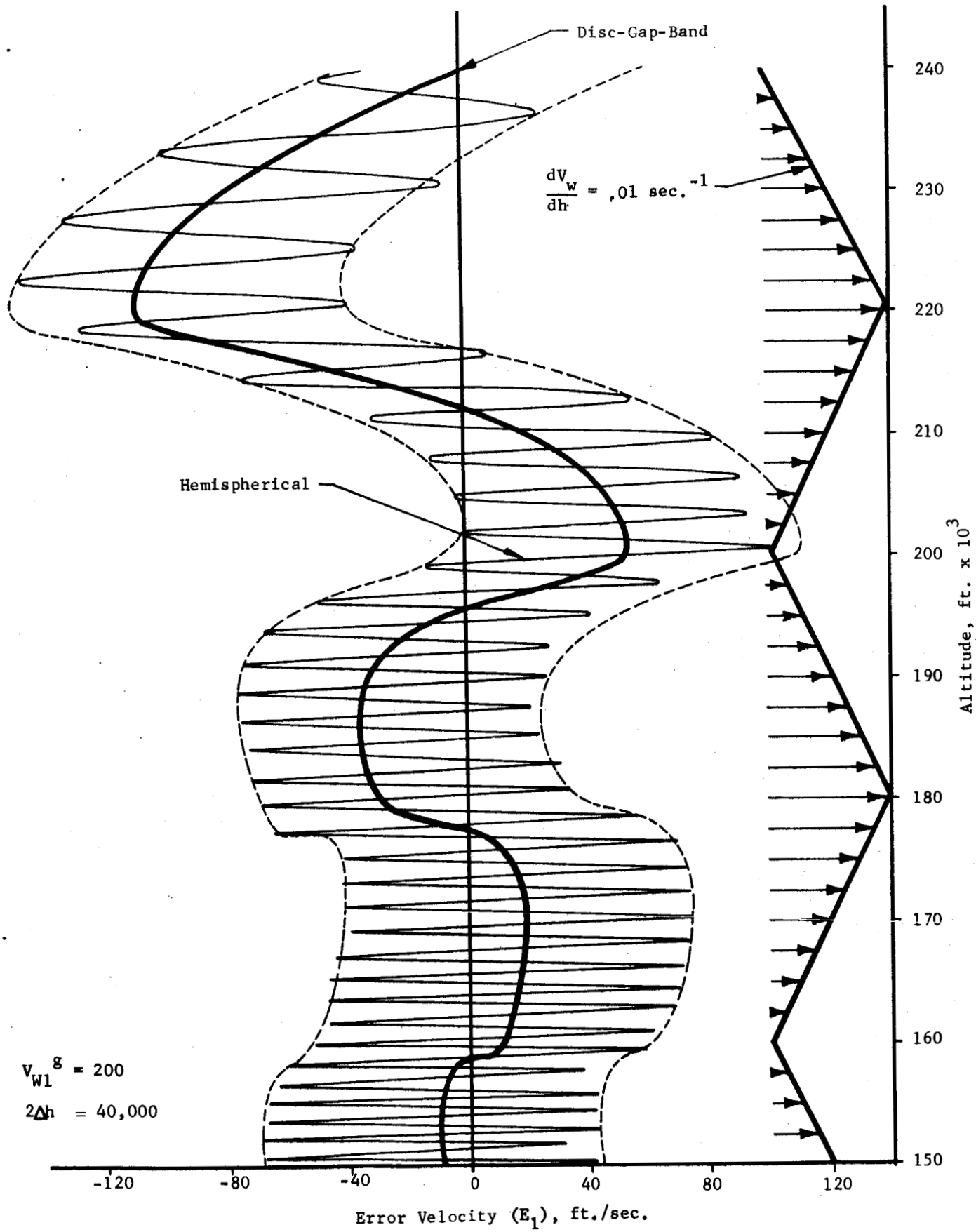

Figure 10. Comparison of Error Velocity vs. Altitude for Both Parachutes

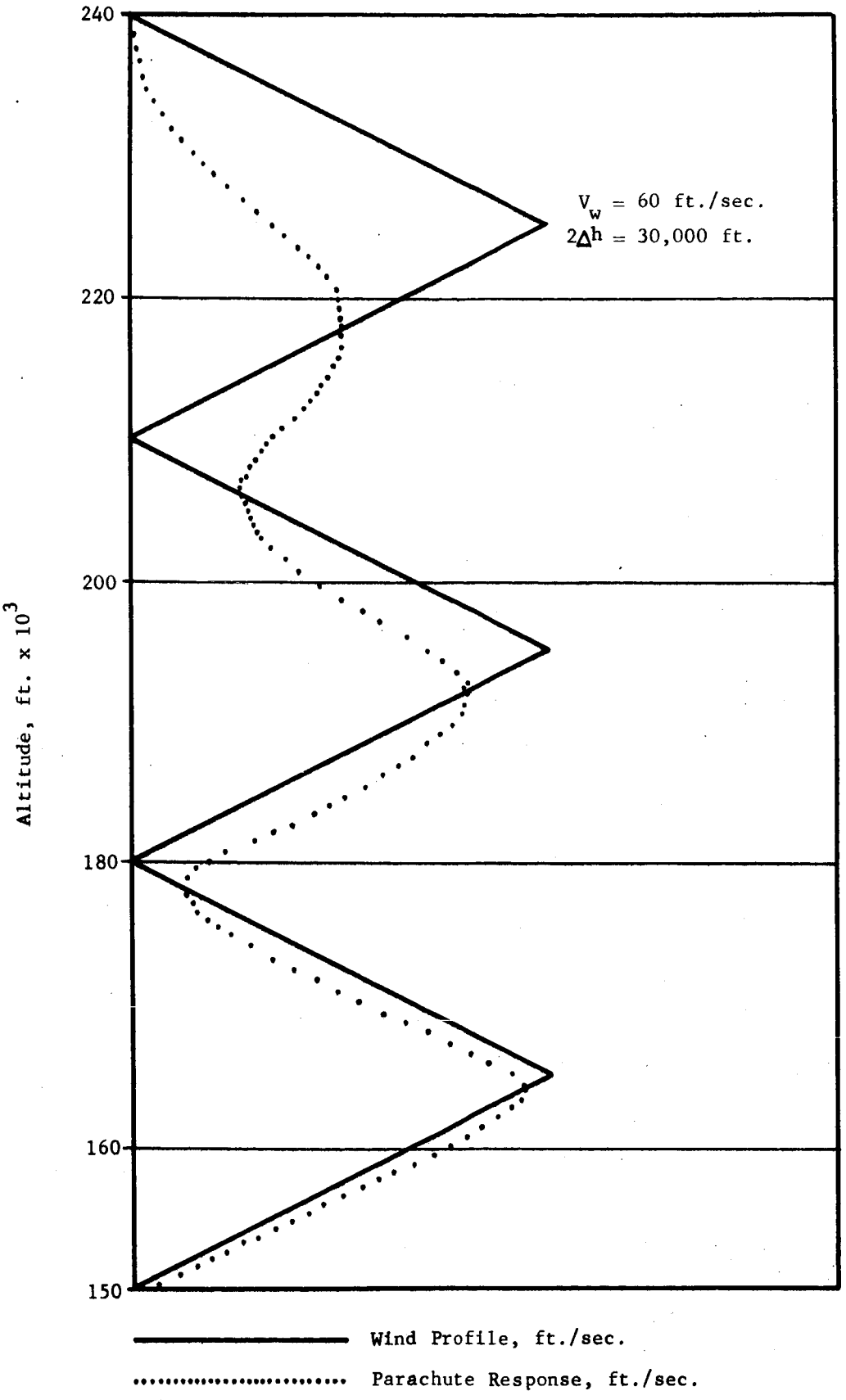

Figure 11. Wind Profile and Parachute Response vs. Altitude for Disc-Gap-Band Parachute

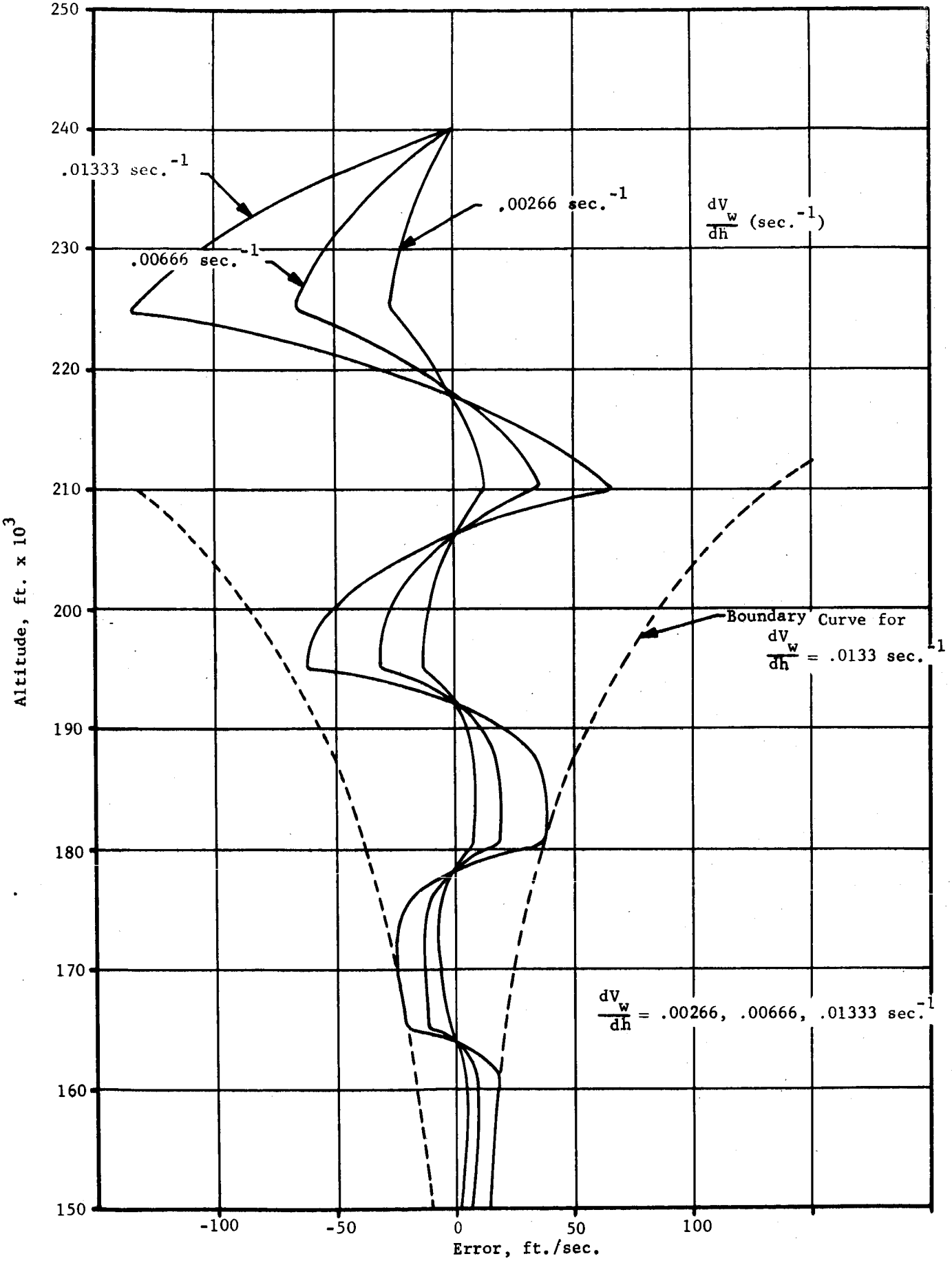

Figure 12. Error vs. Altitude for Disc-Gap-Band Parachute

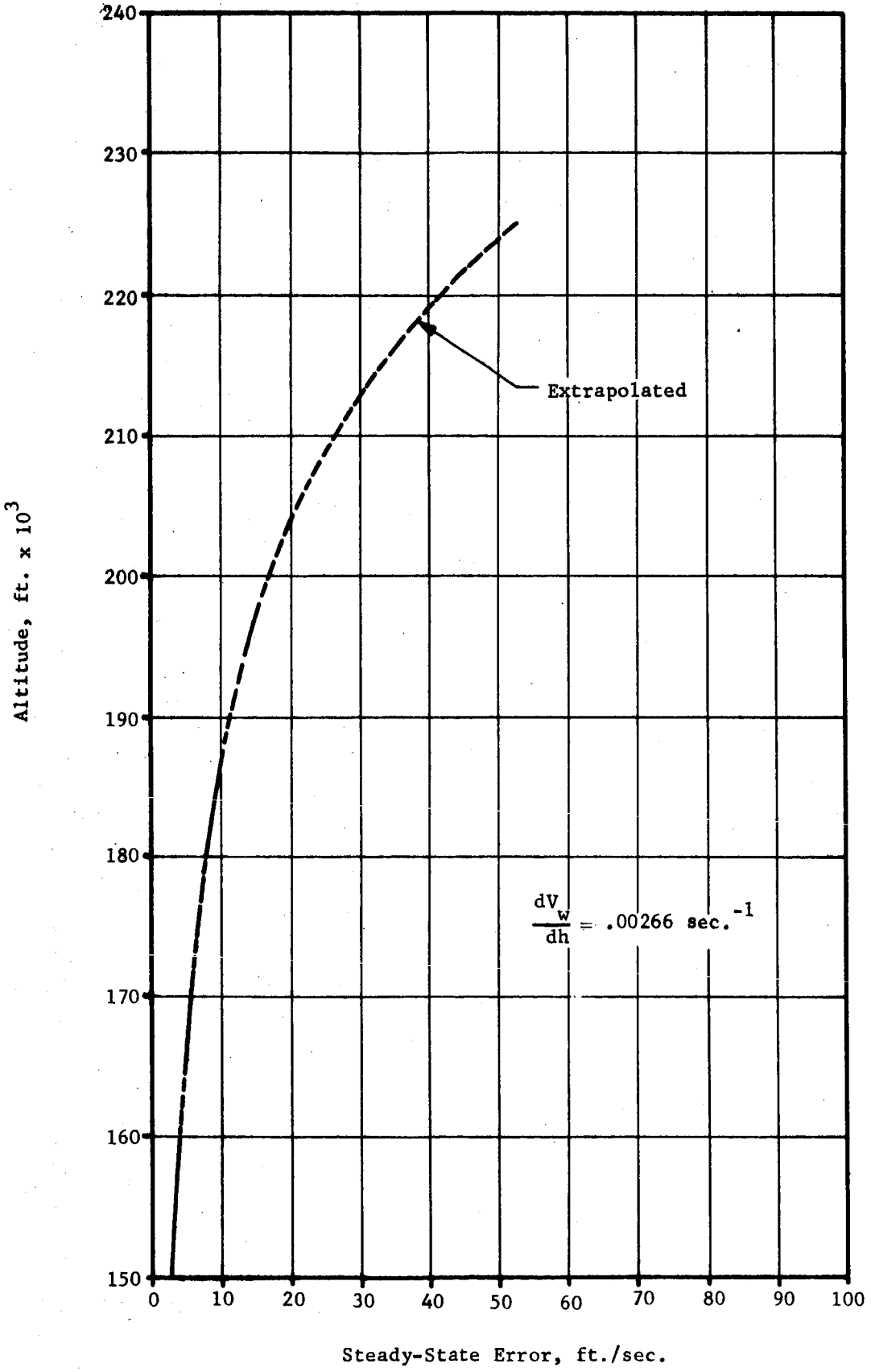

Figure 13. Steady-State Error vs. Altitude for Disc-Gap-Band Parachute

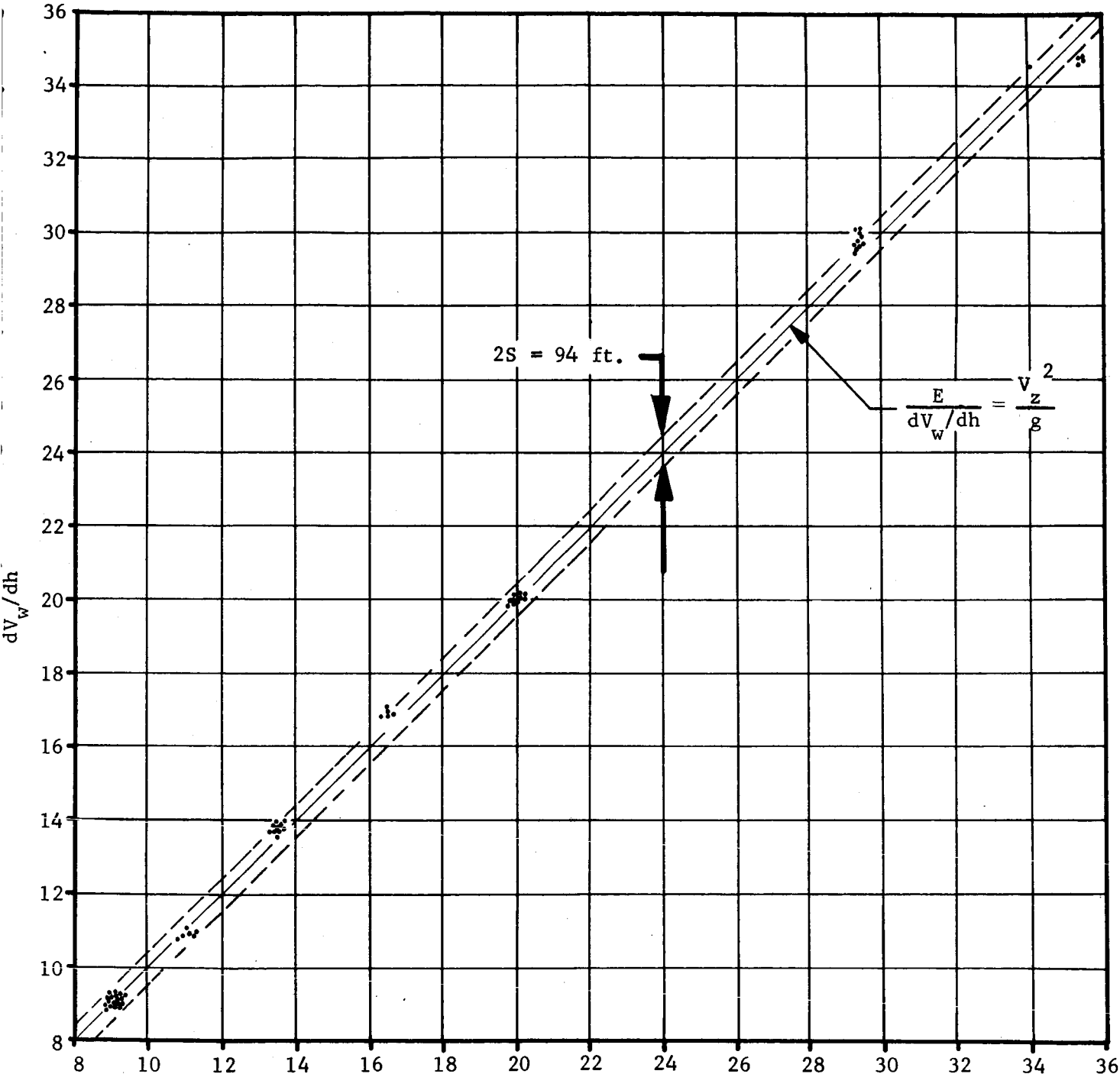

$$S = \left\{ \frac{\left(\frac{E}{dV_w/dh} - \frac{V_z^2}{g} \right)^2}{n} \right\}^{\frac{1}{2}}$$

n = no. of observations

Figure 14. Correlation Plot for Disc-Gap-Band Parachute

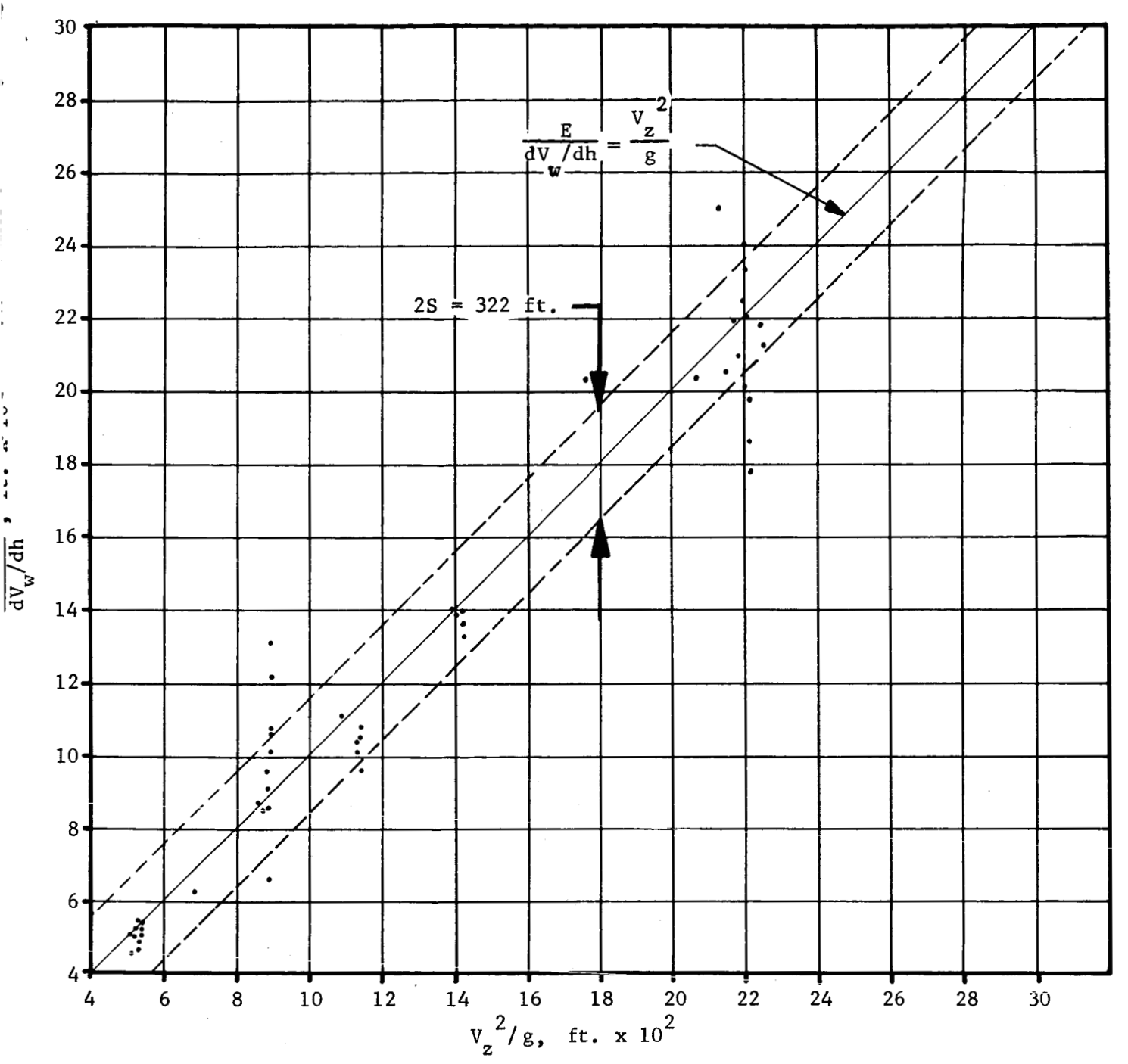

$$S = \left\{ \frac{\left(\frac{E}{dV_w/dh} - \frac{V_z^2}{g} \right)^2}{n} \right\}^{\frac{1}{2}}$$

n = no. of observations

Figure 15. Correlation Plot for Hemispherical Parachute

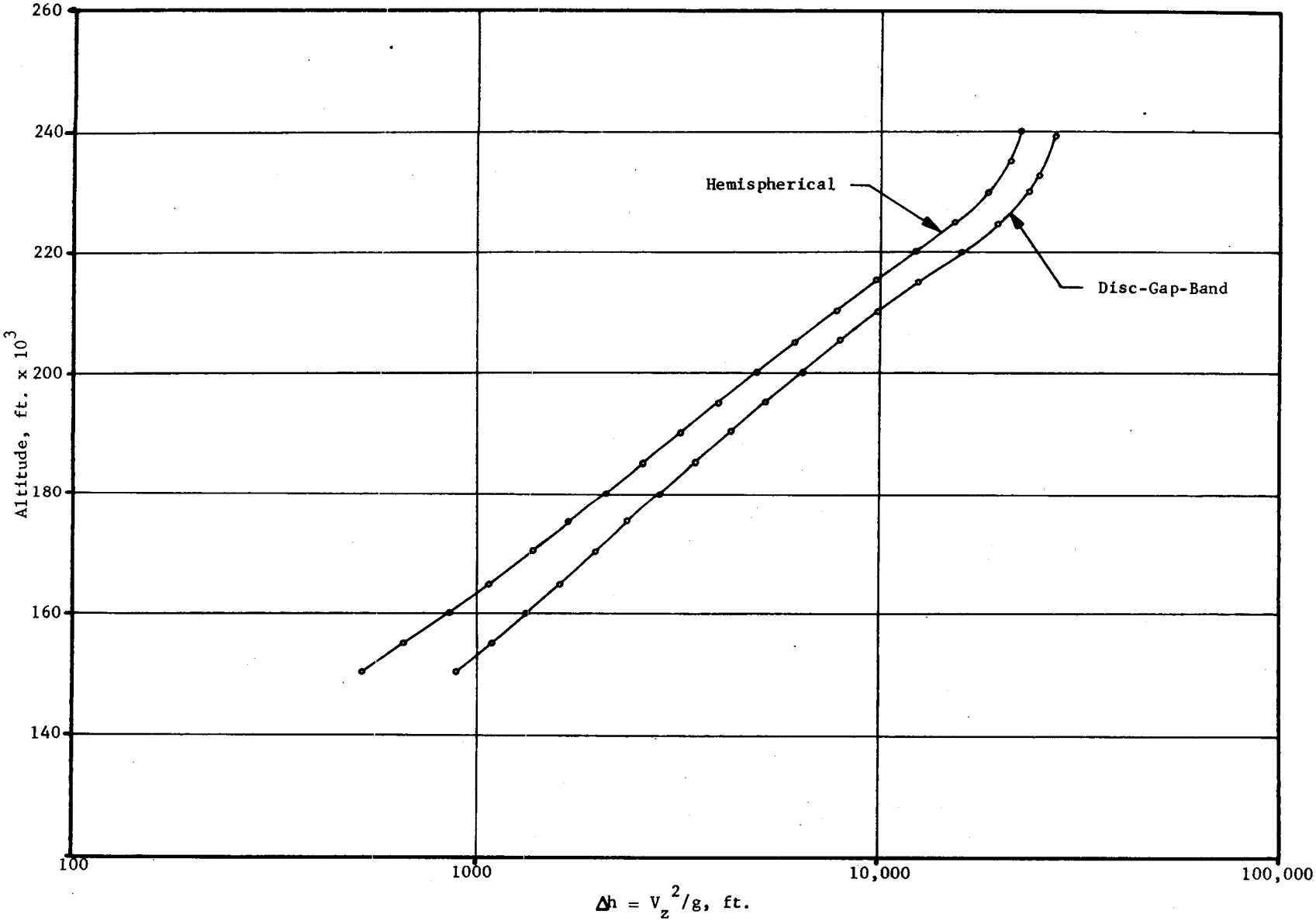

Figure 16. Transient Response Altitude Increment vs. Altitude for Both Parachutes

APPENDIX A

The equations of motion of a parachute falling in a wind field at zero angle of attack can be written:

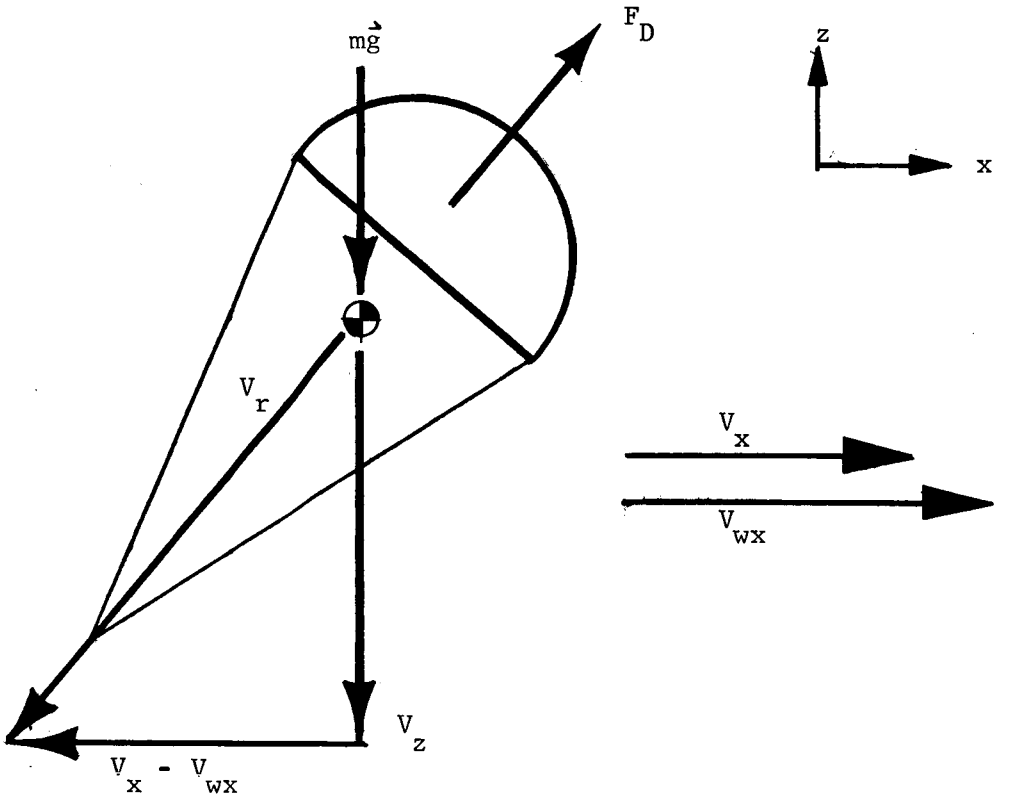

Figure A-1. x-z Plane Projection of Parachute Showing Forces and Velocities

$$F_D = q\, C_D S$$

$$q = \frac{1}{2} \rho\, V_r^{\,2}$$

$$F_L = 0$$

$$m \frac{dV_x}{dt} = q\, C_D S \quad \frac{|V_{wx} - V_x|}{|V_r|}$$

$$m \frac{dV_y}{dt} = qC_D S \frac{|V_{wy} - V_y|}{|V_r|}$$

$$m \frac{dV_z}{dt} = qC_D S \frac{|V_z|}{|V_r|} - mg.$$

These three equations describe the motion of the parachute, when considered as a rigid body under the influence of drag and gravity, with the restriction of zero lift.

The three equations may be rewritten as follows:

$$\frac{dV_x}{dt} = \frac{qC_D S}{m|V_r|} |V_{wx} - V_x|$$

$$\frac{dV_y}{dt} = \frac{qC_D S}{m|V_r|} |V_{wy} - V_y|$$

$$\frac{dV_z}{dt} + g = \frac{qC_D S}{m|V_r|} |V_z|.$$

The common parameter $\frac{qC_D S}{m|V_r|}$ may be eliminated, reducing the three equations to two:

$$\frac{dV_x}{dt} = \frac{\frac{dV_z}{dt} + g}{|V_z|} |V_{wx} - V_x|$$

$$\frac{dV_y}{dt} = \frac{\frac{dV_z}{dt} + g}{|V_z|} |V_{wy} - V_y|.$$

Over a short altitude interval, Δz, the parachute descent velocity V_z may be considered constant, and the first derivative with time $\frac{dV_z}{dt}$ very much less than gravitational acceleration.

Hence, the quantity

$$\frac{\frac{dV_z}{dt} + g}{|V_z|} \rightarrow \frac{g}{|V_z|} \rightarrow \text{constant } (k)$$

over small altitude intervals.

Therefore, the equations for $\frac{dV_x}{dt}$ and $\frac{dV_y}{dt}$ may be rewritten,

$$\frac{dV_x}{dt} + kV_x = kV_{wx} ,$$

and

$$\frac{dV_y}{dt} + kV_y = kV_{wy} .$$

The wind function used in the computer studies is of the form

$$V_{wx} = V_{wxo} + \left(\frac{dV_{wx}}{dz}\right) z ,$$

and

$$V_{wy} = V_{wyo} + \left(\frac{dV_{wy}}{dz}\right) z .$$

The wind field was simulated in only the x-z plane; however, the results are valid for the y-z plane. Over small altitude increments the descent rate V_z may be considered constant; therefore,

$$V_{wx} = V_{wxo} + \left(\frac{dV_{wx}}{dz}\right) V_z t.$$

With this substitution of a linear time function for V_{wx}, the equation of motion of the parachute in the x-z plane may be written:

$$\frac{dV_x}{dt} + kV_x = kV_{wxo} + k\left(\frac{dV_{wx}}{dz}\right) V_z t.$$

The solution of this first-order differential equation for V_x is

$$V_x = e^{-kt} V_{xo} + (1-e^{-kt}) V_{wxo}$$

$$+ \left[t - \frac{1-e^{-kt}}{k} \right] \left(\frac{dV_{wx}}{dz} \right) V_z \ .$$

If the parachute has fallen for a sufficiently long time, t, a "steady-state" condition is approached, and the horizontal velocity may be found by letting

$$e^{-kt} \rightarrow 0 \ ,$$

whence,

$$V_x = V_{wxo} + \left(\frac{dV_{wx}}{dz} \right) V_z t - \frac{1}{k} \left(\frac{dV_{wx}}{dz} \right) V_z \ .$$

The first two terms of this equation are the wind velocity at time, t, (or altitude z); hence the equation for V_x may be written

$$V_x = V_{wx} - \frac{1}{k} \left(\frac{dV_{wx}}{dz} \right) V_z \ .$$

The difference $V_{wx} - V_x$ is defined as the wind-sensing error E and may be seen to be equal to

$$E = \frac{1}{k} \left(\frac{dV_{wx}}{dz} \right) V_z \ .$$

The quantity k was shown earlier to be found by

$$k = \frac{g}{V_z} \ ,$$

from which

$$E = \left(\frac{dV_{wx}}{dz} \right) \frac{V_z^2}{g} \ .$$

$\frac{dV_{wx}}{dz}$ is, of course, the wind shear gradient, and V_z represents the parachute descent rate.

The quantity $\frac{V_z^2}{g}$ may be interpreted as the physical distance between the parachute and an inertialess wind sensor falling at the same rate through the same wind field.*

Of additional interest is the altitude through which the parachute falls while the "steady-state" error is being approached.

For parachute and wind velocities both initially zero,

$$V_x = V_{wx} - \left(1-e^{-kt}\right)\left(\frac{V_z}{k}\right)\left(\frac{dV_{wx}}{dz}\right),$$

and the error E may be seen to be the "steady-state" error, $\frac{V_z^2}{g}\left(\frac{dV_{wx}}{dz}\right)$, multiplied by the factor $1-\frac{1}{e^{kt}}$. The quantity e^{-kt} may be set equal to some known value, and the time t, or altitude increment Δz solved for.

e^{-kt}	t $(k = \frac{g}{V_z})$	$\Delta z = V_z t$	$1-e^{-kt}$
$1/e$	$\frac{1}{k}$	$\frac{V_z^2}{g}$	.6321
$1/e^2$	$\frac{2}{k}$	$\frac{2V_z^2}{g}$	.8647
$1/e^3$	$\frac{3}{k}$	$\frac{3V_z^2}{g}$	.9502

Table A1

*Reed, Wilmer H. III, "Dynamic Response of Rising and Falling Balloon Sensors with Application to Estimates of Wind Loads on Launch Vehicles," NASA TN D-1821, October 1963.

From Table A1 it can be seen that the altitude increment Δz may be found by the equation

$$\Delta z = \frac{bV_z^2}{g} ,$$

where

$$\frac{E}{\frac{V_z^2}{g}\left(\frac{dV_{wx}}{dz}\right)} = 1 - 1/e^b .$$

From these equations it can be seen that when the parachute has fallen approximately three times the "lag distance" $\frac{V_z^2}{g}$, the wind sensing error attains 95% of its theoretical value. This same conclusion was reached in the report referenced on page A-5.

The value of this altitude increment, Δz, should certainly influence data sampling and averaging intervals.

APPENDIX B

The technique for determining error as a function of altitude on the rotating parachute is as follows:

Since the method of superposition holds, the two error components, E_1 and E_2, must be of the form

$$E_1 = A + Bt + C \sin \omega t + D \cos \omega t$$

$$E_2 = C \cos \omega t - D \sin \omega t,$$

where the component $(A + Bt)$ of E_1 represents a linearization of the mean error.

Both E_1 and E_2 are listed at 1-second intervals. From E_2 it is possible to calculate the parachute period of oscillation, τ.

If three points, closely spaced in time, are selected such that

$$t_{-\Delta t} = t_o - \Delta t$$

$$t_o = t_o$$

$$t_{+\Delta t} = t_o + \Delta t ,$$

the three values of E_1 corresponding to the three points in time may be used to find the error $E_1 = A + Bt_o$ at time t_o. This is accomplished by performing the following multiplications and summing

$$(E_1)_{t_o-\Delta t} \times \left(\frac{1}{2 - 2 \cos \theta}\right) + (E_1)_{t_o} \times \left(\frac{- 2 \cos \theta}{2 - 2 \cos \theta}\right)$$

$$+ (E_1)_{t_o} + \Delta t \left(\frac{1}{2 - 2 \cos \theta}\right) = A + Bt_o .$$

The angle θ is found by

$$\theta = \frac{2\pi \Delta t}{\tau} .$$

The term $A + Bt_o$ is the "steady-state" value of error at time t_o.

APPENDIX C

COMPUTER PROGRAMMING

The dynamic model and equations of motion, which are now programmed and operational in an IBM 7040 computer, are summarized below.

Two coordinate systems are utilized: a ground coordinate system based on a flat, nonrotating earth, and a body axis system.

1. Ground Coordinate System, g_i

   Origin - at intersection of plumb line from parachute deployment point and earth's surface

   g_1 - g_2 plane - normal to plumb line

   g_1 axis - east

   g_2 axis - north

   g_3 axis - up, in plumb line direction

   The gravitational force, wind, atmosphere, and initial position and velocity are defined in the g_i system. The parachute position and velocity are specified in this system as outputs, and the error function (the difference between parachute and wind velocity) is expressed in the g_i system.

2. Body Axis System, b_i

   Origin - at the parachute-payload CG

   b_1 - b_2 plane normal to line joining CG with canopy crown

   b_3 - along line joining CG with canopy crown, positive in direction of crown.

Since the axis b_3 is a principal axis, the inertia tensor [I] is defined in the b_i system. The aerodynamic coefficients are defined in this system, and the aerodynamic forces and moments are best suited to computation in this system prior to transformation into the g_i system for trajectory computation.

The transformation between the g_i system and the b_i system is:

$$\vec{V}^b = [a_{ij}]\, \vec{V}^g ,$$

where $[a_{ij}]$ is a time-dependent coordinate transformation matrix specified originally as an initial condition, computed by using the components of the angular velocity vector, $\vec{\omega}^b$, obtained from integration of the differential equations of rotational motion.

3. Symbols

Symbol	Definition	Units
$\vec{b}_1$, $\vec{b}_2$, $\vec{b}_3$	Unit Vectors Along Body Axes	Dimensionless
C_D	Drag Coefficient	Dimensionless
C_L	Lift Coefficient	Dimensionless
C_m	Moment Coefficient	Dimensionless
C_{md}	Damping Moment Coefficient	$ft.^3$
$\vec{D}$	Drag Force	lb.
d	Parachute Great Circle Diameter	ft.
E	Wind-Sensing Error	ft./sec.

Symbol	Definition	Units
$\|G\|$	Gravitational Constant	ft./sec.^{2}
$\vec{G}$	Gravitational Acceleration	ft./sec.^{2}
$\vec{g}_1$, $\vec{g}_2$, $\vec{g}_3$	Unit Vectors Along Ground Axes	Dimensionless
$[I]$	Inertia Tensor	ft.-lb./sec.^{2}
$\vec{L}$	Lift Force	lb.
$\vec{M}$	Aerodynamic Moment	ft.-lb.
$\vec{M}_d$	Aerodynamic Damping Moment	ft.-lb.
M_{mt}	Total Moment Due to Magnus Force	ft.-lb.
M_{m1}, M_{m2}, M_{m3}	Components of Moment Due to Magnus Force	ft.-lb.
m	Mass	lb.-sec.^{2}/ft.
q	Dynamic Pressure	lb./ft.^{2}
$\vec{R}$	Position Vector	ft.
S	Total Parachute Great Circle Area	ft.^{2}
$\vec{V}$	Velocity Vector	ft./sec.
$\vec{W}$	Weight Force	lb.
y	Distance from Parachute Center of Pressure to Center of Gravity	ft.
α	Angle of Attack	radian
μ	Coefficient of Viscosity	lb.-sec./ft.^{2}
ρ	Mass Density	lb.-sec.^{2}/ft.^{4}
$\vec{\omega}$	Angular Velocity	radian/sec.

4. Superscripts

Superscript	Definition
b	Identifies vector resolved into b_i system
g	Identifies vector resolved into g_i system

5. Subscripts

Subscript	Definition
1, 2, 3	Identifies components of vectors along axes of system identified by superscript
P	Refers to parachute
r	Refers to remote conditions
W	Wind

6. $$\dot{\vec{V}}_p^{\,g} = \frac{1}{m} [a_{ji}] [\vec{L}^b + \vec{D}^b + \vec{W}^b] \quad (1)$$

$$[I] \dot{\vec{\omega}}^b = \vec{M}^b + \vec{M}_d{}^b - \vec{\omega}^b \times [I] \vec{\omega}^b \quad (2)$$

$$\dot{\vec{R}}_p^{\,g} = \vec{V}_p^{\,g} \quad (3)$$

$$[a_{ij}] = \begin{bmatrix} 0 & \omega_3{}^b & -\omega_2{}^b \\ -\omega_3{}^b & 0 & \omega_1{}^b \\ \omega_2{}^b & -\omega_1{}^b & 0 \end{bmatrix} [a_{ji}] \quad (4)$$

7. $|\vec{L}| = |q\ C_L S|$

$$\vec{L}^b = \frac{C_L}{|C_L|}\ |\vec{L}|\ \vec{m}^b\ x\left[\frac{\vec{V}_r^{\,b}}{|\vec{V}_r^{\,b}|}\right]$$

$$M_{mt} = C_{mf} q Y_m S$$

$$M_{m1}^{\,b} = M_{mt}\ \frac{V_{r1}^{\,b}}{|V_{r1}^{\,b} + V_{r2}^{\,b}|}$$

$$M_{m2}^{\,b} = M_{mt}\ \frac{V_{r2}^{\,b}}{|V_{r1}^{\,b} + V_{r2}^{\,b}|}$$

$$M_{m3}^{\,b} = 0$$

$$|\vec{D}| = |q\ C_D S|$$

$$\vec{D}^b = |\vec{D}|\left[\frac{V_{r1}^{\,b}}{|\vec{V}_r^{\,b}|}\vec{b}_1 + \frac{V_{r2}^{\,b}}{|\vec{V}_r^{\,b}|}\vec{b}_2 + \frac{V_{r3}^{\,b}}{|\vec{V}_r^{\,b}|}\vec{b}_3\right]$$

$$\vec{W}^b = \left[a_{ij}\right]\ (m\vec{G}^g)$$

8. $|\vec{M}| = |q\ C_m y S|$

$$\vec{M}^b = \frac{C_m}{|C_m|}\ |\vec{M}|\ \vec{m}^b$$

$$\vec{M}_d^{\,b} = -C_{md}\ \sqrt{\mu\rho\omega}\ \vec{\omega}$$

9. $q = \frac{1}{2} \rho \left| \vec{V}_r^{\,b} \right|^2$

$$S = \frac{\pi}{4} d^2$$

$$\vec{m}^b = \frac{V_{r1}{}^b \vec{b}_1 + V_{r2}{}^b \vec{b}_2}{\left| V_{r1}{}^b \vec{b}_1 + V_{r2}{}^b \vec{b}_2 \right|} \times \vec{b}_3$$

$$\vec{V}_r{}^b = [a_{ij}] \vec{V}_r{}^g + (\vec{y}b_3) \times \vec{\omega}^b$$

$$\vec{V}_r{}^g = \vec{V}_W{}^g - \vec{V}_p{}^g$$

$$\vec{G}^g = -[G]\vec{g}_3$$

$$\alpha = \cos^{-1} \frac{V_{r3}{}^b}{\left| \vec{V}_r^{\,b} \right|}$$

$$E_1{}^g = V_{p1}{}^g - V_{W1}{}^g$$

$$E_2{}^g = V_{p2}{}^g - V_{W2}{}^g$$

$$E_3{}^g = V_{p3}{}^g - V_{W3}{}^g$$

$$a_{ji} = \begin{bmatrix} a_{11} & a_{21} & 2_{31} \\ a_{12} & 2_{22} & 2_{32} \\ a_{13} & a_{23} & a_{33} \end{bmatrix}$$

10. C_D, C_L, C_m — Functions of α

    G, u, ρ, $V_W{}^g$ — Functions of $R_{p3}{}^g$

11. $\vec{R}_p{}^g$

    $\vec{V}_p{}^g$

    $[a_{ij}]$

    $\vec{\omega}^b$

    d

    $[I]$

    m

    y

    C_{md}

The output lists the pertinent initial conditions; and lists, as functions of $R_{p3}{}^g$:

$R_{p1}{}^g$, $R_{p2}{}^g$, $V_{W1}{}^g$, $V_{W2}{}^g$, $V_{W3}{}^g$, $|V_W|$, $V_{p1}{}^g$, $V_{p2}{}^g$, $V_{p3}{}^g$,

$|V_p|$, $E_1{}^g$, $E_2{}^g$, $E_3{}^g$, $|E|$, t (Time).